

Frequency Selective Surface based Microstrip Antennas for Wideband Applications

A thesis submitted to the
University of Petroleum and Energy Studies

For the Award of
Doctor of Philosophy
in
Electronics and Communication Engineering

BY
Ankush Kapoor

October 2021

SUPERVISOR (s)

Dr. Ranjan Mishra
Dr. Pradeep Kumar



Department of Electrical and Electronics Engineering
School of Engineering
University of Petroleum and Energy Studies
Dehradun-248007: Uttarakhand

Frequency Selective Surface based Microstrip Antennas for Wideband Applications

A thesis submitted to the
University of Petroleum and Energy Studies

For the Award of
Doctor of Philosophy
in
Electronics and Communication Engineering

BY
Ankush Kapoor
SAP ID: 500072301

October 2021

INTERNAL SUPERVISOR

Dr. Ranjan Mishra
Department of Electrical and Electronics Engineering
University of Petroleum and Energy Studies

EXTERNAL SUPERVISOR

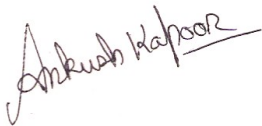
Dr. Pradeep Kumar
School of Engineering
University of KwaZulu-Natal, South Africa



Department of Electrical and Electronics Engineering
School of Engineering
University of Petroleum and Energy Studies
Dehradun-248007: Uttarakhand

DECLARATION

I declare that the thesis entitled as "**Frequency Selective Surface Based Microstrip Antennas for Wideband Applications**" has been prepared by me under the guidance of Dr. Ranjan Mishra, Associate Professor of Electrical and Electronics Engineering, UPES, Dehradun and Dr. Pradeep Kumar, School of Engineering, University of Kwazulu-Natal, South Africa. No part of this thesis has formed the basis for the award of any degree or fellowship previously.



Ankush Kapoor (SAP ID: 500072301)

Department of Electrical and Electronics Engineering,
University of Petroleum and Energy Studies,
Dehradun-248007: Uttarakhand.

Date: 20th October, 2021.



CERTIFICATE

I certify that Mr. Ankush Kapoor has prepared his thesis entitled “**Frequency Selective Surface Based Microstrip Antennas for Wideband Applications**”, for the award of PhD degree of the University of Petroleum & Energy Studies, under my guidance. He has carried out the work at the Department of Electrical & Electronics Engineering, University of Petroleum & Energy Studies, Dehradun.

Dr. Ranjan Mishra

Associate Professor,

Department of Electrical and Electronics Engineering,

University of Petroleum and Energy Studies,

Dehradun-248007: Uttarakhand.

Date: 20th October, 2021.

CERTIFICATE

I certify that Mr. Ankush Kapoor has prepared his thesis entitled “**Frequency Selective Surface Based Microstrip Antennas for Wideband Applications**”, for the award of PhD degree of the University of Petroleum & Energy Studies, under my guidance. He has carried out the work at the Department of Electrical & Electronic Engineering, University of Petroleum & Energy Studies.



Dr. Pradeep Kumar

Discipline of Electrical, Electronics and Computer Engineering

School of Engineering, Howard College Campus

University of KwaZulu-Natal, Durban-4041, South Africa

Date: 20th October, 2021

Discipline of Electrical, Electronic & Computer Engineering

Postal Address: Electrical & Electronic Engineering Building, King George V Avenue,
Howard College Campus, University of KwaZulu-Natal, Durban, 4041, South Africa

Website: www.ukzn.ac.za



1910 - 2010
100 YEARS OF ACADEMIC EXCELLENCE

Founding Campuses:  Edgewood  Howard College  Medical School  Pietermaritzburg  Westville

Abstract

More and more electronic components are being combined onto a single platform due to the demands of downsizing and multi-function in current communication networks. As a result, electromagnetic interference between the signals emanating from the radiating devices must be avoided. It is possible to greatly increase the quality of communication and to avoid the interference by employing the spatial filters.

Spatial filters offer a solution to the problem of improving the performance of communication networks. The use of spatial filters for making stacked apertures has caught a lot of attention. Traditional approaches for developing small, broadband, and high gain antennas are time consuming and costly to implement in practice. Planar frequency selective surfaces (PFSSs) are employed as spatial filters for electromagnetic (EM) waves, which may either transmit or reflect in the required operational frequency band, to achieve these properties. This research work presents a method for creating high gain, compact, and wide band antennas by utilizing PFSSs. This method provides greater antenna capability at a lower cost, as well as a considerable reduction in size and area.

This dissertation describes the overviews and the problems faced in the design of the compact wideband high performance printed patch antennas. The research includes a thorough examination of the compact wideband antennas and the creation of frequency selective surface based spatial filters targeted for sub-6 GHz 5G wideband applications. The characterization of frequency selective surfaces is discussed by using a theoretical and experimental methods. The basic parametric performance analysis, which is critical in the design of the frequency selective surface, is also dis-

cussed in the thesis. Wideband operation is achieved in the printed patch antennas by making use of the slotted ground geometries. The theoretical and experimental research is provided for the two stacked radiating designs which are given as the major emphasis in this thesis. The evolution of a polygon slotted ground printed patch antenna from a normal patch antenna design is fully discussed through experiment and simulation. The influence of various polygon shapes, such as hexagon and 18 segment polygon, on antenna performance is investigated by using the experiments and simulations. Design equations are formulated for implementing the frequency selective surface as spatial filters in the targeted frequency bands and are validated. The frequency selective surface is utilized as a superstrate with the printed patch antenna radiator, and the output performance characteristics are evaluated and reported. The frequency selective surface layer is placed in the two different orientations on the two different proposed printed patch antenna (PPA) designs. In addition, the parametric variation of the height at which the frequency selective surface is positioned above the radiator has been discussed in this thesis. The results of the computational and experimental research on the double layered planar frequency selective surface (DSLPFSS) based stacked design structure are compared for validating the design. This thesis summarizes the results of theoretical and experimental research on a layered architecture of DSLPFSS placed on the PPA. The thesis objective is to design a stacking architecture consisting of a compact wideband high performance radiator which can be utilized in 5G devices consisting of mobile phones, wireless LANs, and other tiny wireless connection terminals.

Acknowledgements

“If each of my remarks were a drop of water, you could see right through them and sense what I’m feeling: appreciation and respect”

Octavio Paz

It is divine, grace and blessings of “**Maa Bhekhi**” that today I have successfully reached yet another milestone of my journey in this endless path of learning that has just begun. After the completion of my thesis work, I feel to convey my indebtedness to all those who helped me to reach my goal. It gives me a great pleasure indeed when I avail this opportunity to express gratitude to those who have contributed in making my research a success.

A plethora of words is insufficient for me to express my profound gratitude to my research guides **Dr. Ranjan Mishra (UPES, Dehradun)** and to **Dr. Pradeep Kumar (UKZN, South Africa)**, whose constant encouragement has enabled me to work enthusiastically, the trust they placed in my abilities was always a great source of motivation. I am really thankful to them for their pioneer guidance and innovative ideas and for spending their precious time in scrutinizing my work at every stage, and this work would not see the light of completion without their continuous encouragement. I feel very much honored as it has been a real privilege for me to get an opportunity to work under their supervision.

I would like to express my profound regards to the **Chancellor** and **Vice Chancel-**

lor of UPES , who gave their kind consent to carry on this work and for providing support throughout this work. I am thankful to the **Dean, School of Engineering of UPES**, for providing consistent motivation to put best effort in this work. I am also thankful to **Dr. Piyush Kuchhal and Dr. S. M. Tauseef**, for providing support and motivation in my research work. I express my sincere thanks and gratitude to **Dr. Raj Gaurav Mishra** , for his valuable support and helping me to start my journey in initial phases by providing his valuable guidance.

Finally I would like to express my profound regards to **Ms. Rakhi Ruhai** for her constant support and also college authorities for providing me the environment which was essential to carry out my work. I express my sincere thanks and gratitude to my fellow colleagues of the **ECE Department, J.N. Government Engineering College, Sundernagar, H.P.** for their constant support and motivation.

Last but not the least all the credit goes to my father **Sh. Vipin Kumar Kapoor** and my mother **Smt. Vijay Kumari Kapoor** for their efforts and blessings by which I am able to reach at this point. I find no words to acknowledge the moral support rendered by my wife **Dr. Sushma Kapoor**, my sister **Dr. Ankita Singh** and brother-in-law **Sh. Ashish Singh** in making this effort a success.

All this has become a reality because of their blessings and above all by the grace of the God.

Ankush Kapoor

Contents

Abstract	i
Acknowledgements	iii
List of Figures	ix
List of Tables	xiv
List of Abbreviations	xvi
1 Introduction	1
1.1 Overview	1
1.2 Printed patch antenna	3
1.3 Performance metrics of the PPA	6
1.3.1 Reflection coefficient	6
1.3.2 Voltage standing wave ratio	7
1.3.3 Impedance bandwidth	7
1.3.4 Gain	8
1.3.5 Directivity	8
1.3.6 Radiation efficiency	9
1.3.7 Fresnel and fraunhofer regions	10
1.3.8 Radiation pattern	11
1.4 Applications	12

1.5	Frequency bands of interest	13
1.6	Planar frequency selective surface (PFSS)	15
1.7	PFSS design methodology	18
1.8	PFSS design challenges	21
1.8.1	Methods for enhancing the bandwidth	21
1.8.2	Miniaturization of PFSS	22
1.8.3	Polarization independence of the PFSS	23
1.8.4	Angular stability of the PFSS	23
1.8.5	Concept of Grating lobes	23
1.9	Applications of the PFSS	24
1.9.1	Spatial filters	25
1.9.2	Electromagnetic shielding	25
1.9.3	Polarizer	26
1.9.4	Security papers	26
1.9.5	PFSS analytical modeling techniques	27
1.10	Research motivation	30
1.11	Research objectives	32
1.12	Research contributions	32
1.13	Organization of the thesis	33
1.14	Summary	35
2	Literature Review	37
2.1	Planar frequency selective surfaces	37
2.2	Outcomes from the discussions	50
2.3	Printed microstrip patch antennas for compact wideband applications	51
2.4	Outcomes from the discussions	54
2.5	Developments of the PFSSs based PPA stacked geometries	55
2.6	Outcomes from the discussions	57

2.7	Summary	57
3	Planar Frequency Selective Surface Design for Sub-6 GHz 5G Ap- plications	59
3.1	Introduction	59
3.2	Double square loop PFSS structure	61
3.3	DSLPFSS analysis	62
3.4	Results formulation for DSLPFSS	67
3.5	DSLPFSS prototype and its measurements	78
3.6	DSLPFSS measurement results	80
3.7	Summary	83
4	Wideband Printed Patch Antennas for Sub-6 GHz 5G Applications	84
4.1	Polygon slotted ground PPA	85
4.2	Interpretation of the results for PSGPPA	88
4.2.1	Reflection coefficient variation with design iterations	88
4.2.2	Radiation intensity	90
4.2.3	Gain and Efficiency	92
4.3	Experimental investigation of PSGPPA.	92
4.4	U- slotted ground PPA (USGPPA)	96
4.4.1	Interpretation of the results for USGPPA	99
4.4.2	Reflection coefficient response along the design iterations	99
4.4.3	Radiation intensity	100
4.4.4	Gain and Efficiency	102
4.5	Experimental investigation for the USGPPA design.	103
4.6	Summary	106
5	Planar Frequency Selective Surface Based Printed Patch Antennas for Sub-6 GHz 5G Applications	107

5.1	Introduction	108
5.2	Design of DSLPFSS based PSGPPA	109
5.3	Interpretation of the results for DSLPFSS-PSGPPA design	111
5.3.1	Reflection coefficient variation with design iterations	113
5.3.2	Radiation intensity	114
5.3.3	Gain and Efficiency	116
5.4	Experimental investigation of the stacked DSLPFSS-PSGPPA design.	118
5.5	Validation of measured results with simulation	120
5.6	Design of DSLPFSS based USGPPA	122
5.6.1	Reflection coefficient variation with design iterations	124
5.6.2	Gain and Efficiency	127
5.6.3	Radiation intensity	128
5.7	Parametric analysis of the height of stacked geometry	129
5.8	Experimental investigation of the stacked DSLPFSS USGPPA design	134
5.9	Validation of measured results with design simulation	138
5.10	Comparison with existing research	139
5.11	Summary	140
6	Conclusion and Future Research	142
6.1	Conclusion	142
6.2	Suggestions for future research	144
	Bibliography	146
	List of Publications	160
	Scholar's Resume	162
	Plagiarism Certificate	164

List of Figures

1.1	Classification of the types of antenna geometries	3
1.2	Figure of merits of the PPA	5
1.3	Illustration of the feeding techniques for the PPA	5
1.4	Basic geometry of the PPA with microstrip line feed	6
1.5	Radiations exhibited by a PPA	11
1.6	Omnidirectional radiation pattern of the PPA	12
1.7	Potential applications of the PPA	13
1.8	Spectrum allocation for 5G deployment	14
1.9	Global snapshot of 5G spectrum finalized by countries (Source Qual- comm)	15
1.10	Most utilized bands of sub-6 GHz 5G spectrum	16
1.11	Illustration of the transmissive behavior of the PFSS	17
1.12	Illustration of operation of a PFSS	18
1.13	Different element geometries of PFSS	20
1.14	Functional description of PFSS	21
1.15	Extracted equivalent circuit parameters of the PFSS	21
1.16	Taxonomy of the PFSS.	25
3.1	Geometry of DSLPFSS unit cell	62
3.2	DSLPFSS as a spatial filter	62
3.3	2x2 array of DSLPFSS.	66
3.4	Lumped circuit of the unit cell of DSLPFSS.	67

3.5	Illustration of the transmissive behavior of the single unit cell DSLPFSS.	68
3.6	Effect on the transmissive characteristics by the variation of $\frac{w_1}{\lambda_1}$ for the DSLPFSS geometry.	70
3.7	Effect on the transmissive characteristics by the variation of $\frac{w_2}{\lambda_2}$ for the DSLPFSS geometry.	71
3.8	Illustration of the two-port network.	72
3.9	Equivalent circuit schematic of the DSLPFSS.	74
3.10	Comparative analysis of the transmission coefficient curve extracted from HFSS and Circuit editor.	75
3.11	Response of DSLPFSS spatial filter at various polarization angles. . .	77
3.12	Response of DSLPFSS spatial filter at multiple incidence angles. . . .	78
3.13	MFEF of the DSLPFSS.	79
3.14	2x2 array of DSLPFSS geometry.	79
3.15	Spatial filtering response of DSLPFSS.	80
3.16	2×2 array of DSLPFSS prototype.	80
3.17	E-Field dispersion of 2×2 array of DSLPFSS.	81
3.18	Testing and measurement set-up of the DSLPFSS.	82
3.19	Comparison of the modeled and the experimental results of the 10x10 DSLPFSS array.	82
4.1	PPA design iterations	87
4.2	Comparative analysis of the output characteristics retrieved from all iterations.	89
4.3	Normalized radiation patterns for the wideband antenna designs comprising hexagon slotted PPA and PSGPPA	91
4.4	3D polar plot depicting the gains exhibited by the two proposed designs	92
4.5	Graphical illustration of the gain (dB), directivity (dB) and the radiation efficiency (%) exhibited by the PSGPPA design.	93

4.6	Photograph of an anechoic chamber used for measurements of the PPA designs.	94
4.7	PSGPPA designed prototype	95
4.8	Measurement set-up for illustrating the output characteristics of the PSGPPA.	95
4.9	Comparative analysis of the output characteristics of the PSGPPA exhibiting a bandwidth of 720 MHz	96
4.10	Design of a simple USGPPA.	97
4.11	Modifications of the ground plane	98
4.12	Comparative illustration of the reflection coefficients obtained from the three design steps consisting of complete ground plane, half ground plane and U-slot defected ground plane (USGPPA).	101
4.13	Normalized radiation patterns of the USGPPA in E-plane and H-plane at 4 GHz resonant frequency.	101
4.14	3D polar plot depicting gains exhibited by USGPPA	102
4.15	Graphical illustration of the gain (dB), directivity (dB) and the radiation efficiency(%) exhibited by the USGPPA design.	103
4.16	USGPPA prototype	104
4.17	Comparative analysis of the output characteristics of the USGPPA retrieved from the simulation and experimental set-up.	104
5.1	Illustration of PFSS based spatial filters in electromagnetic environment.	108
5.2	Incorporation of PFSS as a superstrate with PPAs.	109
5.3	DSLPFSS based PSGPPA design.	110
5.4	Comparison of the radiation region covered by the various designs in terms of the reflection coefficient response versus frequency.	114

5.5	Comparative analysis of the radiation patterns retrieved from the PS-GPPA with and without incorporation of the DSLPFSS superstrate at the 3.75 GHz resonant frequency	115
5.6	3D polar plot depicting the gains exhibited by of DSLPFSS-PSGPPA.	115
5.7	Graphical illustration of the gain (dB), directivity (dB) and the radiation efficiency (%) exhibited by the DSLPFSS-PSGPPA design.	116
5.8	Response of the reflection coefficient (dB) with respect to effective height between PSGPPA and DSLPFSS superstrate for the stacked design.	117
5.9	Variation in the gain of the stacked design by placing DSLPFSS superstrate at different distance above PSGPPA.	118
5.10	Variation in the directivity of the stacked design by placing DSLPFSS superstrate at different distances above the PSGPPA.	118
5.11	Orientation of the DSLPFSS layer over the PSGPPA geometry	119
5.12	Illustration of the design prototypes of PSGPPA and DSLPFSS	120
5.13	Validation of the results retrieved from the experimental set-up and through modeling	121
5.14	Proposed designs of USGPPA and DSLPFSS	123
5.15	Comparative illustration of the reflection coefficients obtained from the three design iterations for making USGPPA.	126
5.16	Comparative analysis of the impedance bandwidth retrieved from the geometry of USGPPA with and without DSLPFSS reflector.	126
5.17	Comparison of the maximum gain of the USGPPA with and without the DSLPFSS.	128
5.18	Comparison of the maximum directivity of the USGPPA with and without the DSLPFSS.	129

5.19	Graphical illustration of the maximum gain (dB), maximum directivity (dB) and the radiation efficiency (%) exhibited by the DSLPFSS-USGPPA design.	130
5.20	Graphical illustration of the radiation patterns for the USGPPA with and without DSLPFSS	131
5.21	Net Magnitude and phase of the reflection coefficient for the unit cell of DSLPFSS.	133
5.22	Reflection coefficient response with respect to effective height between USGPPA and DSLPFSS superstrate for the stacked design.	134
5.23	Variation in the gain of the stacked design by placing DSLPFSS superstrate at different distance above USGPPA.	135
5.24	Variation in the directivity of the stacked design by placing DSLPFSS superstrate at different distances above the USGPPA.	136
5.25	Orientation of the DSLPFSS over the USGPPA geometry	136
5.26	Prototypes of the proposed design	137
5.27	Validation of the results retrieved from the experimental set-up and through modeling.	139

List of Tables

3.1	Parametric specifications of the unit cell of DSLPFSS.	67
3.2	Estimation of the best values of the output loop parameters at a normalized angle of incidence for 3 GHz operating frequency	69
3.3	Estimation of the best values of the innermost loop parameters at a normalized angle of incidence for 5 GHz operating frequency	70
3.4	Numerical results retrieved from the mathematical analysis equations	73
3.5	Resonant frequencies extracted from the lumped circuit parameters. .	74
3.6	Resonant frequencies of operation at different polarization angles. . .	76
3.7	Resonant frequencies of operation at various angles of the incidence. .	77
4.1	Dimensions of proposed PSGPPA (FR4 substrate with $h = 0.02\lambda$) .	87
4.2	Parametric analysis of the results retrieved from the design iterations	90
4.3	Effect on the output characteristics by the variation of the feed width of the PSGPPA.	90
4.4	Output characteristics of the hexagonal slotted PPA and PSGPPA. .	91
4.5	Comparison of the output characteristics retrieved from the simula- tion and the measurements for the proposed PSGPPA	96
4.6	Parametric specifications of the USGPPA	98
4.7	Comparative analysis for the three iterations involved for making final proposed design of USGPPA.	99
4.8	Output characteristics exhibited by USGPPA.	102

4.9	Comparison of the output characteristics retrieved from the simulation and the measurements for the proposed USGPPA.	105
4.10	Comparison of USGPPA design with state of art literature for compactness in sub-6 GHz 5G NR range	105
5.1	Structural configuration of the DSLPFSS-PSGPPA design.	111
5.2	Comparison of the output characteristics retrieved from the simulation and the measurements for the proposed USGPPA.	112
5.3	Experimental results compared with modeled design for DSLPFSS-PSGPPA.	122
5.4	Geometrical configuration of the DSLPFSS with USGPPA.	125
5.5	Comparative analysis of the output performance parameters retrieved from the design iterations comprising of full ground, half ground, U-slot defected ground and with DSLPFSS-USGPPA.	127
5.6	Comparison of simulated and measured results of stacked geometry of USGPPA with DSLPFSS.	138
5.7	Performance comparison of the proposed compact “DSLPFSS-PSGPPA” and “DSLPFSS-USGPPA” with the state-of-art literature.	140

List of Abbreviations

AOI	Angle of Incidence
EM	Electromagnetic
5G	Fifth Generation
DSLPFSS	Double Square Loop Planar Frequency Selective Surface
ECM	Equivalent Circuit Modeling
FDTD	Finite Difference Time Domain
FEM	Finite Element Method
FR1	Frequency Range 1
FR4	Flame Retardent 4 Substrate
IOT	Internet of Things
NR	New Radio
PFSS	Planar Frequency Selective Surface
PPA	Printed Patch Antenna
PSGPPA	Polygon Slotted Ground Printed Patch Antenna
RCS	Radar Cross Section
RF	Radio Frequency
TE	Transverse Electric
TM	Transverse Magnetic
USGPPA	U- Slotted Ground Printed Patch Antenna
VNA	Vector Network Analyser

Chapter 1

Introduction

1.1 Overview

Electromagnetic environment is greatly influenced by both natural and human factors. The expansion of electronics and electrical equipment in numerous industries, such as the networking sector, wireless communication industry, and high-speed computation, etc necessitates the operation of several systems near to one another. All of the applications of electronics in the communication industry will emit electromagnetic radiations, which may be categorized as either deliberate or man-made. Humans are inherently surrounded by electromagnetic radiations which are emitted by some of the other antennas as radiating apertures. When the electromagnetic radiation is emitted from a source, then it travels to a far-field distance. The voltages and currents are further induced in the neighboring circuits due to electromagnetic induction which is known as radiated coupling. There is no requirement for a conducting channel in this case, unlike in regular impedance coupling. To see the influence of distant fields, radiation coupling must be investigated. Most of us find it fascinating that currents running in one circuit may cause currents to flow in another circuit across the room or even many miles away. The presence of electromagnetic waves can be felt in the radiations which were identified far back

by James Clerk Maxwell in the year 1864. In his research, he determined the wave propagation velocity along with reflection and diffraction behavior. In modern communication systems, wireless connectivity is taken for granted. Even though the technology which is used to generate and transmit electromagnetic waves remains sophisticated, many engineers believe that electromagnetic radiations are both difficult to make and detect. Almost all the wireless circuits emit detectable amounts of ambient electromagnetic fields. The most difficult task for electronic engineers is to design antenna radiators that do not release excessive electromagnetic radiation. Hence, there is a need to develop a mechanism to mitigate the stray electromagnetic fields.

In addition, as the communication industry has evolved from 1st generation wireless mobile systems to 5th generation wireless mobile systems, there has been a desire for small miniaturized antennas that take up less space while yet delivering adequate performance. The antennas that must be developed must be light, small, and simple to manufacture. An antenna is a component of any wireless communication system that is used to transmit or receive radio waves. It is an electronic device that helps to broadcast electromagnetic waves into the air by converting all the supplied electrostatic energy into the radio waves and performs a reverse phenomenon at the receiver end [1]. Antennas are embedded in all the wireless technologies which include wireless television remote control, telematics devices, high-speed spacecraft and aircraft, and satellite communications. With the introduction of integrated circuit technology and the development of miniaturized electronic devices, the need for compact and low-profile antennas is growing. Antenna design is a crucial component of growing wireless technology which has experienced a flourishing phase from the 1940s until the 21st century [2]. This is because of the technological advancements which have occurred by the addition of several new design methodologies and innovation of new structures such as lens antennas, parabolic reflectors,

rhombic antennas, and microstrip antennas which have contributed to its success [1]. Downsizing the communication equipment has been constrained by the size of the antennas. The major drawback of the low profile antennas is their small values of the impedance bandwidth, with low gain and directivity [2]- [4]. There is a trade-off in maintaining a wide bandwidth with adequate gain and directivity, as an increase in one parameter tends to reduce the other. Hence, many techniques are suggested in the available literature which makes use of the complex designs that can be implemented in almost all personal wireless communication devices. These difficulties can be mitigated by proper designing of the antennas which makes this field of research more appealing. Figure 1.1 depicts some of the most common types of antennas used in the communications sector.

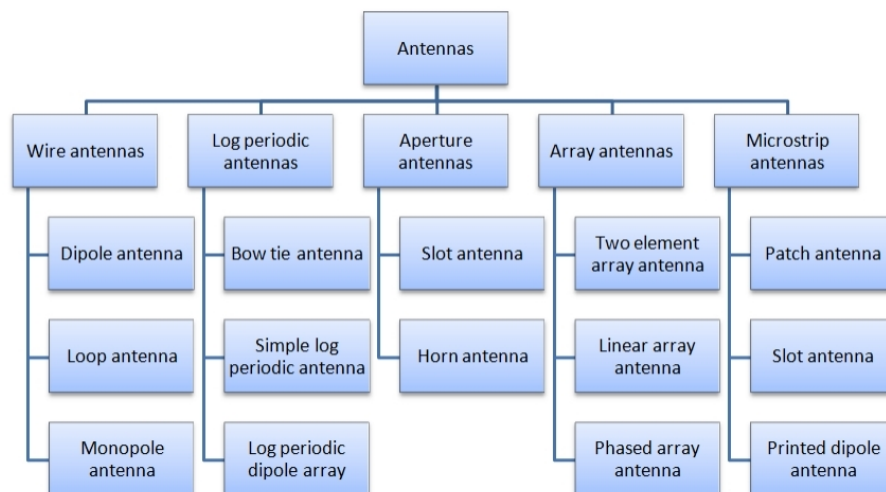


Figure 1.1: Classification of the types of antenna geometries

1.2 Printed patch antenna

The printed patch antenna (PPA) is cutting-edge technology in the design of radiating apertures. It is commonly utilized in wireless communication systems because it offers inherent advantages of simplicity and compatibility with printed circuit technology. Microstrip geometries that emit electromagnetic waves were first considered

in the early 1950s [3]. Deschamps firstly proposed the concept of microstrip antenna in the year 1953 [3]. In 1955, the patent was granted to Gutton and Baissinot for the microstrip antenna [4]. PPA may now be found in nearly all wireless systems. It's utilized to send and receive electromagnetic signals in the microwave range, and it's employed in wireless communications.

The shape and material characteristics of the substrate on which the antenna is printed has an influence on the performance and operation of the PPA. Engineers have been required to create scaled-down electronic frameworks as a result of improvements in the communication industry, allowing researchers to cope with both embedded systems and patch antenna innovation. Due to a few attractive qualities, PPAs have become a crucial component of scaled-down electronic systems. The PPAs are made up of a metallic transmission patch created over a dielectric substrate and supported by a metallic ground plane in their most basic form. It can be found in virtually all generations of mobile phone receivers. In recent wireless communications generations, such as industry 4.0 and internet of things devices, PPAs have gotten a lot of attention. Regardless of its numerous areas of interest, it has a significant disadvantage in form of low value of gain and reduced amount of bandwidth. To overcome this issue, many design approaches for increasing the narrow bandwidth of PPAs have been devised. Due to its various advantages over typical microwave antennas, PPAs have proven to be an efficient radiator for a variety of applications. Figure 1.2 highlights some of the most important advantages of the patch antennas. Several feeding strategies for enhancing the PPA's output performance characteristics have been offered. The incident energy is fed into the radiating aperture using the feeding technique. It is crucial because it serves as a link between the air interface and the radiating aperture. Figure 1.3 depicts some of the PPA feeding strategies.

The direct contact microstrip line feed is a widely utilized feeding technology as

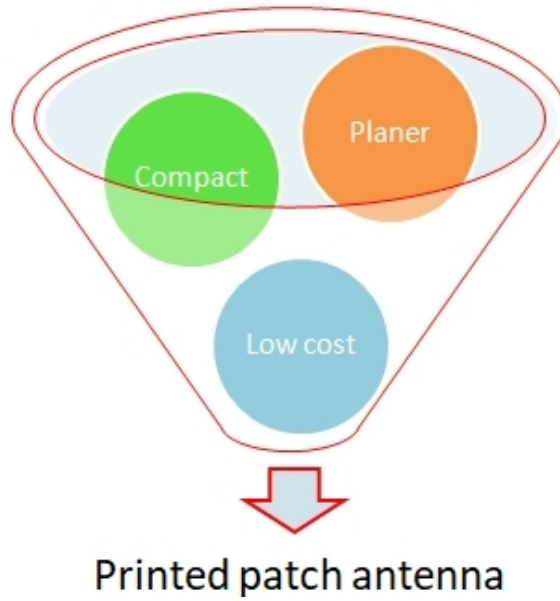


Figure 1.2: Figure of merits of the PPA

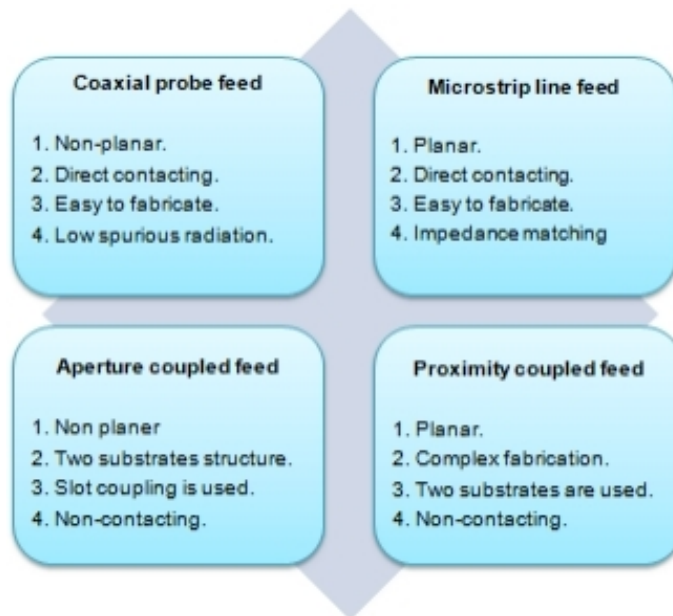


Figure 1.3: Illustration of the feeding techniques for the PPA

it is easy to fabricate. As seen in Figure 1.4, a conducting strip is attached directly to the margin of the microstrip patch. The dimensions of the radiating patch extend beyond the conducting strip. The feed-in form of conducting strip may be etched on the same substrate as that of the patch, giving it a flat appearance. This feeding technique offers with simple manufacturing, modeling, and impedance matching. However, this feeding technique suffers from a strong limitation. Surface waves and spurious feed radiations rise as the thickness of the dielectric substrate increases,

limiting the antenna's bandwidth.

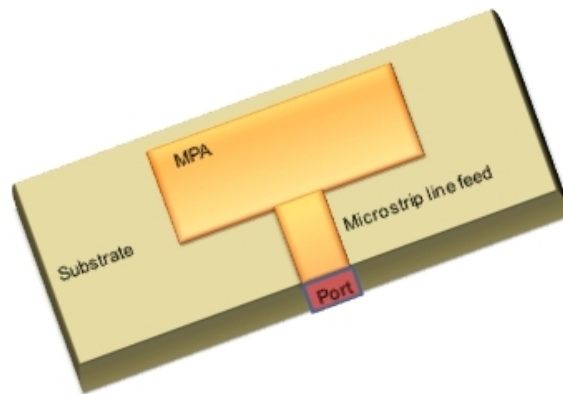


Figure 1.4: Basic geometry of the PPA with microstrip line feed

1.3 Performance metrics of the PPA

PPA forms the backbone of today's mobile communication systems. They obey the reciprocity property which implies that the antenna geometry maintains the same features in the transmitting as well as in the receiving mode. The design of the PPA is targeted to achieve adequate values of the performance metrics as described below:

1.3.1 Reflection coefficient

The reflection coefficient of the PPA forms important design criteria and in terms of the scattering parameters, it is given by the S_{11} coefficient. It signifies the percent of the total power of the source which is reflected in the overall power output. The amount of radiation is calculated by looking at the reflection coefficient, which should be as small as feasible. It's a statistic that quantifies of how much an electromagnetic wave is reflected back owing to a transmission medium impedance discontinuity.

1.3.2 Voltage standing wave ratio

The voltage standing wave ratio (VSWR) is basically a measurement of how well input power is transferred through the PPA for radiation purposes. The PPA is connected by the feedline from the source generator. When the source, feedline, and PPA impedances are correctly matched, the energy created by the source is entirely transmitted to the surroundings through the antenna interface. The transceivers and the feed lines are designed for exhibiting 50-ohm impedance and therefore if the impedance offered by the PPA differs from 50 ohm, then there is a mismatch which results in energy loss [1]- [3]. An optimal communication system radiates all the incident power given to an antenna. This requires a perfect impedance matching between the source, feedline, and the PPA. In real-world systems, if any impedance mismatch occurs at the interface of these systems, then it might cause some amount of energy to be reflected in the source. This creates a standing voltage across the line, and consequently, the reflection generates the destructive interference and thus causing the voltage to fluctuate at different points along the line. So, VSWR helps to measure the voltage fluctuation along with the targeted frequency band.

1.3.3 Impedance bandwidth

Another essential feature of the PPA antenna is its bandwidth, which is defined as the range of frequencies across which the antenna can transmit or receive energy correctly. As a result, bandwidth is a crucial aspect to consider when building a PPA for a certain application. The term fractional percentage bandwidth is utilized to explain the broadband characteristics of the designed antennas which are given by:

$$Bandwidth = \frac{HigherFrequency - LowerFrequency}{MiddleFrequency} \quad (1.1)$$

1.3.4 Gain

Gain of the PPA is defined as the ratio of the overall radiation intensity (RI) of the proposed PPA design in a given direction to that of its value that would be produced by a lossless isotropic PPA. Also, the effective radiation intensity of the lossless isotropic PPA is equal to the ratio of the amount of power that enters into the radiating aperture and the solid angle of 4π steradians.

Mathematically,

$$Gain = \frac{4\pi RI}{P_{in}} \quad (1.2)$$

Gain of a PPA is measured usually in dB and a gain of 10 dB which when equated to an isotropic antenna is termed as 10dBi. The amount of radiation exhibited by an isotropic antenna is equal in all directions. In the real-world, the isotropic antenna doesn't exist, but it surely helps to retrieve the antenna parameters. The measurement of the gain is done by equating the test antenna with a standard calibrated antenna. An antenna doesn't generate power, so the total amount of the power radiated from an antenna is equal to that of an isotropic antenna, but it is non-uniformly distributed.

1.3.5 Directivity

When a uniform quantity of power is radiated, the directivity may be calculated by dividing the power density in the direction of highest value by the power density of an ideal isotropic antenna. It is a measurement of the radiation pattern directionality of an antenna. An isotropic antenna is a lossless antenna that radiates evenly in all directions. It has a perfect spherical radiation pattern in free space, which means that the electric strength of the field radiated by an isotropic antenna is the same at every point on an imagined spherical surface. As a result, if an isotropic antenna

outputs total power P_t in watts and is positioned in the centre of a transparent (or fictional) far-field sphere of radius R metres, the power density throughout the whole spherical surface is given by:

$$P_{isotropic} = \frac{P_t}{4\pi R^2} W/m^2 \quad (1.3)$$

As the total amount of input power P_t is spread equally throughout the entire surface area of the sphere and the radiation is being felt uniformly, hence the above equation holds valid. Practical antennas possess some degree of non-uniformity in their emission patterns; hence an isotropic radiator is not physically possible. A practical antenna, which is essentially a non-isotropic radiator, has a directed pattern because it radiates more power in certain directions than others. Despite emitting the same total power, a directional antenna will produce more power in its maximum radiation direction than an isotropic antenna. Directivity is essentially a statistical measure of an antenna's ability to concentrate radiated power per unit solid angle in a certain direction.

1.3.6 Radiation efficiency

The radiation efficiency of the PPA is calculated by taking the ratio of the net amount of power supplied at the input terminal to the power emitted from the output terminal. For a highly efficient antenna, a major portion of the power delivered at the antenna's input must be radiated out. But in a practical scenario, the majority of the power is absorbed due to losses inside the PPA. An important feature exhibited by the PPA is in the form of having an ability to maintain the same efficiency when applied in the transmitter or at the receiver side. The radiation efficiency is determined by dividing the net radiated power by the total provided input power of the PPA and is expressed as follows:

$$\epsilon_r = \frac{P_{emitted}}{P_{input}} \quad (1.4)$$

The value of the radiation efficiency lies between 0 and 1. Usually, the value is taken in percentage such as efficiency of 0.5 equals to 50 % and it is commonly expressed in decibels (dB).

1.3.7 Fresnel and fraunhofer regions

The radiation pattern of the PPA fluctuates with the distance at which the radiation is measured. It basically consists of two forms of energy that is reactive energy felt in the near fields and radiating energy felt in the far fields as shown in the Figure 1.5. Therefore, the antenna vicinity is classified into three distinct regions which are classified as: (a) Reactive fresnel field region, (b) Radiating fresnel field region, and (c) Fraunhofer field region. The reactive energy oscillates to and fro from the antenna in the reactive fresnel field area. This area has a significant disadvantage in that it is unable to emit energy, thus the entire energy component is stored in it. The final place where its presence is sensed is at:

$$X_1 = 0.62\sqrt{\frac{D^3}{\lambda}} \quad (1.5)$$

where X_1 represents the distance of the radiating field measurement from the antenna surface, D denotes the greatest dimension of the antenna aperture, and the operating wavelength is denoted by λ .

The radiating fresnel field region is located between the reactive fresnel field and the fraunhofer field region. In this area, the value of reactive fields is smaller than that of radiating fields, and radiation fields begin to dominate. Its influence may be visible up to the outermost layer, which is located at a distance of:

$$X_2 = 2\sqrt{\frac{D^2}{\lambda}} \quad (1.6)$$

where X_2 denotes the distance from the surface of antenna. The third region consists of the fraunhofer field region which exists beyond the distance of X_2 . This region experiences lack of the reactive fields and only the effect of the radiating fields are felt. It is crucial to notice that the angular field distribution is unaffected by the distance between the PPA and the observer.

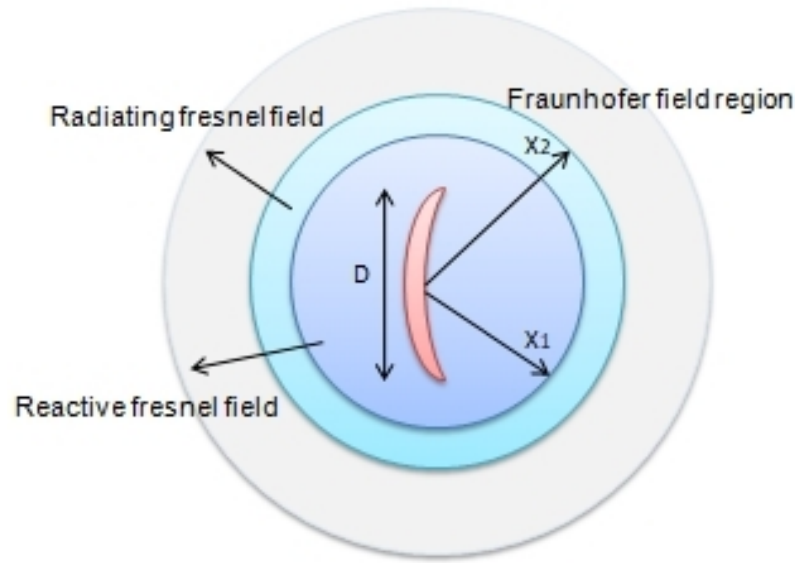


Figure 1.5: Radiations exhibited by a PPA

1.3.8 Radiation pattern

The term "radiation" is used to describe the emission or reception of a wavefront at the PPA interface, which further specifies its intensity. The radiation pattern of the PPA is a sketch created to illustrate its radiation as a function of direction. The parameters such as the gain and directivity may be easily deduced by looking at its radiation pattern. When the power is emitted from the PPA, then it has an influence in both the near and distant fields. The radiation emitted from the PPA depends on the angular position of the receiver and also on the radial distance at which it is measured. The radiation pattern's mathematical representation can be

expressed in terms of spherical co-ordinates such as $E(\theta, \phi)$ and $H(\theta, \phi)$. Figure 1.6 depicts an omnidirectional radiation pattern, which is defined as the uniform emission of radiation in all directions.

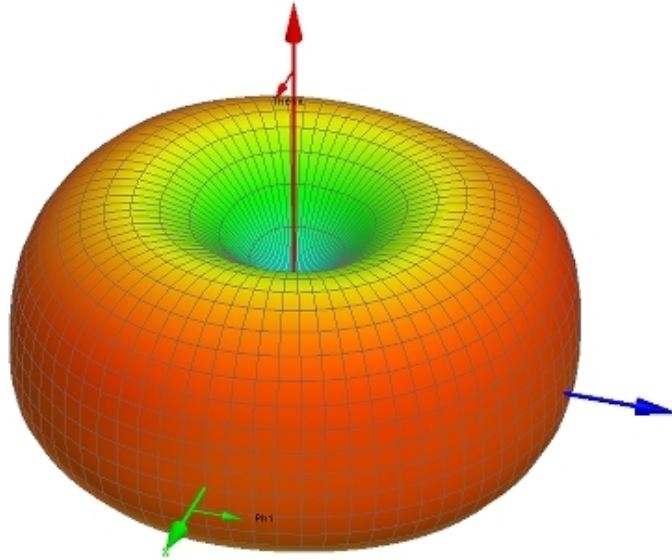


Figure 1.6: Omnidirectional radiation pattern of the PPA

1.4 Applications

PPA forms the backbone of almost all mobile communication devices. They find their usage in a variety of areas such as in satellite communication, RFID (radio frequency identification), mobile communication systems, and in healthcare systems. Satellite links, for example, need circularly polarized radiation characteristics, which may be realized by using either a square or circular patch microstrip antenna. Circularly polarized transceivers are employed in global positioning satellite (GPS) systems as they are quite small and highly costly. These are used in telemedicine applications operating at 2.45 GHz. Wearable microstrip antennas are an appropriate candidates for wireless body area networks. RFID (radio frequency identification), wireless telephones, and healthcare systems are some of the applications which employ microstrip antennas. An RFID system is made up of a tag

and a reader which incorporated PPAs. Microwave radiation is believed to be the most effective technique of generating hyperthermia in the treatment of malignant tumours. The radiators used for this function should be compact, easy to handle, and durable. These requirements can only be met by use of the PPA. The earliest microstrip radiator designs for generating hyperthermia in medical applications were based on printed dipoles and annular rings built on S-band. Some of the potential uses of PPAs are depicted in Figure 1.7 below:

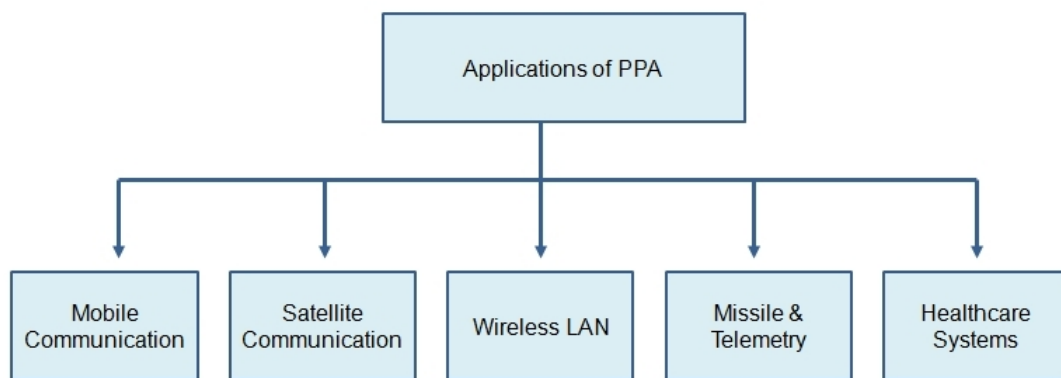


Figure 1.7: Potential applications of the PPA

1.5 Frequency bands of interest

Fifth generation (5G) mobile communication is the most recent generation of cellular technology, and it promises to deliver seamless coverage, high data rates, minimal latency, and extremely dependable communications. It will increase the system's energy efficiency, spectrum efficiency, and network efficiency. It will serve as an information conduit, connecting billions of Internet of Things (IoT) devices while also providing faster and more reliable access. The 5G enabled communication systems will deliver higher quality video services possessing high speed mobility. The delivery of information and data will be through billions of connected devices. They will support the delivery of vital services such as telesurgery and self-driving vehicles,

ensuring low latency and ultra-reliability networks. It will increase the productivity by providing high-quality and real-time data. Historically, India's technological deployment has lagged behind that of the world's most industrialized countries. India, on the other hand, is meticulously preparing to install 5G technology ahead of the rest of the world. The lifeblood of every wireless communication system is its spectrum. 5G spectrum caters to three different frequency bands consisting of low frequencies (less than 1 GHz) which allows IoT for low data rate applications and provides wide area and deep indoor coverage throughout urban, suburban, and rural regions. The second one is the medium range of the frequencies (1 GHz –6 GHz) which offers excellent coverage and speed. However, in dense installations, the higher-order frequencies (lying above 6 GHz) hold significant potential for providing very high data rates and system capacity. The three different 5G frequency bands are illustrated in Figure 1.8 as mentioned below.

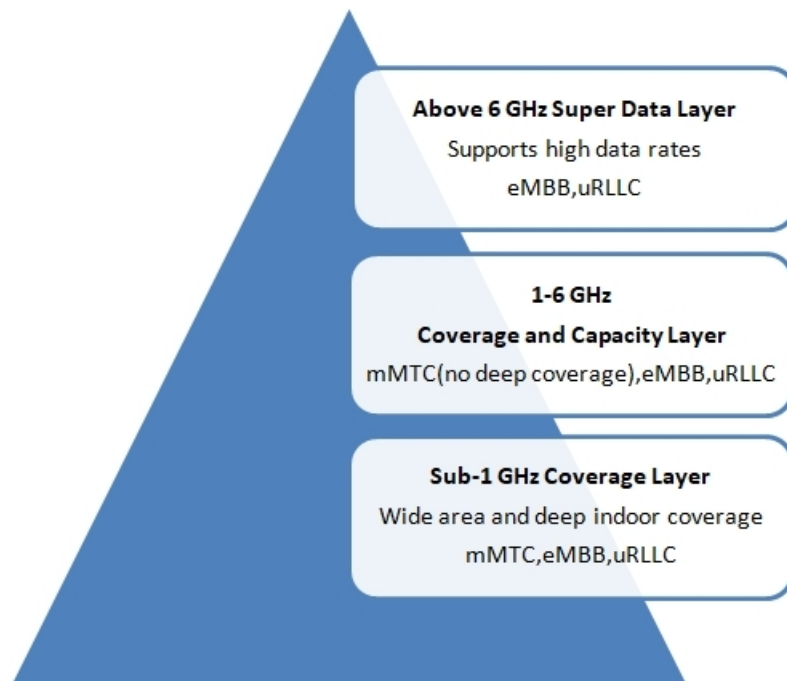


Figure 1.8: Spectrum allocation for 5G deployment

The sub-6 GHz FR1 bands of 5G communication are mostly used for enhanced

mobile broadband (eMBB), massive machine-type communication (mMTC), and ultra-reliable low latency communications (uRLLC) [5]. In the recent decade, technological improvements in wireless communication have made tiny patch radiators a viable option for large-scale deployments on existing 4G and projected sub-6 GHz 5G cellular networks. At the moment, mobile users want faster data speeds and better service efficiency. The FR1 band will be of significant value as a result of recent advancements in the communication industry and the introduction of 5G devices, as it will bridge the technological gap between the present 4G and 5G networks. As indicated in Figure 1.9, many nations have finalised their frequency bands for deployment.



Figure 1.9: Global snapshot of 5G spectrum finalized by countries (Source Qualcomm)

Some of the most common frequency bands which are allocated and are in use for the sub-6 GHz 5G spectrums are illustrated in Figure 1.10.

1.6 Planar frequency selective surface (PFSS)

Planar frequency selective surfaces (PFSS) are made up of a series of randomly distributed metallic patches (capacitive) or apertures (inductive) with symmetrical

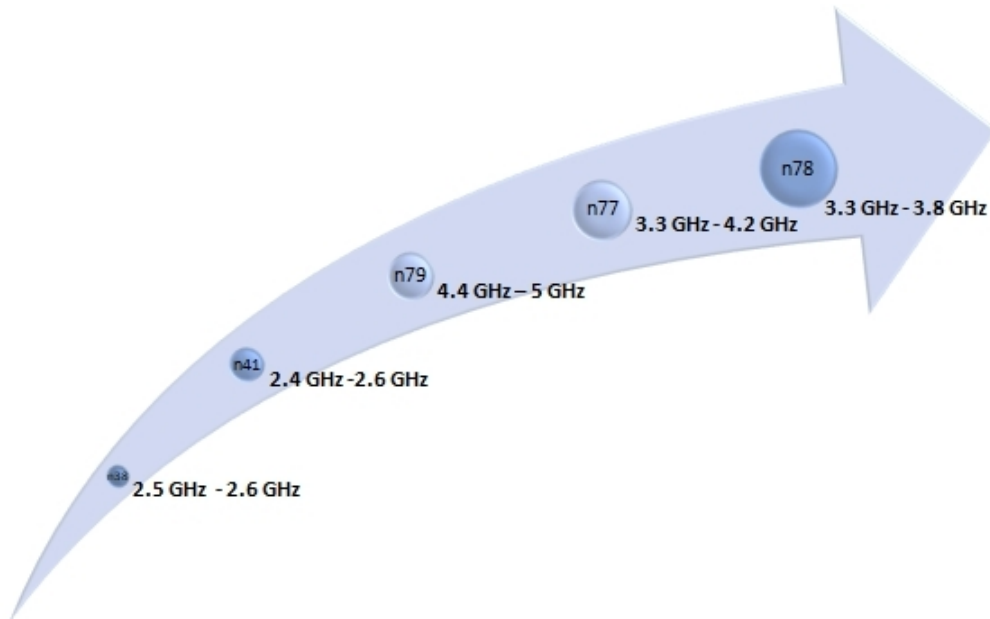


Figure 1.10: Most utilized bands of sub-6 GHz 5G spectrum

or asymmetrical geometries on a dielectric substrate that act as a spatial filter for electromagnetic (EM) waves at specific resonant frequencies within a given range of incident angles and polarization [6]. The PFSS are classified as spatial filters in terms of high-pass, low-pass, band-pass, and band-stop filters based on the kind of element and array structure. Aforesaid filtering characteristics help in the usage of PFSS in radomes, Cassegrain sub-reflectors, electromagnetic shielding, spatial filtering, microwave absorbers, and in the applications which are directly related to security and efficiency of wireless communications. [6]- [13]. The basic functioning concept of the PFSS structure is comparable to the study of diffraction gratings in optics, which aid in dividing a beam of non-monochromatic light into its spectrum components. In the mid-1960s, researchers were interested in the comprehensive investigation of PFSS and their interaction with EM waves. In addition, from the year 1919 onwards, different kinds of literature describing the uses of the PFSS have been discovered [6]. Let us consider the simplest symmetrical geometry of square loop PFSS, which acts as a band stop filter for the frequencies corresponding to its unit cell dimensions. Whereas, on the other hand, its analogous structure comprising of

aperture based square slot structure, gives a band-pass response at frequencies determined by its aperture size while rejecting all the out-of-band frequency components. The type of chosen element, its size, and inter-element spacing with the dielectric substrate parameters are the factors that impact the overall resonance frequency, bandwidth, and the angle of incidence (AOI) dependence along with polarization behavior of the planar incoming wave [14]- [16]. As a result, while building an FSS structure for the desired frequency response, the appropriate selection of geometrical features is important. These variables have the potential to significantly affect the PFSS's output characteristics. The resonant frequency of operation of the PFSS is also affected by the dielectric material utilized and the number of PFSS layers through which the wave passes. The relationship between the operation's resonant frequency (f_r) and the relative permittivity (ϵ_r) of the dielectric substrate is critical to consider throughout the design phase. Hence, it can be said that the choice of the dielectric material impacts the resonant frequency of operation. A simplified schematic of the PFSS explaining the concept of operation is depicted in Figure 1.11 and variation of the response on the basis of the type of element is depicted in Figure 1.12. The designed PFSS structure can be a single layer PFSS or a cascaded kind with many PFSS layers. Depending upon the targeted applications, PFSSs can be constructed with single, dual, or broadband frequency responses.

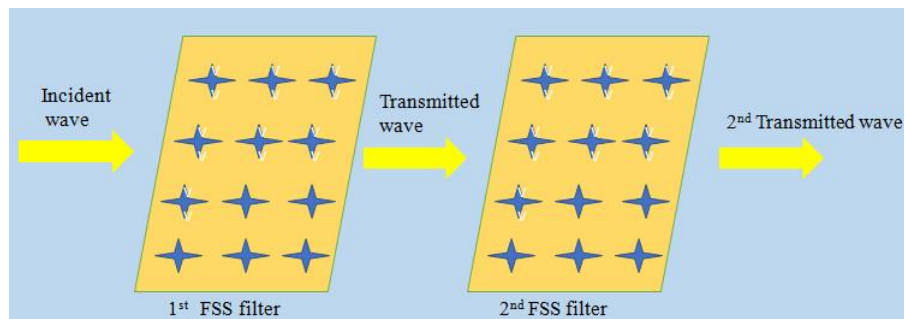


Figure 1.11: Illustration of the transmissive behavior of the PFSS

Miniaturization, polarization independence, and angular independence are three

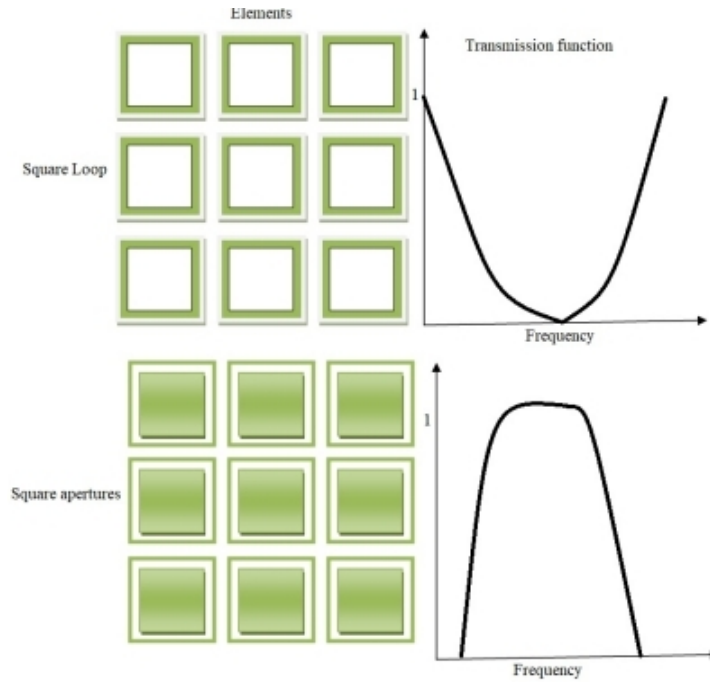


Figure 1.12: Illustration of operation of a PFSS

main characteristics that must be considered while designing PFSS for most applications. The performance of the PFSS's is investigated by creating an infinite number of unit cells, even though real deployment needs a finite number of unit cells. Miniaturization of unit cells is a difficult process that must be accomplished without changing the resonant frequency of operation.

1.7 PFSS design methodology

The shape of unit cells is essential in the formation of PFSS. According to Floquet's theory, an array of periodic elements exhibits the same behavior as the unit element used to construct the array [17]. The periodic elements generated by the unit cell design and the substrate utilized define the PFSS's band stop or band-pass characteristics. The unit cell components of periodic surfaces can be constructed by using patch or aperture type elements depending upon their applications. Various forms of PFSSs have been reported in the literature, with some fundamental geometries including loop, dipole, cross, and patch-shaped PFSSs. As shown in [6], the

geometries are classified based on their output properties and are as follows:

- Group A: is formed by assembling of dipoles, tripoles, square spirals, and Jerusalem crosses.
- Group B: consists of loops such as circular, square, and hexagonal loops.
- Group C: consists of diverse forms of solid interior patch kinds.
- Group D: consists of hybrid forms of the solid interior patch kinds in a variety of forms.

Figure 1.13 depicts diagrammatic examples of the aforementioned groupings. PFSS functionality may be shown using a complementary self-resonating network, as seen in Figure 1.14. Electric currents are induced when an electromagnetic wave impacts the PFSS structure. The magnitude of the induced currents is determined by the coupling energy level. These induced currents act as electromagnetic sources, generating further dispersed fields. As a consequence, the total field in the PFSS area is made up of incident electromagnetic fields combined with dispersed fields. As shown in Figure 1.13 , group (A) is made up of dipole-type patch components that are intended to act as bandstop filters for incident plane waves as well as complete reflecting surfaces over a limited frequency range. The slot aperture components, like those in group B, exhibit band-pass properties, which mean they behave as semi-reflecting surfaces to incoming electromagnetic waves within the operational frequency band. Despite meeting the practical criteria, the geometries exhibit insufficient filter response, low angular stability, and limited bandwidth, restricting their applicability to a limited range of electromagnetic applications.

The equivalent circuit modeling technique is used to evaluate and forecast the characteristics of PFSSs, as shown in Figure 1.15, which shows two unique types of

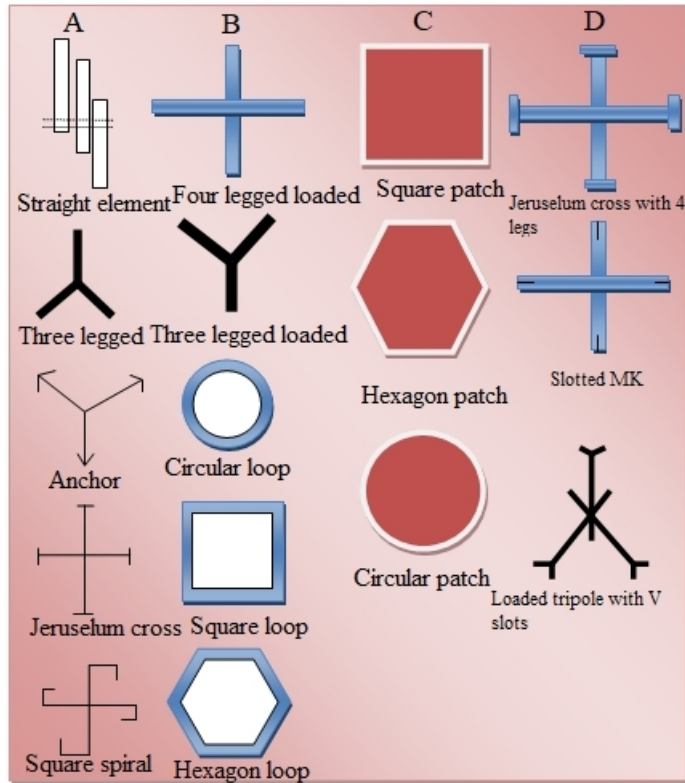


Figure 1.13: Different element geometries of PFSS

elements in array shape with low and high pass responses [6]. Resistance (R) and inductance (L) are created by PFSS metallic patches in an equivalent circuit modeling technique, while capacitance (C) is formed by gaps between each FSS component. Consider the components of an analogous circuit model in which L is derived from metallic plates and C is represented by the distance between each individual array member. The electrostatic theory is taken as a reference for controlling the output characteristics of PFSSs. As a result, the necessary filtering response may be created by combining these comparable capacitive and inductive components. Simultaneously, altering the FSS dimensional parameters changes the values of equivalent L and C .

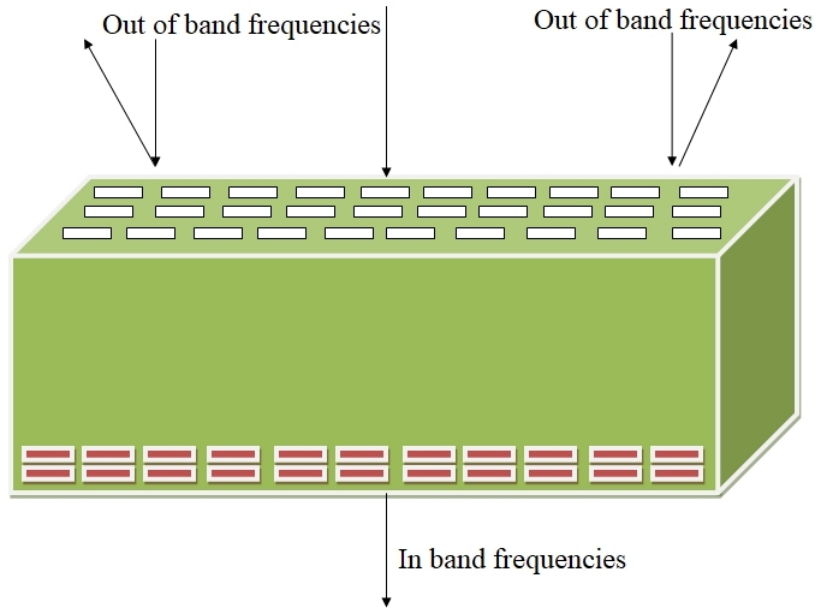


Figure 1.14: Functional description of PFSS

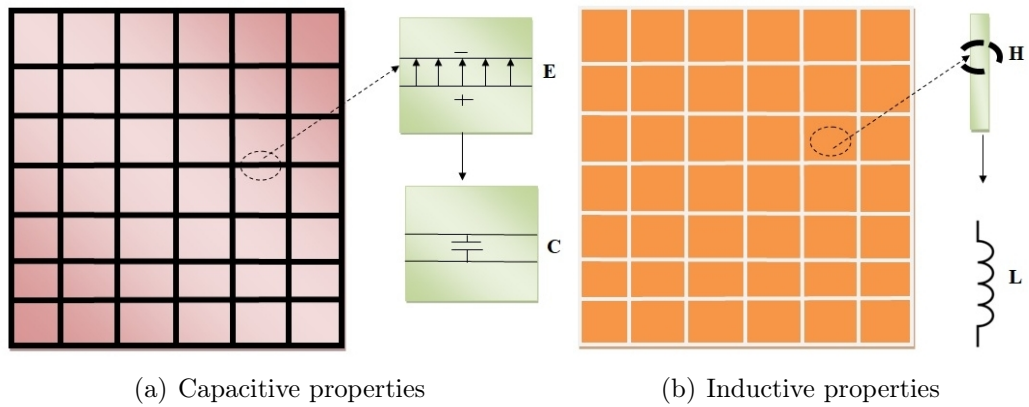


Figure 1.15: Extracted equivalent circuit parameters of the PFSS

1.8 PFSS design challenges

1.8.1 Methods for enhancing the bandwidth

When designing the PFSS, the major focus is kept on the bandwidth. The spacing between the individual elements of an array plays a vital role in getting adequate bandwidth. By decreasing the element spacing, the operating bandwidth increases [18]. An important advantage of using the PFSS is in the reduction of the overall impedance by the application of the PFSS as a ground plane. Furthermore, the impedance can be decreased by constructing the PFSS structure in such a way

that all capacitive components cancel out all inductive ones. An important factor to consider is that an array element has a lower impedance than an identical unit isolated in free space, which helps to increase bandwidth. A single element has an ability to store charge from its edge to infinity. So, when it is organized in form of an array then it exhibits the potential to store charge from its edge to roughly half the distance to its next element. A fair rule of thumb states that by making a 20% decrease in the inter-element spacing in a single direction gives a 20% increase in the bandwidth. Whereas making a 20% decrease in the inter-element spacing in both directions gives a 40% increase in the bandwidth. When the inter-element distance is shortened, the resonant frequency of components with the high end capacitance, such as closely spaced patch or loop elements, rises significantly. The resonance frequency may be adjusted to lower values if needed by increasing the size of the elements for a given element space and to higher values by reducing the size of the elements for a certainly given element spacing [7]. Another method to increase the bandwidth is by stacking two identical PFSS arrays in front of each other. The stacking of two identical PFSS arrays permits the bandwidth to retain almost perfect reflection behavior throughout a broad range of frequencies and causes the reflectivity to fall down drastically at the stop-band frequency notches.

1.8.2 Miniaturization of PFSS

The PFSS is analyzed by using an infinite number of unit cells, but a real-time applications require just a finite number of unit cells to design. Miniaturization is crucial for lowering the size of unit cells for extracting the best performance features. It also helps in overcoming the edge effects by relocating the resonant frequency of operation away from the grating lobe regions. Some of the techniques adopted for achieving miniaturization are by making the use of fractals, complicated structures, and space-filling curves.

1.8.3 Polarization independence of the PFSS

Polarization is defined in the free space as the orientation of the E-field in the direction of wave propagation. In electromagnetic waves, there are three forms of polarization: transverse electric (TE), transverse magnetic (TM), and transverse electromagnetic (TEM). The PFSS holds the versatility in finding its applications in different areas of technological innovations. The design of PFSS must be such that it depicts identical responses in both the TE and TM polarization modes. In real-time applications, PFSS can be oriented in any direction such that their response must be identical for all the modes of incident radiations. The identical response is achieved by using the symmetrical structures of the PFSS.

1.8.4 Angular stability of the PFSS

The design of PFSS for targeted applications requires angular stability which means that the proposed design of the PFSS should offer a steady response irrespective of the angle at which it strikes the surface. The stability feature is influenced by the chosen geometry of the PFSS. The concept of miniaturization is used to construct a PFSS array for ensuring angular stable response.

1.8.5 Concept of Grating lobes

The concept of grating lobes helps to predict the behavior of the PFSS. The origin of grating lobes can be understood is analyzing its concept from the field of optics. The rays emitted from the two different collinear point sources are delayed in phase by a factor given by:

$$\psi = r \sin \theta \cos \phi \tag{1.7}$$

account of phase delay which when equals to 2π radians, then the two sources will be having same phase and thus will be added together creating a grating lobe. The minimum distance will occur when the equation $\sin \theta \cos \phi=1$ exists. Also, in

other terms we can say that

$$Radiation = \frac{2\pi r_m}{\lambda} \quad (1.8)$$

which is equal to 2π when $r_m = \lambda$. However, if an element does not emit energy in the direction of a grating lobe, then the lobe will not be able to emit energy. This is simply demonstrated by assuming that an array pattern may be created by multiplying patterns, which asserts that

$$E(\theta, \phi) = E_u(\theta, \phi)E_x(\theta, \phi)E_y(\theta, \phi)E_z(\theta, \phi) \quad (1.9)$$

where E_u denotes the pattern of a unit cell of the FSS, E_x , E_y and E_z shows the patterns of a linear array composed of point sources in the x, y and z directions respectively [6]. Thus, it can be said that if the source doesn't radiate then it means no energy is emitted from an array in desired direction. For many applications, the presence of the grating lobes severely reduces an antenna's performance. This means that when an antenna is used in receivers then it will receive signals from the intended directions as well as from the directions in which the grating lobes are present.

1.9 Applications of the PFSS

PFSS has recently got a lot of attention from the academics which resulted in its expansion in plenty of the applications. Some of the potential applications include their usage as spatial filters, shielding devices, polarizer's and as security papers. The taxonomy of the PFSS is illustrated in the Figure 1.16 as shown below.

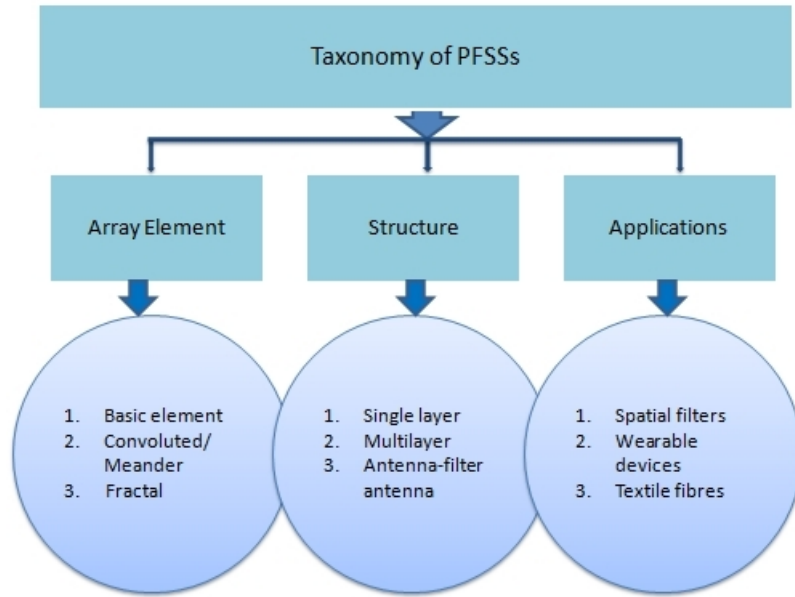


Figure 1.16: Taxonomy of the PFSS.

1.9.1 Spatial filters

In the latest research, PFSS is readily accepted to be used as spatial filters. The filtering phenomenon is exhibited by using PFSS structures which allow certain radiations to pass through while blocking all other radiations. The design of the PFSS as band stop filters finds their usage in the substrate of patch antenna design which is meant for increasing the bandwidth and in the radomes for getting the radar cross section (RCS) reduction. Also, the PFSS acts as band pass filters, thus finding their usage in placing them as superstrate above the patch antennas for augmentation of gain and directivity. Patch type structures such as dipoles find their applications in form of band stop filters while aperture type structures such as loops and rings help to create band pass responses.

1.9.2 Electromagnetic shielding

The use of electromagnetic radiations for transmitting information from one place to another has reached its peak by the innovations in wireless communication, which require electromagnetic shielding to be implemented. In the face of high EM pol-

lution, the devices should provide the necessary performance with no deterioration. This is made feasible through shielding, which offers adequate separation from the unwanted electromagnetic radiations which may harm the system. PFSS forms the best candidates for providing a solution to these ever present electromagnetic interferences by filtering out the undesired radiations.

1.9.3 Polarizer

The application of the PFSS structures to be used as a polarizer helps to transform the linearly polarized electromagnetic radiations into circularly polarized waves and vice versa. Satellite communication has become an essential component of all the technological advancements. This concept is applied in the satellite communication in which the radiations have to travel through different levels of the atmosphere. The fluctuation in the polarization of the incident field has a significant impact on the receiver's performance. An important property of circularly polarized waves is their performance which remains unaffected as they strike the receiver. So, to reduce the impact on the receivers from the variation of the polarization, these converters play a major role.

1.9.4 Security papers

PFSS finds its suitability for implementation as security papers. As in airports, bus stands, and many places of public importance, security check machines are present. Also, if any documentary proof is to be carried containing information related to national importance then it may be leaked. Hence, PFSS is placed on both sides of documents in such a way that when these documents are passed through a security gate with transmitting and receiving antennas that are capable of detecting radio frequency (RF) signals, then no detection takes place. An important point to consider is that while building a security paper, stability for angles of incidence

must be taken into consideration.

1.9.5 PFSS analytical modeling techniques

Several numerical approaches are used to compute the electromagnetic fields dispersed by the PFSS. Various researchers have used numerical approaches to study the reflection and transmission properties of various PFSS structures, and the results have been confirmed by the experimental observations. All numerical approaches, however, are based on the well-known Maxwell equations, and in general, these approaches are unable to provide accurate solutions to the electromagnetic phenomenon, and thus preferring to provide approximate answers with acceptable precision. Plenty of analytical modeling techniques have been identified by researchers consisting of Plane Wave Expansion method [19], Spectral-Domain method [20]- [21], Method-of-Moment (MoM) [22], Finite-Difference-Time-Domain (FDTD) method [23], Finite-Element Method (FEM) [24], and the most widely accepted Equivalent Circuit Modeling technique (ECM) [25]. The choice of the best approach for performing the numerical modeling of the PFSS structure is still up in the air. Several numerical algorithms available in the reported literature for the modeling of electromagnetic difficulties associated with PFSS structures are briefed. Initially, the MoM approach was applied by Chen for analyzing the scattering properties of the PFSS in the frequency domain [26]. In his approach, the current was accessed on the metallic pattern of the PFSS by matching the fields prevailing on the surface of the unit cell element and thus integral equations were formulated to extract the values of the unknown current which in turn was dependant on the values of the unknown electric fields. In the last phase of the analysis, the MoM was applied to break the set of integral equations further into a set of algebraic equations.

The analysis of the electromagnetic scattering phenomenon by using MoM can be explained using the following steps:

1. The unknown function to be extracted is expanded in terms of a set of N basis functions consisting of unknown coefficients.
2. The boundary conditions are enforced for generating a linear system of N equations.
3. The linear system of N equations is then solved for extracting unknown coefficients.

Many new modifications are extracted by various researchers in the MoM method for reducing computational complexity [27]- [33]. The prime advantage offered by this technique is in terms of exhibiting the potential for evaluating the scattering characteristics with angular stability but it certainly has a restriction of supporting only symmetrical structures on homogeneous substrates. The FDTD and FEM techniques are an excellent computational tools for investigating the complicated PFSS structures that are supported by an in-homogeneous dielectric substrate [34]. These two approaches are classified as finite techniques. In a single simulation run, the FDTD methodology explores the scattering properties of the PFSS structure in the time domain and spans over a wide frequency range. This method provides a straightforward solution to Maxwell's time-dependent equations [33]. Following steps that are offered in the FDTD method for solving scattering problems as:

1. Initially, the solution region is separated into grids of nodes by dividing it into two different sets of nodes constituting one for the calculation of the magnetic field and the other for the calculation of the electric field.
2. The mathematical formulation is then approximated by a finite difference equivalent, which relates the dependent coefficients in one part of the solution region to their values in another region. The magnetic field value at one instant is evaluated by the electric field values at previous instants.

3. Further, the set of equations are solved using defined boundary conditions [34]- [35].

In addition, as stated in [36]- [38], several other scientists have studied the numerical modeling of various PFSS structures using the FDTD. Another important technique to analyze the scattering phenomenon of the radiations emitted by the antennas is the FEM technique. It analyses scattering characteristics in the frequency domain using partial differential equation solutions based on the set of Maxwell's equations. The following are the generalized phases in this FEM-based synthesis procedure:

1. Firstly, the solution region is divided into a finite number of sub-regions, marking each corner as a node which helps to determine the field quantities.
2. The set of equations are formed for typical sub-regions.
3. After that the process of integration is performed combining all sub-regions for the entire geometry.
4. Then the entire sets of equations are solved for the entire sub-region.

Various scholars have highlighted the technological developments in the FEM, as stated in [39]- [41]. Out of all the methods described, the ECM method is a lot easier than the intense approaches. The ECM technique is based on the transmission line analogy. In this technique, the lumped parameters which were extracted from the ECM synthesis technique are determined by reporting the inductive and capacitive behavior of its geometrical features [42]- [44]. In this technique, the modeling is confined to linear polarizations and basic symmetrical PFSS geometries. However, the effect of the dielectric substrate and incidence angles have been included in the ECM equations, but the correctness is dependent on the assumptions made in the study. Using the ECM approach, many studies examined various PFSS

configurations such as square loops [45]- [46], circular loops [47], dipoles elements [48]- [50], and Jerusalem crosses [51]. The ECM technique gives the approximate analysis as compared to other numerical approaches. However, it gives a physical insight of the filtering behavior of the PFSS structures; hence it is chosen as the analytical tool for this research.

1.10 Research motivation

Sub-6 GHz 5G spectrum is entirely new, and the allocated frequency range 1 (FR1) aims to achieve both coverage and the capacity with even more advantages. There is a need to create antennas radiating in the specified frequency range to meet the demands of communication devices required in the wireless sector. The design emphasized in this study is intended for use in the 5G new radio's n77 and n78 band of the FR1 spectrum new radio (NR). Patch radiators have been an everlasting topic of research due to their capability of exhibiting properties such as compact shape, light in weight and have an ease of alignment with several other circuits and modules. The miniaturization is most revolutionary topic in microstrip patch antenna architecture which is catching an eye of sight of antenna experts. The integration of the patch antennas into the cell phone is an essential application in which miniaturization plays an important role. Further, there is a need to increase number of users utilizing same data speed at a particular instant due to which market is switching over to 5G. However, a major limitation of using the existing low profile radiators is their capacity to handle adequate amount of users with same data speed which is termed as narrow bandwidth by many researchers. Due of the inborn narrow band behavior, designing of a small wideband microstrip patch antenna is extremely difficult. Our major design applications will be in the field of broadband mobile, which will include extremely dependable and low latency services requiring large machine-based technologies. Although techniques such as partial ground plane integration

have previously been used to expand the bandwidth of rectangular PPA's, but they have failed to improve the active antenna characteristics such as gain and directivity. Hence, in addition to visualize the effects of incorporation of various defected ground geometries, the performance enhancement of the active parameters by the addition of the PFSS layer is studied. The main issue in this area of research is that for a low-profile antenna such as PPA, the design of PFSS screens should be compact, easy to fabricate, and must be commercially viable. Another consideration is determining the distance between the PFSS screens and the PPA, which must be kept in mind in order to enhance antenna gain and directivity. The PPA and the PFSS designs are to be formulated separately and then integrated together. The design constraints are faced by the PFSS layers as in this the range of the frequency bands and the dimension of the unit cell increases and is comparable to wavelength of operation. Also, the choice of the PFSS shapes is of great concern which depends on the type of filtering response needed at the output. The numerical modeling of the PFSS is performed by using the ECM technique which gives a highly correct response. It is to be noted that the numerical approaches such as MoM, FDTD, and FEM requires large computation and mathematical manipulations whereas the ECM technique requires lesser computations and computer resources with the accurate results. In the earlier approaches, researchers have explored a limited spectrum of electromagnetic radiations and a limited PFSS design operability due to availability of the limited resources. However, technological advances in computer approaches have transformed the way in which electromagnetic behavior is explored. As a result, nearly all antenna and microwave engineers analyze and design the novel PFSS systems by using the computer techniques. There are several commercial electromagnetic simulators which are available, the most of which used are CAD FEKO, CST Microwave Studio, ADS Designer, Ansys HFSS and Circuit Designer. In this thesis, the validation of the analytical behavior is achieved from the simulation results obtained from Ansys HFSS and Circuit Designer tools. The validation is also done by performing the

experimental measurements which helps to report the most realistic and trustworthy analyses of the scattering properties of the PFSS structure. Development of the PFSS structure is necessary for presenting experimental results related to scattering characteristics. Making a design prototype is a time consuming, expensive, and irreversible process. Despite these limitations, experimental measurements of the PFSS structures are critical as they provide the most realistic and trustworthy results in terms of the scattering properties. In fact the design of the stacked geometry comprising of PFSS based PPA is entirely new and not explored to an extent. So, an initiative is taken to report the results of integration of PFSS with the PPA for improving the characteristics of the PPA in the sub-6 GHz frequency range of 5G spectrum.

1.11 Research objectives

1. Design and simulation of the planar frequency selective surface and its integration with microstrip patch antenna (sub-6 GHz) to enhance the overall performance metrics.
2. Fabrication and measurement of the designed planar printed patch antenna and the PFSS elements.
3. Validation of the frequency selective surface behavior through the equivalent circuit method of the analysis.

1.12 Research contributions

The following are the outcomes and perspectives of the study described in this thesis:

1. Using an idea of the defected ground substrate, the enhancement of the bandwidth of the printed patch antennas (PPA) which are targeted for wideband

applications is visualized.

2. PFSS has been designed with two different geometries comprising square loop and circular ring shapes for providing band-pass frequency response in the sub-6 GHz frequency spectrum.
3. Analytical modeling of the designed PFSS geometries is done using equivalent circuit model technique and the results are validated from HFSS simulator and from the measurements.
4. Stacked geometry of PFSS-PPA is designed and validated by comparing results of HFSS simulator with the measurements.

1.13 Organization of the thesis

The dissertation is divided into the six chapters. The chapter-wise summary of the thesis is listed below.

- **Chapter 1:** The first chapter presents an overview of the electromagnetic radiation. The sources of these radiations, which are the antennas are being focused and classified. The microstrip patch antennas are explained in detail with their feeding techniques, applications and desired characteristics. 5G spectrum is briefed with targeted frequency ranges in form of sub-6 GHz FR1 spectrum. The advantage of choosing sub-6 GHz (1 GHz - 6 GHz) is explained in terms of coverage and capacity. After that, the frequency selective surfaces with their design problems and applications are discussed. This chapter also comprises of the motivation, research objectives, research contributions and a brief description of the thesis content. The formulation of the thesis objectives is primarily based on the current trends of the research in the field of microstrip patch antennas as discussed.

- **Chapter 2:** The second chapter provides an in-depth and comprehensive analysis of the state-of-the-art literature for microstrip patch antennas, frequency selective surfaces, and stacked geometries combining PPA and PFSS. In this chapter, different slot shapes which are engraved for making defected ground substrate to enhance the overall bandwidth of a PPA in the literature is discussed. Various PFSS designs and their applications are elaborated. The review of PFSS based antenna designs is performed chronologically. The merits and demerits of incorporating PFSS above and below the antennas are discussed in detail. Finally, research gaps were identified, which served as the foundation for our research.
- **Chapter 3:** In this chapter different designs of PFSS are proposed for sub-6 GHz 5G frequency ranges. The basic design namely double square loop PFSS is formulated. The numerical modeling for this design by using the equivalent circuit modeling approach is completed. The transmission and reflection characteristics of the unit cell of double square loop PFSS designs is also investigated in the targeted sub-6 GHz frequency ranges. At last, the simulation and the measurement results of the proposed design is depicted and validated.
- **Chapter 4:** This chapter gives a brief description of the microstrip patch antenna designs formulated to operate in the sub-6 GHz 5G frequency ranges. Various techniques are included for enhancement of the bandwidth of the microstrip patch antennas by utilizing different shapes of the patches and defected ground geometries. The design, optimization, fabrication, and measurement of the two different conventional rectangular shaped microstrip patch antennas with different defected ground plane geometries are completed. The effect of inserting the various types of slots in form of polygon shaped and a U-shaped are discussed. This chapter is concluded with the comparison of the proposed work with the existing literature.

- **Chapter 5:** This chapter presents the design, parametric optimization, fabrication, and measurement of the stacked designs composed of PPA and the PFSS geometries. The PPA's designed in the chapter 4 are combined with the PFSS designs proposed in the chapter 3. The distance between the two geometries comprising of PFSS and PPA is optimized by choosing the best suitable value at which both the gain and bandwidth attain the maximum values. The fabrication is completed in the computerized mechanical etching PCB fabricator. Vector network analyzer (VNA) is used for measuring the reflective behavior of the stacked designs and for providing the validation of the simulated results. Parametric analysis is also conducted and presented in this chapter to validate the converged design. This chapter is concluded with the comparison of the proposed work with the existing literature.
- **Chapter 6:** The achievements of this thesis are reviewed in this chapter, and the future work which can be extended in the research approach is recommended.

1.14 Summary

This chapter presents an overview of the electromagnetic radiation. The sources of these radiations, which are the antennas are being focused and classified. The microstrip patch antennas are explained in detail with their feeding techniques, applications and desired characteristics. 5G spectrum is briefed with targeted frequency ranges in form of sub-6 GHz FR1 spectrum. The advantage of choosing sub-6 GHz (1 GHz - 6 GHz) is explained in terms of coverage and capacity. After that, the frequency selective surfaces with their design problems and applications are discussed. This chapter also comprises of the motivation, research objectives, research contributions and a brief description of the thesis content. The formulation of the thesis objectives is primarily based on the current trends of the research in

field of the microstrip patch antennas as discussed.

Chapter 2

Literature Review

This thesis highlights the latest developments and presents an analysis of various designs of printed patch antennas (PPAs) and planar frequency selective surfaces (PFSSs). The list of previous works on the design of PPAs and PFSSs are summarized in this chapter. The literature review is an essential component of the study. It aids in the identification of research gaps as well as the limits of current research efforts. For both the design and implementation of the structures in stacked form, a comprehensive examination was undertaken. This chapter provides a thorough overview of various technologies and designs produced by various researchers for the PFSSs, PPAs for sub-6 GHz, and stacked geometries produced by the combination of PPA with PFSS. In the sub-6 GHz 5G frequency spectrum, recent advancements in the field of PFSSs and PPAs have also been mentioned.

2.1 Planar frequency selective surfaces

Planar frequency selective surfaces (PFSSs) are the passive structures which offer spatial filtering characteristics when exposed to electromagnetic radiations. Many researchers have worked in this area and provided some innovative designs which offer excellent characteristics. In this section, some of the state-of-art literature works related to design of PFSSs have been referred and discussed.

Bagby et al. [52] illustrated the conceptual and numerical analysis of integrated dielectric wave guiding systems. An integral equation is presented which is applied to the axially uniform waveguides. Method of the moments and quasi closed form of solution technique is used for obtaining the numerical results for the propagation characteristics of step- and the graded-index rectangular strip and rib waveguides.

Koshiba et al. [53] suggested a computational technique for dealing with scattering caused by H-plane and the E-plane waveguide connections. This analysis method combines the boundary element technique and the statistical procedure. Using quadratic components, a generic computer programme was created.

Schimert et al. [54] proposed a double periodic PFSS operating in the mid infrared region ranging from 4-12 μm . The analysis of the proposed design is completed involving the solution of an electric field integral equation. Fabrication process is completed by using photolithographic techniques. These structures are targeted for exhibition of a spectral band-stop characteristic in the transmittance.

Agahi et al. [55] investigated on the filtering characteristics of the PFSS towards electromagnetic radiation for separating the S and K bands in a communication satellite. The problems were identified and mitigated for synthesizing a dual frequency band PFSS in form of a sub-reflector over the frequency range of 2 GHz -30 GHz. The spectral-Galerkin method along with the cascading technique is utilized to identify the reflection and transmission properties of PFSS screens.

Kunz et al. [56] described the FDTD numerical modeling approach in detail. This approach helps to facilitate the computation of electromagnetic interaction for complicated issue geometries. This approach investigates the design geometries' stability, outer radiation boundary conditions, and various coordinate systems.

Lambea et al. [57] proposed a hybrid method for calculating the generalized scattering matrix of a regularly perforated metal sheet with arbitrarily shaped holes by cascading the connections of the individual cells. This technique is utilized as a building block for evaluating the multilayer PFSS with varied shapes.

Rozanov et al. [58] presented the analytical properties of the reflection coefficient of a multilayer metal backed slab. The recovered information is in the form of a dispersion connection between the entire thickness and the slab's averaged static permeability. The $1/17^{th}$ fraction of the greatest operational wavelength is recovered from a 10 dB broad band dielectric radar absorber. Bardi et al. [59] proposed the use of the finite element method (FEM) for analyzing the reflection/transmission coefficients, effective permittivity, and permeability of the periodic structures. The study of PFSSs produced from photonic band gap materials (PBGs) and composite materials with negative effective permeability and permittivity is provided.

Farahat et al. [60] proposed a novel approach for evaluating the influence of thickness on the frequency response of an PFSS using a periodic variant of the finite difference time domain (FDTD) algorithm.

Gianvittorio et al. [61] designed the PFSS by using fractal iterative techniques. The fractals were created by multiplying the several scaled copies of the initial shaped structure. The suggested design employs Minkowski and Sierpinski carpet fractals with two or three stop bands. Because of their symmetrical nature, these surfaces provide the dual polarization.

Kern et al. [62] proposed that by using a PFSS, it is possible to create a multiband artificial magnetic conducting (AMC) surfaces. The inclusion of fractal-based PFSS screens helps to utilize the AMC design approach with multiband behavior. The multiband AMC surfaces are synthesized by using a genetic algorithm.

Blackburn et al. [63] proposed a sub-domain version of the periodic method of moments for the study of rectilinear wire-type PFSSs. The convergence of the impedance matrix for an PFSS, which is aligned with the unidirectional elements, is examined, indicating the influence of individual oscillatory and decaying components.

Kiani et al. [64] proposed an active band pass PFSS over a single layer of the substrate. At the operational resonant frequency of 2.45 GHz, the design has high

angle of incidence stability. The design consists of a circular loop aperture with four PIN diodes in each unit cell. At a resonant frequency of 2.45 GHz, the device produced almost 12 dB of average variance between the two switch states.

Chiu et al. [65] proposed a miniaturized PFSS exhibiting band pass frequency response. The designed PFSS demonstrates excellent frequency stability at different polarizations and incidence angles. The size of the unit cell of the designed miniaturized PFSS is of the order of one tenth of the wavelength.

Chen et al. [66] presented a unique solution for realizing a symmetric dual-layer PFSS based radome which is integrated on a planar slotted waveguide antenna. Integration of the PFSS radome has resulted in a significant performance improvement of the slotted PPA. The presented PFSS radome exhibited good transmission characteristics in form of wide bandwidth at the resonant frequency of 9.5 GHz.

Yang et al. [67] discussed about the comprehensive and applications specific survey of electromagnetic band gap (EBG) structures. This survey provides an insight to understand EBG applications in antenna engineering.

Liu et al. [68] describes the design technique for a downsized PFSS utilizing lumped reactive components. In the metallic patches, capacitive and inductive components are used to produce current loops similar to those seen in the band-pass aperture type PFSS. Using full field predictions, the paper covers topics such as the consequences of component loss and oblique incidence.

Mudar et al. [69] provided a complete synthesis process for creating a compact, band-pass PFSS made out of non-resonant constituent components arrays of sub-wavelength periodic structures which are used in the proposed PFSSs. The intended design provides low-profile and ultra-thin structures with acute frequency selectivity and consistent frequency responses.

Campos et al. [70] investigated on a Minkowski island fractal type of PFSS. The design is oriented to provide band stop frequency response with resonant frequencies of 9 GHz and 10 GHz, respectively.

Roig et al. [71] proposed a tunable PFSS which works as a transmission array possessing the beam steering capability. The PFSS is engraved on a screen printed with thick film of barium-strontium titanate. The presented design acts as a band pass filter. The design prototype exhibits a maximum phase shift of 116° at 10 GHz, while keeping the transmission and reflection levels at constant values.

Sun et al. [72] reported a design of a broadband meta-material absorber composed of a lossy PFSS with a metallic ground plane. The design consisted of a crisscross and fractal square patches which couple with each other. The enhancement of the bandwidth is reported in the frequency range of 2 GHz-18 GHz.

Jang et al. [73] discussed about the chip-less passive wireless sensor system by using the PFSS. They reported that the electromagnetic characteristic change of PFSS is used to assess mechanical strain or structural deterioration. Nondestructive structural health monitoring (SHM) is a new area of research which is making use of the wireless sensor network.

Song et al. [74] presented a technique for the construction of label-free sensing platforms by the use of metamaterials possessing dimensions smaller than that of operating wavelength. Equivalent circuit analysis was performed using a numerical modeling approach to determine the essential sensing design criteria for creating periodic arrays made up of capacitive and inductive components.

Lazaro et al. [75] proposed an ultra-wideband (UWB) radio identification system which is based on modulating an actively controlled PFSS. An improved characteristic of the tag is achieved in form of the modulation of the backscattered time-domain response into an input ultra-wide band pulse response. Low power UWB radar is utilized as the reader in this system.

Li et al. [76] proposed a new three dimensional band pass PFSSs possessing multiple transmission zeros. A two-dimensional array of insulated microstrip lines is suggested in the proposed design. In addition, metallic plates in rectangular “T-type” constructions are placed in the air area of insulated microstrip lines. The

suggested architecture contributes to the generation of numerous transmission zeros located outside the pass band.

Cure et al. [77] presented a theoretical and practical investigation into a low-profile, 2.4 GHz dipole antenna that uses a PFSS in conjunction with varactor-tuned unit cells. The tunable unit cell is a square patch with varactor diodes implanted on either side. The observed bandwidth extends from 2.15 GHz to 2.63 GHz, with maximal broadside gains ranging from 3.7 dBi to 5 dBi.

Zhang et al. [78] suggested a unique technique for constructing an electrically beam steerable antenna system utilizing active PFSS (APFSS). With a null point of -59 dB, the suggested design has a front-to-back ratio of more than 30 dB. A maximum gain of 7.0 dBi is obtained. Pan et al. [79] proposed a new filtering antenna consisting of active PFSS aimed at displaying filtering and beam steering features. A metallic rectangular ring and a patch make up the PFSS unit cell. The design is set up in such a manner that the transmission phase of the emitted wave may be adjusted by varying the bias voltage provided to the varactor diodes. The described horn antenna with active FSS can provide beam steering in both the E- and H-planes with a range of 30° at a resonance frequency of 5.3 GHz and a bandwidth of 180 MHz.

Jazi et al. [80] suggested an electronically sweeping radiating antenna for 2.45 GHz operation utilizing a novel active cylindrical PFSS (ACPFSS). The antenna radiation properties are controlled using a novel reconfigurable hybrid unit cell, which is used in the construction.

Agarwal et al. [81] investigated upon the reflection coefficient phase for four distinct artificial magnetic conductors with conventional PFSS type two-dimensional periodic configurations. These structures are used as back reflectors for aperture antennas. They also aid in converting the bidirectional circularly polarized radiation of the octagonal-shaped aperture antenna to a unidirectional one.

Moharamzadeh et al. [82] A modified microstrip triangular slotted antenna in-

tegrated with a novel triple-band PFSS for X-band operation was suggested. The PFSS is made up of three conductor-based split-ring resonators linked together. The topic finishes with the periodicity's influence on the finite PFSS. The impact of changing the distances between the antenna and the PFSS surfaces has been thoroughly investigated.

Seager et al. [83] presented fabric-based PFSS structures. The suggested PFSSs are created by the use of a screen printing and weaving process. In addition, the screening approach is examined by employing a collection of fabric hangings and wall coverings from the fabric-based PFSS.

Natarajan et al. [84] suggested a PFSS based stable band stop filter with unit cell dimensions on the order of $66mm^2$. The suggested design is intended to block 5 GHz WLAN band transmissions while also acting as a shield for the open area. It responds symmetrically in both the azimuth and elevation axes of polarization.

Genovesi et al. [85] explored the decrease of the radar cross section (RCS) of array antennas. In this research, a microstrip slot array is used to demonstrate the radar cross section reduction technique. The study discovered that using an array of periodic resistive components results in a significant decrease of the radar cross section throughout a frequency band. The usage of metallic parasitic components is expanded for the purpose of increasing antenna gain.

Smith et al. [86] suggested a shared aperture antenna for simultaneous L-band and Ka-band operation. The presented antenna is a stacked construction made up of a Ka-band reflect-array antenna and an FSS-based ground-plane. The proposed reflect-array has maximum directivity of 36.4 dBi at 20.0 GHz and 38.5 dBi at 29.8 GHz, respectively.

Rashid et al. [87] investigated on the classification of the three dimensional PFSS which exhibit superior filtering responses as compared to the conventional two dimensional PFSS. Basically, a three dimensional PFSS is composed of a periodic array of multimode cavities arranged in a two dimensional structure coupled with

the air. These structures exhibit a high performance filtering response. Lopez et al. [88] presented a circular polarizer constructed with a multilayer PFSS. The design structure utilizes a group of split rings which are bisected by a metal strip. The added advantage which is exhibited by this geometry is in the form of low cross-polarizations value and low sensibility with respect to the incidence angle. Axial ratio of lower than 3 dB is obtained for the variation of the incident angles over the frequency range of 25.5 GHz-36.5 GHz.

Abdelrahman et al. [89] proposed a new design of transmit array antennas by encircling them with multilayer PFSS type of elements. It is identified that the transmission phase limits lies at 54° , 170° , 308° , and 360° for a single, double, triple, and four-layer PFSS. Also, it is identified that if 3-dB criteria is being used, then a triple-layer PFSS exhibits a full 360° phase range.

Abadi et al. [90] introduced a new technique for designing miniaturized band-pass PFSS. Several metallic and dielectric layers make up the suggested design. Two-dimensional capacitive patches or inductive grids make up each metallic layer. The design's dimensions are on the wavelength scale. The design has a second-order band pass response and is aimed at operating at 3.0 GHz with a fractional bandwidth of 20%.

Abadi et al. [91] presented the design of a broadband and compact multi-beam antenna. The suggested system makes use of numerous feed components located at the focal plane of a microwave lens. A novel modeling approach is provided that considerably simplifies the design's full-wave electromagnetic analysis. The approach was used to create a prototype multi-beam antenna that operates in the 8 GHz to 10 GHz frequency range. The retrieved data indicate similar radiation characteristics over the full operational spectrum, with several beams visible near 45° .

Shi et al. [92] designed a miniaturized 2.5D PFSS in form of a closed loop. The proposed PFSS is a compact shape with dimensions as $0.048\lambda \times 0.048\lambda$. The proposed design offers the angular and the polarization stability.

Yu et al. [93] proposed a new ultra-miniaturized 2.5D element of PFSS. The suggested element is made up of two major parts: a planar tapered meandering line and a vertical via-based meandering line. At diverse polarisation's and incidence angles, the suggested element has a good resonant stability.

Li et al. [94] presented a miniaturized band pass PFSS based on a stepped-impedance resonator (SIR) structure for suppressing unwanted radiations. A dual layer periodic array of etched metallic rods and plates is used to construct the suggested PFSS. The suggested design may provide a band-pass response with two transmission poles and has a very large stop-band.

Abdelrehman et al. [95] gave a comprehensive design study of a multiple conductor layers transmit array antenna with a slot type element and no dielectric substrate. A transmit array antenna with quad-layer cross slot components is included in the suggested design. The intended prototype has a gain of 23.76 dB at the resonance frequency of 11.3 GHz.

Li et al. [96] proposed a polarization reconfigurable converter which is composed of multilayer PFSS. The square patches and grid lines are placed in an array as the first design phase. In the second stage, the corners of the square patches are shortened, resulting in a 90° phase difference between the two orthogonal linear components for circular polarization. The suggested design has a fractional bandwidth of more than 15% when compared to the operating frequency of 10 GHz at a normal angle of incidence.

Xu et al. [97] proposed a compact second order miniaturized PFSS which is composed of a metallic mesh and its complementary structure. The arrays of modified triples distort the composite structure. The proposed PFSS has an overall thickness of $\lambda/18$ and is made up of three metallic layers sandwiched between two electrically thin dielectric substrates. The suggested design achieves a -3 dB bandwidth of around 8.2 GHz with a frequency range of 6.9 GHz to 15.1 GHz and a fractional bandwidth of roughly 75%. The design provides steady performance at incidence

angles ranging from 50° to 60° .

Mahgoub et al. [98] investigated on the PFSS structures targeted for the applications in the area of ultra-high frequency (UHF) radio frequency identification (RFID). The initial structure is a square patch PFSS exhibiting a total reflection characteristics for the entire UHF RFID region ranging from 840 MHz - 960 MHz, whereas the second structure is square slot PFSS exhibiting a total transmission band for the UHF RFID region. The proposed structure finds its applications in different electromagnetic interference / compatibility (EMI / EMC) applications.

Wang et al. [99] suggested a two-dimensional leaky wave antenna based on graphene (LWA). It employs a graphene sheet as a tuning component of the ground plane's high-impedance surface (HIS). It is investigated if the reflection phase of the HIS may be changed by varying the graphene conductivity.

Jia et al. [100] demonstrated a high gain, wideband mushroom antenna with a low radar cross section over a wide range of frequencies. At the operational frequency, the mushroom structure shows resonant activity, which aids in the reduction of radar cross section. It employs the band-stop PFSS to replace the antenna's metallic ground while maintaining high gain.

Kapoor et al. [101] introduced a new method of creating spatial filters based on PFSS, which are widely utilized in a variety of microwave and optical systems. The electromagnetic wave transmission and reflection behavior of the complicated thick/thin metallic PFSS is examined.

Hashemi et al. [102] proposed the usage of the PFSSs for shielding rooms against the incident electromagnetic radiations. This helped in achieving secure indoor communications and reduced the human exposure to the external fields. Double layer PFSSs are used for designing the secure room using s FR4 substrate targeted to cover 10 GHz - 12 GHz frequency band. Bio-tissue is utilized inside the PFSS walls which results in the specific absorption rate.

Yao et al. [103] presented a design of the three PFSSs for analyzing electrical

behavior. A novel PFSS is proposed with the phase compensation structure which consists of a short-ended circular waveguide array. The PFSS designs are targeted to work on the 119 GHz and 183 GHz reflection bands simultaneously.

Milici et al. [104] presented a feasibility analysis of utilizing modulated PFSS as a semi-passive tag for body sensing applications in the open license 2.45 GHz ISM band. The authors demonstrated two prototypes consisting of a breathing sensor and a skin thermometer. The breathing sensor detects changes in airflow temperature caused by respiration. The NTC resistor is also utilized for the breathing sensor, which is placed directly into the skin. It detects temperature made up of dual layered metallic patterns. The bottom PFSS layer filters out-of-band signals from in-band signals, while the top layer of EBG cells reduces backward scattering radiations. The suggested construction allows the antenna signal to be broadcast in the S-band with minimal insertion losses while also providing a wideband low-scattering response in the X and Ku bands. It is used in the radome applications.

Hussain et al. [105] investigates the feasibility of utilizing vias for the downsizing of PFSSs. The study provided a novel method for knitting loop-type PFSS components. The proposed miniaturized PFSS has a consistent frequency response for a wide range of incidence angles and polarizations.

Sarika et al. [106] investigated a new design of a PFSS reflector possessing a wideband response for 4G, X-band and Ku-band of microwave spectrum. The PFSS reflector comprises of a cascaded double layer patch type PFSS formulated on the separate layers of FR4 substrate. The proposed design is targeted for a frequency range of 5-16 GHz. A numerical analysis is also performed for the designed unit cell using an equivalent circuit (EC) modeling.

Huang et al. [107] proposed a method for achieving a high-efficiency transmission and wideband scattering reduction. It makes use of integration of a PFSS and an electromagnetic band-gap (EBG) surface which is composed of dual layered metallic patterns. The bottom PFSS layer helps in filtering out out-of-band signal

from the in band signal, while the top layer is of *EBG* cells helps in reducing the backward scattering radiations. The proposed structure makes the antenna signal to be transmitted in the S-band with small insertion losses and it simultaneously provides a wideband low-scattering response at X and Ku band. It finds its usage in the radome applications.

Hui et al. [108] suggested a tiny, low-cost; double-layer PFSS-based band-pass filter for terahertz operation. The PFSS structure seen here is made of double-layer tin foil with a hexagonal lattice array of round holes. The proposed structure has a flat pass-band with a 3-dB bandwidth extending from 0.81 to 1.01 THz.

Anwar et al. [109] gave an introduction of the fundamental ideas, kinds, methods, and experimental investigations of today's cutting-edge PFSSs. PFSSs have been thoroughly researched, and there has been a tremendous increase in the field of their design and application. The authors showed new research on the various types of PFSSs based on structural design, array element utilized, and applications. The emphasis is on key performance metrics with a focus on developments in the field of PFSS.

Elzwawi et al. [110] suggested a switched-beamforming antenna built with active PFSS. The suggested antenna design comprised of two parts namely a source with an omnidirectional radiation pattern and an active triangular PFSS (ATPFSS) that surrounded the source. Each unit cell of the ATPFSS structure is made up of two diamond-shaped patches that are linked together by a high frequency pin-diode. The findings are obtained in terms of beam directions, reflection coefficient, and gain at a resonant frequency of 5.8 GHz.

Zhao et al. [111] presented a 2.5-dimensional Jerusalem cross structure-based compact PFSS for 5G applications. The suggested element is made up of two major parts: consecutive segments of metal traces alternatively arranged on the two sides of the substrate and vertical vias linking traces. The suggested design's transmission curves show a considerable size reduction as well as good angular and polarization

stability.

Anwar et al. [112] revealed a novel method for broadening the bandwidth of a multilayer antenna-filter antenna-based PFSS. The suggested fractal PFSS with centre square slots is composed of three metallic layers separated by two dielectric substrates. The design includes centre square holes in the exterior Minkowski fractal patches to boost the capacitive effect. At a normal angle of incidence, the design displays a steady response with 3 dB fractional bandwidth reaching 87.4% and 92%, respectively.

Kanth et al. [113] proposed a band-pass PFSS which are based on substrate integrated waveguide technology has been suggested. The concept was submitted with the intention of being used in airborne radome applications. The PFSS element's unit cell is made up of two tapering cross-slots on either side of the substrate. The element is encased in metal vias. Within the working band, the structure has the capacity to enable the desired electromagnetic radiations to flow through it. The design is stable in terms of angle of incidence and has strong roll-off performance characteristics at the working band's boundaries. With a frequency range of 9.5 GHz to 10.8 GHz, the -10 dB relative bandwidth (BW) is 12.8%.

Peralvo et al. [114] presented an inductive PFSS based dichroic sub-reflector. In the Ku, K, and Ka bands of the microwave spectrum, it operates in such a way that it permits transmission of two frequency bands while reflecting in the third. The design was created with earth-to-space and earth-to-earth satellite communications in mind. A Jerusalem cross and a Brigid's cross are incorporated into the proposed design.

Sahai et al. [115] suggested an I-shaped PFSS structure with negative permittivity and permeability in the microwave C and S bands. Because the I-shaped PFSS structure is contained within a set of two rectangular split ring resonators, it shows negative properties. The rectangular split ring exhibits inductive characteristics, whereas the capacitor exhibits capacitive properties. The response of the unit cell's

I-shaped PFSS structure exhibits pass band and stop band behavior in the X and Ku bands.

Kapoor et al. [116] presented a study on numerous slots based PFSSs comprising of a rectangular, circular, hexagonal and elliptical geometries possessing angular stability. The proposed PFSS designs are targeted to provide spatial filtering in the n77, n78 and n79 sub-6GHz 5G spectrum bands. A wide rejection bandwidth ranging from 3.30 GHz to 5.00 GHz is achieved by using simple geometries.

Li et al. [117] proposed dual-layer PFSS geometry with an extended cross-dipole structure. The PFSS is a tiny device that has a band-stop frequency response of 1.6 GHz. The suggested PFSS has a footprint of 5 mm x 5 mm. The design is symmetrical in rotation and has high polarization stability. The suggested PFSS architecture provides up to 60 degrees of angular stability. The suggested design's prototype has a shielding efficacy of more than 26 dB.

Alvarez et al. [118] designed a spherical dome PFSS with the goal of improving angular stable band-pass filtering performance in the near-field area of an antenna source. This article offered a comparison of the conformal PFSS and a finite planar PFSS at frequencies ranging from 26 GHz to 40 GHz in order to demonstrate the benefits of using the conformal PFSS in the near-field.

2.2 Outcomes from the discussions

It is seen that the equivalent circuit model analysis for band pass filters is not studied to an extent and is only applied to basic single square loop and single circular loop in the available literature. Also, in the sub-6 GHz frequency range, the dimensions of the unit element of PFSS are comparatively larger which makes it difficult for formation of large dimensional array. Further, the angular sensitivity and polarization stability of the proposed structures are not fully explored.

2.3 Printed microstrip patch antennas for compact wideband applications

The advantages of the printed microstrip patch antennas (PPAs) are in the form of their simplicity of the design and superior reflection and radiation performance. In this section, the state-of-art literature on PPA is discussed which highlight the designing techniques for wideband applications.

Tang et al. [119] proposed new antenna designs for the three Chinese operators' operational frequency bands encompassing the three 5G bands, comprising 2.515 GHz - 2.675 GHz, 3.4 GHz - 3.6 GHz, and 4.8 GHz - 4.9 GHz. The design was created by altering the ground plane's structure. The recovered reflection coefficient has a frequency range of 2.32 GHz to 5.24 GHz, which is suitable for Wi-Fi, Bluetooth, and WLAN applications. The suggested design's highest gains in the three bands are 2.52 dBi, 3.04 dBi, and 4.31 dBi at resonance frequencies of 2.55 GHz, 3.5 GHz, and 4.75 GHz, respectively. Meneses et al. [120] proposed a wide bandwidth slotted PPA operating in the range from 3.1 GHz - 4.2 GHz targeted for 5G applications. The proposed design will cater Internet of Things (IoT) applications.

Huang et al. [121] suggested a small hybrid-mode antenna for use in communications below 6 GHz. The slotted rectangular patch, a feeding dipole, and a balun are all part of the proposed design. The suggested device has a 56.87° impedance bandwidth, spanning from 2.97 GHz to 5.33 GHz, with an average gain of around 8.00 dBi. The suggested architecture has applications in sub-6 GHz communication for micro-base stations.

Yerlikaya et al. [122] suggested a design of a broadband patch antenna targeted for sub-6 GHz 5G mobile systems. With an overall dimension of $10.7 \times 22.5 \text{ mm}^2$, the proposed 5G antenna is small in size. The pattern is made up of a log-periodic patch in the shape of an equilateral triangle and a rectangular shape in the shape of a ground plane. The planned 5G antenna operates at frequencies ranging from 3.4

GHz to 4.2 GHz. With all of the radiation and physical qualities as demonstrated, the proposed log-periodic patch antenna finds its applications in the sub-6 GHz 5G frequency ranges.

Gopal et al. [123] explored a cross dipole antenna for base station applications. The suggested antenna is made up of a basic dipole and a modified balun construction. The suggested architecture is useful for 4G and sub-6 GHz 5G base station applications. In the frequency range of 1.341 GHz to 3.834 GHz, the suggested antenna design achieves a maximum gain of 13.8 dBi. It has a consistent radiation pattern and gain over the frequency range.

Khalifa et al. [124] researched innovative ideas for supplying high bandwidth and data speeds to a big number of customers. A novel antenna design is being researched that is based on the different forms and dimensions of the monopole antenna. The working bandwidth is divided into two bands, 1.24 GHz - 2.64 GHz and 3.34 GHz - 5 GHz, with gain and efficiency of 5 dBi and 80%, respectively.

Melchiorre et al. [125] suggested the study and optimization of a bio-inspired spiral shell dielectric resonator antenna constructed using Gielis' super formula, with the objective of increasing antenna bandwidth. The suggested device has an operating range of about 2 GHz, with an acceptable gain of approximately 5 dBi at 5 GHz.

Saurabh et al. [126] explored a small two-element multiple input multiple output (MIMO) antenna for potential sub-6 GHz 5G applications were explored. The two identical rhombus-shaped radiating components are arranged in the same orientation on a common rectangular ground in the suggested design. For better impedance bandwidth and isolation, the design employs a T-shaped ground stub between a pair of radiating components. The design runs in the 3.34 GHz to 3.87 GHz frequency range, with a bandwidth of 530 MHz.

Zaidi et al. [127] studied a wide-band and tri-band flexible antenna for the fifth-generation (5G) sub-6-GHz communication systems. The tri-band antenna resonates

in three different allotted frequency bands in the sub-6 GHz 5G spectrum at 2.45 GHz, 3.5 GHz, and 4.7 GHz, whereas the wideband antenna radiates between 2.8 GHz and 5.35 GHz. For the intended output response, hexagonal split-ring resonators have been included.

Jha et al. [128] proposed a partial ground architecture antenna design for sub-6 GHz applications. The antenna has a small footprint, measuring 40 x 30 x 1.6mm³. Radiation in the frequency range of 3 GHz to 5.64 GHz is produced by the suggested design. The suggested design's average gain increases from 1.73 dB to 3.22 dB, and the radiation efficiency reaches a maximum of 90 °.

Azim et al. [129] proposed a low-profile multi-slotted PPA for long-term evolution (LTE) and fifth-generation (5G) communications. A stepped patch with a ground plane is the proposed design. The slots are etched within the patch to obtain the necessary characteristics, and it contributes to a working band extending from 3.15 GHz to 5.55 GHz, which covers the full n77/n78/n79 bands of the sub-6 GHz 5G wireless range.

Mishra et al. [130] presented a multi-band resonant small antenna for operating in the sub-6-GHz frequency range. The authors demonstrated a small microstrip inverted slotted antenna. Split ring resonators are used to boost the performance of a single-layer slotted antenna. The suggested design has good reflections and radiation characteristics at 3 GHz and 4 GHz. The given design has a 200 MHz impedance bandwidth and a peak gain of 4 dBi. The antenna is suitable for future 5G applications in the LTE and sub-6-GHz bands.

Aathmanesan et al. [131] suggested the design of a slotted hexagonal patch antenna for 5G wireless applications operating from 3.5 GHz to sub-6 GHz. The suggested antenna is made up of a slotted radiator placed in a modified ground plane measuring 25 x 20mm². The antenna's bandwidth is 130 MHz, with a gain of 3.93 dBi and an efficiency of around 96.65 percent. This design is used in sub-6 GHz 5G wireless applications with a resonance frequency of 3.5 GHz.

Hakanoglu et al. [132] provided a thorough examination of a stub loaded rectangular patch antenna. The suggested concept runs in 5G sub-6 GHz frequencies and Wi-Fi 5.8 GHz bands. The concept achieves a significant size reduction from roughly $0.322mm^2$ to $0.162mm^2$, implying a reduction of over 50% for each antenna with improved radiation characteristics.

Ishteyaq et al. [133] proposed a MIMO antenna design for mutual coupling minimization approaches. The suggested design addresses virtually all elements of 5G, including antenna design types and performance metrics linked to MIMO design. The authors underlined the frequencies designated for 5G, which include sub-6 GHz and mm-wave bands.

Zada et al. [134] offers a small dual-function antenna for 5G mobile applications that operates at 3.5 GHz and in the mm-wave spectrum. A microstrip patch is connected to a meandering radiating structure with the use of a radio frequency PIN diode in the proposed antenna. The PIN diode is used to assist facilitate frequency reconfigurability between the two operational bands. With a broad decoupling of 7.4% and 4.8% at the low and high frequency bands, respectively, the suggested antenna system demonstrated adequate MIMO capabilities. The suggested antenna technology will be used in 5G mobile portable devices in the future.

2.4 Outcomes from the discussions

It is seen that many designs are proposed with modified structures of the radiating apertures and the ground plane which increases the design complexity. The mechanism to remove the electromagnetic interference in the sub-6 GHz frequency range requires further exploration as much of the band is congested with 4G LTE and free ISM bands. Also the variation of gain and directivity requires further development.

2.5 Developments of the PFSSs based PPA stacked geometries

Planar frequency selective surfaces (PFSSs) are finding their usage in the manufacturing of spatial filters. These surfaces are being utilized along with the PPA designs for improving the output characteristics of the PPAs. The stacked geometry (PFSS-PPA) so designed must be compact and of low cost. The placement of PFSS can be in form of substrate or superstrate depending upon the characteristics required to be exhibited. Some of the works related to the development of the stacked designs are presented in this section.

Chaimool et al. [135] presented a design by using a reflective metasurface (RMS) as a superstrate to boost the gain and bandwidth. For the RMS, two alternative structures are proposed: the double split-ring resonator (DSR) and the double closed-ring resonator (DCR). The proposed antenna achieves a high gain of over 9.0 dBi with a wide impedance bandwidth of over 13% utilizing the RMS as a superstrate.

Sharma et al. [136] developed a circularly polarized slotted PPA with a large gain and low radar cross-section (RCS). We utilized a meta-surface that is made up of a 6x6 array of corner-truncated square patches that are layered on top of the higher substrate. In the frequency range of 4.29 GHz to 5.75 GHz, the suggested antenna has an impedance bandwidth of around 29.08 % . In the broadside direction, a gain of 9.9 dBi is attained. In the frequency range of 4 GHz to 13 GHz, this design aids in RCS reduction.

Cure et al. [137] presented a flexible low profile dipole antenna with the use of a FSS added with the inter-digital barium strontium titanate (BST) varactor-tuned unit cells. The proposed design demonstrates the capacity of tunability ranging from 2.42 GHz to 2.66 GHz.

Rana et al. [138] presented a PFSS to be used as a superstrate for a dual-polarized

dielectric resonator antenna (DRA). With a gain of 3.4 dBi, the planned PFSS is positioned half a wavelength above the ground plane. With a maximum gain of 8.9 dBi, the suggested design has a 5.1% impedance bandwidth that covers the full frequency range from 6.4 GHz to 6.74 GHz.

Rabbani et al. [139] showed two PFSSs, each with 12 patch components can boost the gain of an extended size PPA up to 18.5 dBi in the X-band (8-12 GHz).

Imran et al. [140] created a compact cylindrical antenna for the microwave radiology imaging applications. The folded PFSS meta-material structures are layered on a cylindrical profile in this concept. The suggested design's measurements are 32 mm in height and 20 mm in diameter. The frequency range covered by the given design is 7.8 GHz to 15 GHz.

Gunes et al. [141] presented a PPA which utilizes a modified cross shaped PFSS. The performance enhancement is visualized in the ISM band at around 2.45 GHz.

Singh et al. [142] proposed a rectangular PPA operating at 2.45 GHz in the ISM band for wireless communication. The proposed design consists of defected ground plane which helps to achieve a miniaturization of 37.9% along with enhancing the radiation performance.

Shukla et al. [143] proposed a high gain rectangular PPA. The design exhibits a gain of 9.5 dB at a resonant frequency of 9.5 GHz. The gain enhancement is achieved by backing the antenna with the PFSS of 5x5 array constituted with square loops.

Hussein et al. [144] suggested a design for operating at 60 GHz that consists of a rectangular PPA and a PFSS. In order to create the PFSS layer, the basic square loop unit cell is used. Gain, return loss, and bandwidth are among the output parameters that have been improved by the design.

Nassr et al. [145] demonstrated an PFSS-integrated wideband planar antenna. The PFSS array screen is studied by constructing a unit cell of the PFSS using a simple square ring. For a steady frequency response, the antenna is positioned in parallel above the PFSS at a distance of 28 mm. The suggested design improves

directivity and gain by roughly 6.5 dB and 5.1 dB, respectively along the broadside direction.

Raj et al. [146] discussed about the radiation characteristics of the PPA stacked with the PFSS based absorbing layer. It is reported that the radiation characteristics of the PPA are controlled by placing an absorbing layer in between the PPA and the ground plane. The formulation of the stacked geometry helps to reduce the back lobe radiations.

Kumar et al. [147] presented a new approach for increasing the gain of a PPA. The design uses a slot antenna with a modified circular loop PFSS, and it works in the sub-6 GHz 5G band. The suggested design's operational bandwidth, which is loaded with polarization insensitive single-layer PFSS, ranges from 3.6 to 6.1 GHz, with a realized gain of 7.87 dB.

2.6 Outcomes from the discussions

In the available state-of-art literature, no work on the polarization and angular stability has been reported. Recently, this topic of the PFSS based PPA structures has been actively taken by researchers but still implementation in the sub-6 GHz 5G range is not yet reported.

2.7 Summary

This provides an in-depth and comprehensive analysis of the state-of-the-art literature for microstrip patch antennas, frequency selective surfaces, and stacked geometries combining PPA and PFSS. In this chapter, different slot shapes which are engraved for making defected ground substrate to enhance the overall bandwidth of a PPA in the literature is discussed. Various PFSS designs and their applications are elaborated. The review of PFSS based antenna designs is performed chronologi-

cally. The merits and demerits of incorporating PFSS above and below the antennas are discussed in detail. Finally, research gaps were identified, which served as the foundation for our research.

Chapter 3

Planar Frequency Selective Surface

Design for Sub-6 GHz 5G

Applications

Planar frequency selective surfaces (PFSS) can function as band pass or band stop filters for incoming electromagnetic waves, and these characteristics of the PFSS aid in enhancing the performance of the printed antennas. Today, these advancements in PFSS have created new entry points for a wide range of applications. A handful of difficulties must be overcome to fully comprehend the capabilities of PFSS. In the past, much of the research work has been focused on the designing portion, with relatively little effort have been put into analyzing the performance characteristics. This chapter develops a mathematical framework for modeling the resonance characteristics of a PFSS while focusing on electromagnetic factors.

3.1 Introduction

Spatial filters helps to protect a transreceivers from the interferences which are caused by undesired signals emitted by adjacent electronic equipment. When used

with an antenna, these filters provide acceptable performance by implementing a frequency selective function. Furthermore, these aid in the suppression of undesired radiations on the antenna aperture. The inclusion of the PFSS with the antennas allows for the implementation of spatial filtering features. PFSSs have been the focus of extensive investigation in recent years due to their ability to impart filtering characteristics in the spatial domain. The PFSS is made up of the metallic components organized in the form of geometry and put in the shape of apertures on a dielectric substrate. These surfaces comprise with regular periodic patterns and they exhibit the filtering behavior. Their application may be observed in the electromagnetic spectrum while processing or blocking radio waves. Electromagnetic interference (EMI) created by the wireless devices poses a significant threat to the performance of a wireless system. The PFSS geometries are created by assembling the metallic structures periodically. Many geometrical forms that might be utilized in the electromagnetic spectrum have been collected and proposed by the researchers, including a square loop, a circular ring aperture, an elliptical shape, a hexagonal structure, and a cross dipole element [148]. These surfaces have a benefit over other techniques in that they may be integrated into a wireless system, providing strong isolation from interfering signals due to their low profile and lightweight. Another advantage of PFSS is its ease of manufacture. There are several PFSS structures available. When compared to all other PFSS geometries, the square-shaped loop and circular-shaped ring have the added benefit of being less sensitive to changes in angle of incidence, making them popular. When constructing PFSS structures, the consequences of polarization change and angular stability must be addressed. The parametric dimensions of the periodic unit cells, as well as the range at which unit cells are replicated to produce an array, are both common features of the PFSS architecture. In this chapter, the PFSS is used to create the spatial filters for the sub-6 GHz 5G frequency range, and a mathematical study is also presented to provide an insight into the electromagnetic behavior.

3.2 Double square loop PFSS structure

The double square loop planar frequency selective surface (DSLPFSS) is appealing for the creation of spatial filters due to its simple design, large operating bandwidth, and virtually omnidirectional radiation coverage. This section describes the DSLPFSS setup. The DSLPFSS structure is analyzed and synthesized by using the equivalent circuit model (ECM) method. The geometrical parameters for the proposed DSLPFSS-based spatial filter are shown. The design exhibits a strong band pass behavior, allowing it to be used as spatial filters in the sub-6 GHz range. It should be noted that the unit-cell part of the planar spatial filters must be checked for functioning in accordance with Floquet's theorem. On the basis of the Floquet theorem, the field characteristics show an identical behavior for the PFSS array and that of the single element comprising a unit cell [149]. The dimensions of the PFSS structure are used to calculate the lumped circuit components such as inductance and capacitance during the equivalent circuit construction. These components are the side length of the loop (l), the periodicity (pe), the effective width of the conducting loop (w), an angle of incidence (for TE and TM), the wavelength exhibited by the incident ray (λ), and an overall distance between the two loop structures (g). Figure 3.1 depicts a diagrammatic representation of the DSLPFSS. It comprises of a patch constructed of a copper sheet with a thickness of 0.02 mm. The patch is then put on a dielectric with a height (h) of 1.6 mm and a relative permittivity of 4.4. Figure 3.2 illustrates the DSLPFSS operating as spatial filters in open space . However, it is desirable to define the size as well as the effective periodicity of the square loop structure in the design of a DSLPFSS in order to establish resonance at the necessary frequencies operable at a particular planned bandwidth. A successful synthesis strategy has been published in the literature, which served as the foundation for our precise numerical synthesis utilizing an analogous circuit model approach [150]- [151]. Furthermore, the values of the equivalent circuit elements gen-

erated from the numerical modeling are affected by the periodicity (p_e), the effective width of the square loop (w), a net incidence angle (θ, ϕ), and the effective mode of incidence, which might be either transverse electric (TE) or transverse magnetic (TM).

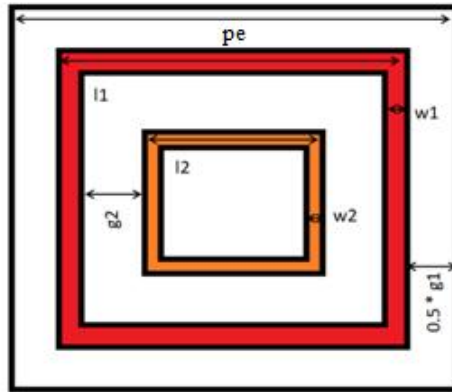


Figure 3.1: Geometry of DSLPFSS unit cell

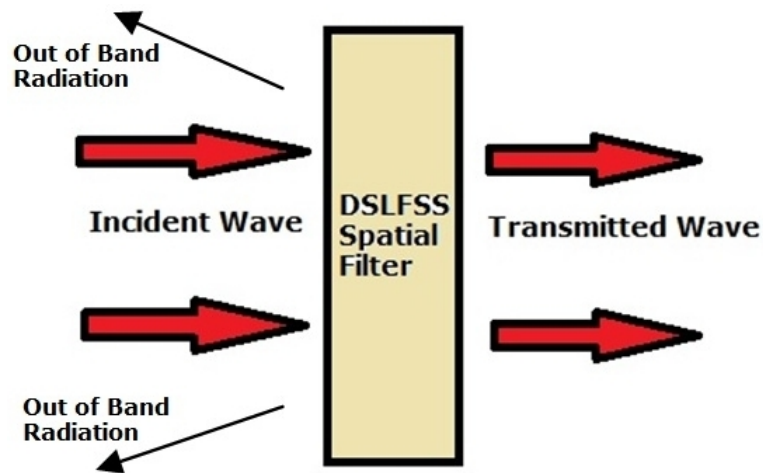


Figure 3.2: DSLPFSS as a spatial filter

3.3 DSLPFSS analysis

When the plane polarized wave in a transverse electric (TE) mode is impacted on the PFSS structure, the equivalent circuit components for each individual square loop structure may be recovered by using following equations:

$$\frac{\omega_r L}{Z_o} = \frac{l}{p_e} \cos(\theta) \times F(p_e, w, \lambda, \theta) \quad (3.1)$$

$$F(p_e, w, \lambda, \theta) = \frac{p_e}{\lambda} \left[\ln \csc \left(\frac{\pi w}{2p_e} \right) \right] + G(p_e, w, \lambda, \theta) \quad (3.2)$$

$$\frac{\omega_r C}{Y_o} = 4 \frac{l}{p_e} \sec(\theta) \times F(p_e, g, \lambda, \theta) * \epsilon_{eff} \quad (3.3)$$

$$F(p_e, g, \lambda, \theta) = \frac{p_e}{\lambda} \left[\ln \csc \left(\frac{\pi g}{2p_e} \right) \right] + G(p_e, g, \lambda, \theta) \quad (3.4)$$

In the above mentioned equations, the terms $\epsilon_{eff}, Z_o, Y_o, G(p_e, w, \lambda, \theta)$ and $G(p_e, g, \lambda, \theta)$ signifies for the effective value of the dielectric permittivity, characteristic impedance, characteristic admittance and for the correction terms of the values of the inductance and capacitance associated with the designed PFSS surface. The flaws in the PFSS analysis were found using the aforementioned equations, and it was recommended to take normalized wave reactance into consideration [152]. Some generalized formulations were provided for the adjustment terms indicated in the equations (3.1) to (3.4). The first order correction term $G(\cdot)$ is calculated as follows:

$$G(p_e, w, \lambda, \theta) \text{ or } G(p_e, g, \lambda, \theta) = \frac{A}{B} \quad (3.5)$$

where

$$A = 0.5 (1 - \beta^2)^2 \left[\left(1 - \frac{\beta^2}{4} \right) (C_+ + C_-) + 4\beta^2 C_+ C_- \right] \quad (3.6)$$

$$B = \left(1 - \frac{\beta^2}{4} \right) + \beta^2 \left(1 + \frac{\beta^2}{2} - \frac{\beta^4}{8} \right) (C_+ + C_-) + 2\beta^6 C_+ C_- \quad (3.7)$$

$$\beta = \sin \frac{\pi w}{2p_e} \quad (3.8)$$

$$C_n = \frac{1}{tS_n} - \frac{1}{mod_n} \quad (3.9)$$

where $n = \pm 1, \pm 2, \dots$

For TE incident ray

$$tS_n = \sqrt{\left(\frac{p_e \sin \theta}{\lambda} + n\right)^2 - \frac{p_e^2}{\lambda^2}} \quad (3.10)$$

For TM incident ray

$$tS_n = \sqrt{\left(\frac{p_e \sin \phi}{\lambda}\right)^2 + n^2 - \frac{p_e^2}{\lambda^2}} \quad (3.11)$$

So, by ignoring the correction factor terms, the computations become simpler as depicted in the equations (3.12) and (3.13) respectively.

$$\frac{\omega_r L}{Z_o} = \frac{l}{p_e} \cos(\theta) \times \frac{p_e}{\lambda} \ln \csc \frac{\pi w}{2p_e} \quad (3.12)$$

$$\frac{\omega_r C}{Y_o} = 4 \frac{l}{p_e} \sec(\theta) \times \frac{p_e}{\lambda} \ln \left[\csc \left(\frac{\pi g}{2p_e} \right) \right] \times \epsilon_e f f \quad (3.13)$$

Equations (3.12) and (3.13) holds true only if $w \ll p_e$, $l \ll p_e$, and $p_e \ll \lambda$. If air acts as a substrate, then by multiplying the equations (3.12) and (3.13) yields:

$$\omega_r^2 LC = 4 \left(\frac{l}{p_e}\right)^2 \left(\frac{p_e}{\lambda}\right)^2 \times \ln \left[\csc \left(\frac{\pi w}{2p_e} \right) + \csc \left(\frac{\pi g}{2p_e} \right) \right] \quad (3.14)$$

The resonance phenomenon is depicted on the left side of the following equation, which is a measure of the overall quality factor. In the case of a PFSS that is entirely reflecting, the net result of the left hand side attains unity value, as seen in

this scenario $\omega_r^2 = \frac{1}{LC}$. Hence, the above equation may be rewritten as:

$$1 = 4 \left(\frac{l}{p_e} \right)^2 \left(\frac{p_e}{\lambda} \right)^2 \times \ln \left[\csc \left(\frac{\pi w}{2p_e} \right) + \csc \left(\frac{\pi g}{2p_e} \right) \right] \quad (3.15)$$

Rewriting on simplification we get:

$$1 = 4 \left(\frac{l}{p_e} \right)^2 \left(\frac{p_e}{\lambda} \right)^2 \times \ln \left[\left(\frac{1}{\sin \left(\frac{\pi w}{2p_e} \right)} \right) + \left(\frac{1}{\sin \left(\frac{\pi g}{2p_e} \right)} \right) \right] \quad (3.16)$$

Considering a special case in which $w \ll 2p_e$ and $g \ll 2p_e$, the expression reduces to:

$$1 = 4 \left(\frac{l}{p_e} \right)^2 \left(\frac{p_e}{\lambda} \right)^2 \times \ln \left[\left(\frac{2p_e}{\pi w} \right) + \left(\frac{2p_e}{\pi g} \right) \right] \quad (3.17)$$

It is anticipated that the value of g will be larger than the value of w . Hence, the ratio $\left(\frac{2p_e}{\pi w} \right)$ has larger impact as compared to $\left(\frac{2p_e}{\pi g} \right)$ and with ignoring the precision the equation may be rewritten as:

$$1 = 4 \left(\frac{l}{\lambda} \right)^2 \times \ln \left[\left(\frac{2p_e}{\pi w} \right) \right] \quad (3.18)$$

It is demonstrated and documented in the literature that an angle of incidence (θ) and net amount of periodicity (p_e) have a significant influence on the performance of PFSS based spatial filters. The equation presented in [151] provides a strong relationship between θ and p_e along with wavelength and is given as:

$$p_e(1 + \sin(\theta)) < \lambda \quad (3.19)$$

The generalized expression for linking the aforementioned parameters may be provided after additional simplification.

$$p_e = C\lambda \quad (3.20)$$

where the term C denotes the constant of proportionality and attains the maximum value of unity. By substituting the equation (3.20) in (3.18), following expression is retrieved:

$$1 = 4 \left(\frac{l}{\lambda} \right)^2 \times \ln \left[\left(\frac{2C\lambda}{\pi w} \right) \right] \quad (3.21)$$

The overall dimensions of the loop are therefore retrieved and optimized using equations (3.19) and (3.21). The square loop PFSS has an inherent feature of being polarization independent. The equations as elaborated are equally true for TM mode. For visualization of the resonance condition, the left hand side (L.H.S.) of equation (3.14) has been set to numeric value 1. But in reality, the result on L.H.S. attains the value lesser than unity which represents the out of band resonance. The net value retrieved is used to determine the concentration of reflections at a certain set of frequencies. The designed DSLPFSS structure behaves as a LC filter where L denotes the inductance and C signifies the values of capacitance. The diagrammatic illustration is provided in the Figure 3.3 and Figure 3.4.

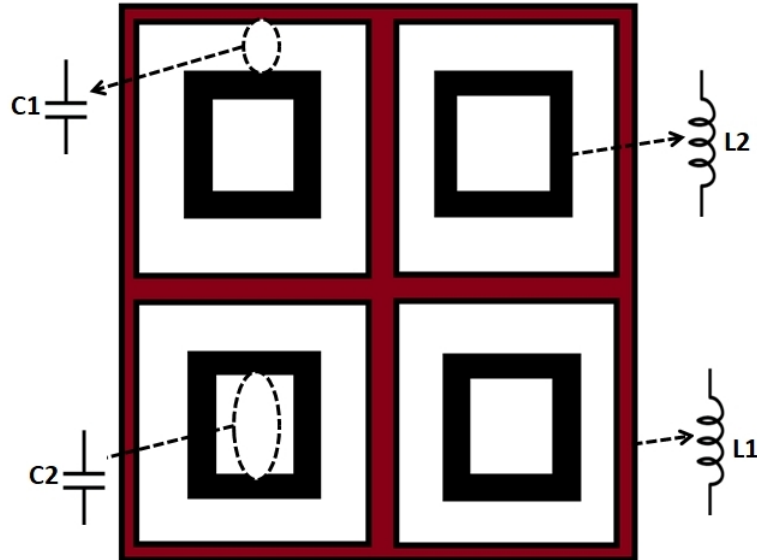


Figure 3.3: 2x2 array of DSLPFSS.

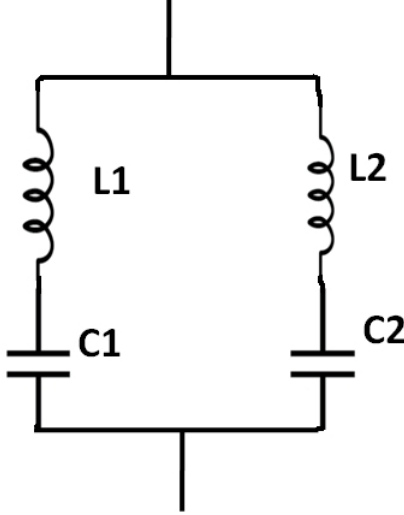


Figure 3.4: Lumped circuit of the unit cell of DSLPFSS.

3.4 Results formulation for DSLPFSS

A comprehensive synthesis process for providing the validation to the proposed hypothesis is presented. The system parameters of the suggested DSLPFSS-based spatial filter are determined by using the design parameters for operation in the sub-6 GHz FR1 frequency spectrum, i.e. from 3 GHz to 6 GHz. The coefficients of the transmission and the reflection are computed and displayed using the DSLPFSS dimensions. The HFSS v20 software, which is based on the FEM technique and is used to assess the physical parameters. The retrieved results are then compared with the output characteristics of the equivalent circuit retrieved from the ANSYS electronic desktop circuit editor. Furthermore, a prototype of the suggested DSLPFSS architecture is built and tested experimentally. The DSLPFSS is a polarisation independent structure and its characteristics alter dramatically depending upon the angle at which the ray strikes. The first stage is to examine the dimensions of the DSLPFSS unit cell at $\theta = 0^\circ$ which are mentioned in the Table 3.1.

Table 3.1: Parametric specifications of the unit cell of DSLPFSS.

f_1	f_2	p_e	l_1	l_2	w_1	w_2
2.90 GHz	5.38 GHz	0.55λ	0.40λ	0.14λ	0.01λ	0.02λ

where the terms of the Table 3.1 can be defined as: f_1 is the lower frequency of resonance, f_2 is the higher frequency of resonance, λ denotes the wavelength at middle frequency, p_e signifies the periodicity, l_1 denotes the length of outer loop, l_2 denotes the length of the inner loop, w_1 signifies the width of outer loop of DSLPFSS and w_2 denotes the width of inner loop of DSLPFSS.

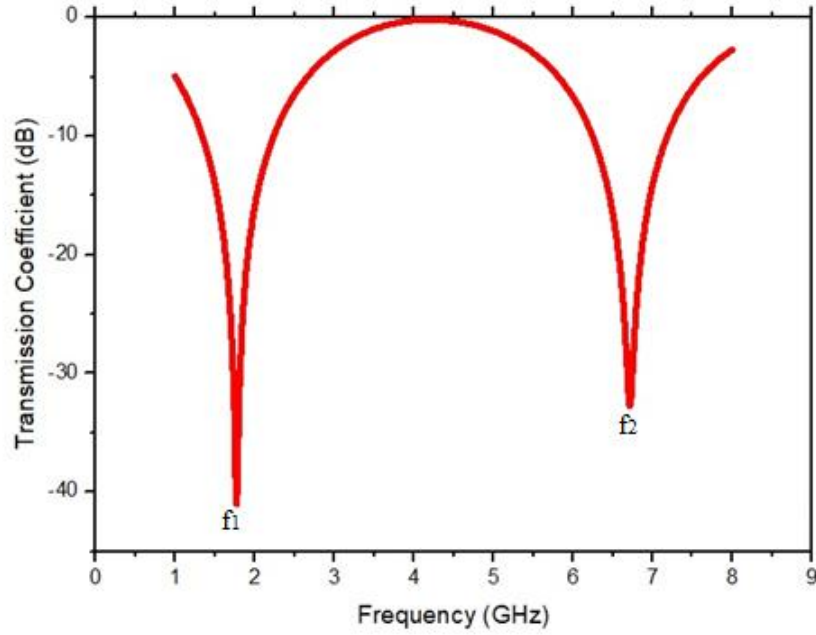


Figure 3.5: Illustration of the transmissive behavior of the single unit cell DSLPFSS.

Periodicity is an important characteristic to consider when developing spatial filters using the PFSS array, and it must be evaluated. To compute its value at the appropriate frequency ranges of operation while disregarding grating lobes, equation (3.19) must be satisfied. So, when the outer loop in the 5G sub-6 GHz band is examined for $\text{AOI} = 0^\circ$, equation (3.19) simplifies to:

$$p_e < \lambda \quad (3.22)$$

$$p_e = \frac{\lambda}{2.27} \quad (3.23)$$

Furthermore, the dedicated formula from equation (3.20) for the outermost loop

in the sub-6 GHz band is obtained as:

$$p_e = 0.44\lambda \quad (3.24)$$

After determining the value of C , the dimensions of the individual loops i.e. l_1 and w_1 are evaluated by gradually varying the $\frac{w}{\lambda}$ values using the equation (3.21). The values are mentioned in the Table 3.2 for the 3 GHz resonant frequency and in the Table 3.3 for 5 GHz resonant frequency of operation. Figures 3.6 and 3.7 visually depict the net amount of the percentage deviation of the simulated frequencies from the specified intended value of the frequencies.

Table 3.2: Estimation of the best values of the output loop parameters at a normalized angle of incidence for 3 GHz operating frequency

w_1/λ_1	p_e	l_1	w_1	f_1 (simulated)	% deviation of f_1 from 3 GHz
0.01	0.4 λ	0.2783 λ	0.01 λ	2.90 GHz	3.3
0.02	0.4 λ	0.3077 λ	0.02 λ	2.87 GHz	4.3
0.03	0.4 λ	0.3345 λ	0.03 λ	2.81 GHz	6.3
0.04	0.4 λ	0.3583 λ	0.04 λ	2.74 GHz	8.6

The higher extreme end frequency of 5 GHz is considered for the innermost loop parameters and for normalized angle of incidence, the equation (3.19) reduces to:

$$p_e < \lambda \quad (3.25)$$

$$p_e = \frac{\lambda}{1.36} \quad (3.26)$$

Furthermore, the appropriate expression from equation (3.20) for the innermost

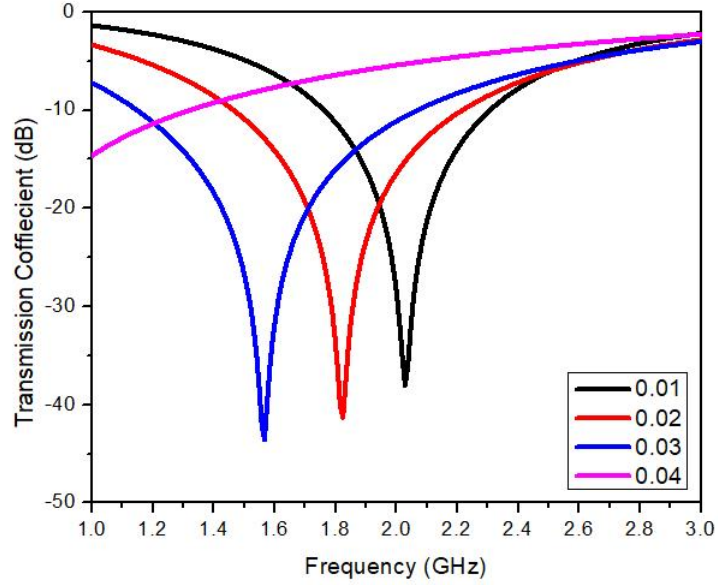


Figure 3.6: Effect on the transmissive characteristics by the variation of $\frac{w_1}{\lambda_1}$ for the DSLPFSS geometry.

loop in the sub-6 GHz region is recovered as:

$$p_e = 0.73\lambda \quad (3.27)$$

Table 3.3: Estimation of the best values of the innermost loop parameters at a normalized angle of incidence for 5 GHz operating frequency

w_2/λ_2	p_e	l_2	w_2	f_2 (simulated)	% deviation of f_2 from 5 GHz
0.01	0.66λ	0.17λ	0.01λ	5.20 GHz	4.1
0.03	0.66λ	0.17λ	0.03λ	5.38 GHz	7.6
0.05	0.66λ	0.18λ	0.05λ	5.57 GHz	11.4
0.06	0.66λ	0.18λ	0.06λ	5.61 GHz	12.2

The resonant operating frequency is calculated as the value at which the transmission coefficient drops to -3dB. Tables 3.2 and 3.3 provide different estimations of the loop dimensions, such as l_1 , l_2 , w_1 and w_2 , for a fixed value of periodicity p_e . This study discovered that changing the estimations of the $\frac{w}{\lambda}$ ratio for a particu-

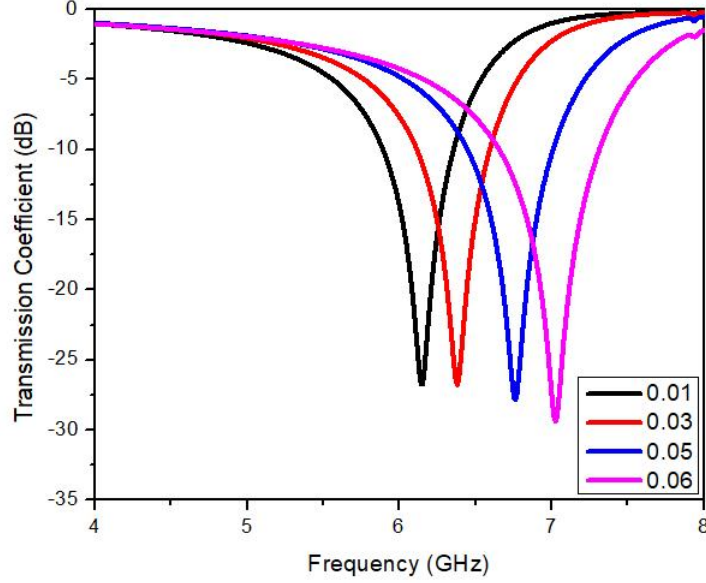


Figure 3.7: Effect on the transmissive characteristics by the variation of $\frac{w_2}{\lambda_2}$ for the DSLPFSS geometry.

lar estimated value of the periodicity p_e increases the relative deviation percentage from the expected recurrence. Figures 3.6 and 3.7 illustrate that at a normalized incidence angle and with a change in the $\frac{w}{\lambda}$ ratio, the lower and higher resonant frequencies repel at a given rate, expanding the transmission bandwidth. According to the study given in Tables 3.2 and 3.3, it is seen that by increasing the size of the loop helps in reduction of the overall inductive influence of the suggested topology. The scattering parameters are related to each other for which the relation holds true as $[S_{11}]^2 + [S_{21}]^2 = 1$, valid for the lossless environment. The S_{11} parameter denotes the overall magnitude of the reflection coefficient, whereas the S_{21} parameter denotes the magnitude of the transmission coefficient. At any given resonant frequency of operation, the above relationship clearly indicates that the responses of S_{11} and S_{21} are reciprocal to each other.

$$\begin{bmatrix} b_1 \\ b_2 \end{bmatrix} = \begin{bmatrix} S_{11} & S_{12} \\ S_{21} & S_{22} \end{bmatrix} \begin{bmatrix} a_1 \\ a_2 \end{bmatrix} \quad (3.28)$$

Where b_1, b_2 are the output coefficients and a_1, a_2 are the input coefficients. S_{11}

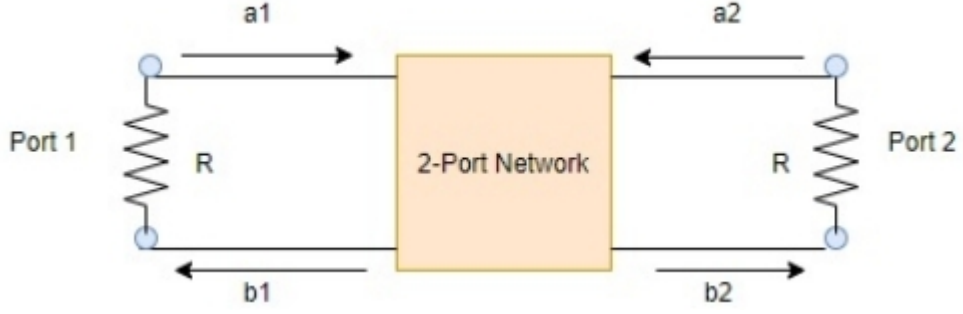


Figure 3.8: Illustration of the two-port network.

denotes the reflection coefficient at the input terminal, S_{12} parameter reflects the transmission gain at the opposite terminal, S_{21} signifies the transmission gain at the input terminal and S_{22} constitutes to the value of the reflection coefficient at the output terminal.

$$S_{11} = \left[\frac{b_1}{a_1} \right]_{a_2=0} \quad (3.29)$$

$$S_{22} = \left[\frac{b_2}{a_2} \right]_{a_1=0} \quad (3.30)$$

$$S_{21} = \left[\frac{b_2}{a_1} \right]_{a_2=0} \quad (3.31)$$

$$S_{12} = \left[\frac{b_1}{a_2} \right]_{a_1=0} \quad (3.32)$$

Furthermore, the mathematical analogous relationship that exists between the loop structure's impedance parameter (Z) and scattering parameters (S) is investigated in order to study the idea of linear rise or fall in the maximum transmission frequency [153].

$$\begin{bmatrix} Z_{11} & Z_{12} \\ Z_{21} & Z_{22} \end{bmatrix} = Z_o \begin{bmatrix} \frac{(1+S_{11})(1-S_{22})+S_{12}S_{21}}{(1-S_{11})(1-S_{22})-S_{12}S_{21}} & \frac{2S_{21}}{(1-S_{11})(1-S_{22})-S_{12}S_{21}} \\ \frac{2S_{21}}{(1-S_{11})(1-S_{22})-S_{12}S_{21}} & \frac{(1-S_{11})(1-S_{22})+S_{12}S_{21}}{(1-S_{11})(1-S_{22})-S_{12}S_{21}} \end{bmatrix} \quad (3.33)$$

where the term Z_o indicates the characteristic impedance of the proposed designed structure. The above study demonstrates the process for evaluating equivalent circuit characteristics such as inductance and capacitance, as shown in Figure 3.4. The retrieved parameters are shown in Table 3.4.

Table 3.4: Numerical results retrieved from the mathematical analysis equations

Parameters	Values
f_1 Simulated	2.90 GHz
f_2 Simulated	5.38 GHz
p_e	0.55 λ
w_1	0.01 λ
l_1	0.40 λ
w_2	0.02 λ
l_2	0.14 λ
Input to output	
L_{f1} (mathematically evaluated)	3.555 nH
L_{f2} (mathematically evaluated)	10.511 nH
C_{f1} (mathematically evaluated)	0.866 pF
C_{f2} (mathematically evaluated)	0.073 pF
f_1 (mathematically evaluated)	2.86 GHz
f_2 (mathematically evaluated)	5.71 GHz

The frequency response model of DSLPFSS shows that the transmission coefficient (S_{21}) reaches a relatively low value at the two resonant frequencies (f_1 and f_2). The outer and inner loops regulate the values of f_1 and f_2 , respectively such that the outer loop manages the inner resonant frequency and vice-versa. By using the electromagnetic principles, the structure's equivalent circuit inductance and capacitance can be utilized to extract the resonant frequencies.

$$f_1 = \frac{1}{2\pi\sqrt{L_{f1}C_{f1}}} \quad (3.34)$$

$$f_2 = \frac{1}{2\pi\sqrt{L_{f2}C_{f2}}} \quad (3.35)$$

As per the information retrieved from the Table 3.5, it is reported that the variance of the resonant frequencies as recovered from the mathematical analysis

Table 3.5: Resonant frequencies extracted from the lumped circuit parameters.

Parameters	Values
L_{f1} (mathematically evaluated)	3.555 nH
L_{f2} (mathematically evaluated)	10.511 nH
C_{f1} (mathematically evaluated)	0.866 pF
C_{f2} (mathematically evaluated)	0.073 pF
Input to output	
f_1 (GHz)	2.86
f_2 (GHz)	5.71
% deviation from lower resonant frequency of 2.90 GHz	1.37
% deviation from higher resonant frequency of 5.38 GHz	6.13

is within the limits. These discrepancies are attributable to approximations used while assessing the parameters and can be tolerated. The parameters collected from the ECM method are simulated using ANSYS circuit editor to evaluate the transmission properties and confirm our results. The corresponding circuit diagram for the proposed architecture is shown in Figure 3.9.

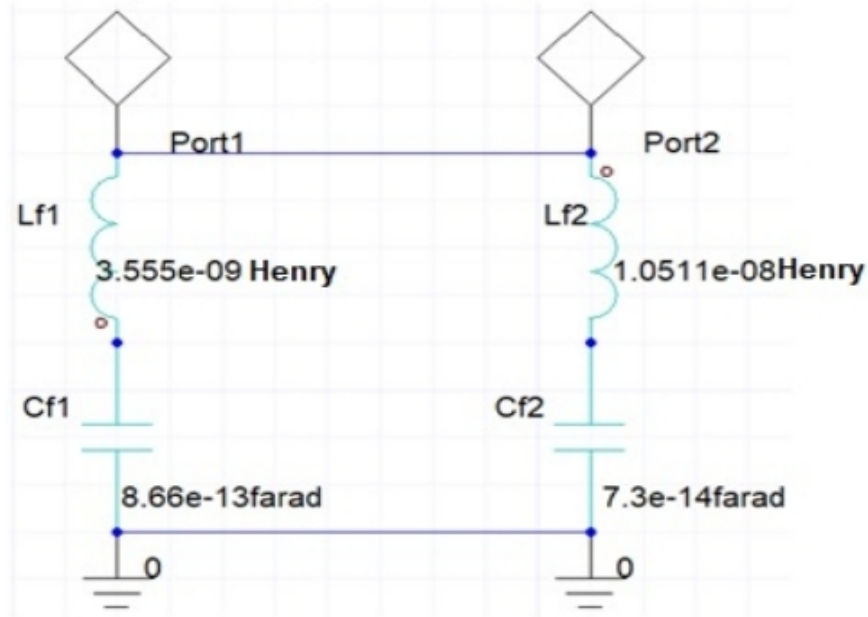


Figure 3.9: Equivalent circuit schematic of the DSLPFSS.

The transmission coefficient values recovered from this hypothesis are consistent with those obtained from the HFSS simulator which provides an authorization to proceed with the building of an array. An essential characteristic to illustrate is the

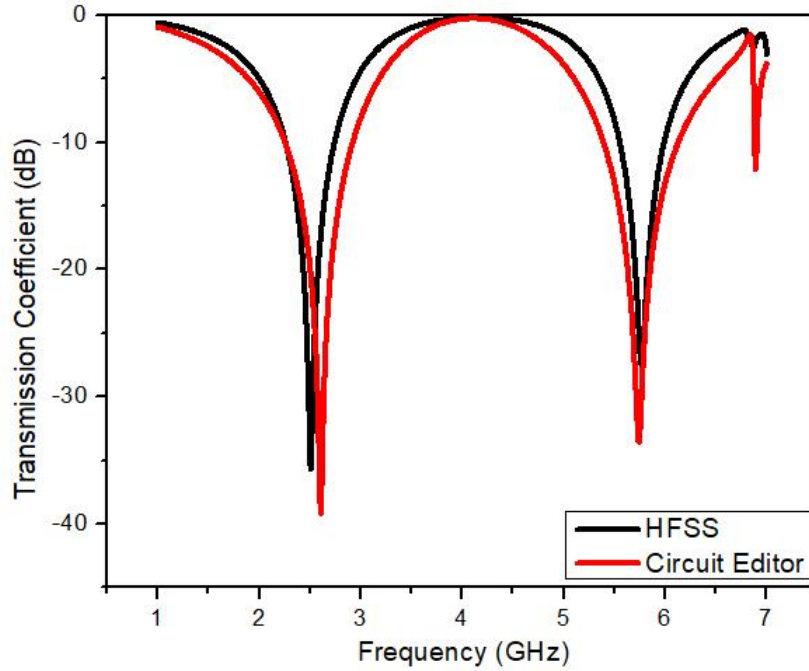


Figure 3.10: Comparative analysis of the transmission coefficient curve extracted from HFSS and Circuit editor.

effect of the angle at which a wave is impacted on the surface of the spatial filter. The DSLPFSS has the inherent property of having the same characteristics only for a narrow range of incidence angles. It also exhibits polarization independent behavior, as seen by the results provided in Table 3.6. Figure 3.11 depicts the fluctuation in transmission coefficient response at various polarization angles. When a wave travels down the Z-axis, the polarization angle is defined as the angle created between the electric/magnetic field vector and the coordinate axis. Table 3.6 shows that there is very little variance in the lower resonant frequency range and almost no change in the upper resonant frequency values.

The proposed DSLPFSS offers polarization insensitive behavior, as the resonant frequencies remain almost constant when the angle ' ϕ ' changes, ranging from 0° to 90° . Furthermore, as shown in Figure 3.12, the planned structure investigation is carried out for various oblique angles of incidence. The maximum angle of incidence for which this design can work is 30° and must satisfy the following equation:

Table 3.6: Resonant frequencies of operation at different polarization angles.

Polarization angle(ϕ)	f_1 (GHz)	f_2 (GHz)	Bandwidth (GHz)	% deviation of lower resonant frequency from 2.9 GHz	% deviation of upper resonant frequency from 5.38 GHz
0 °	2.9	5.38	2.48	0	0
30 °	2.82	5.37	2.55	2.75	0.18
60 °	2.82	5.38	2.56	2.75	0
90 °	2.8	5.38	2.58	3.44	0

$$p_e(1 + \sin 30^\circ) < \lambda \quad (3.36)$$

Minor variations are visible in the resonant frequencies ranging from 0° to 30°. The average bandwidth is therefore essentially unaffected by the angular shift, and it is reported that at larger incidence angles, such as 30°, the structure performs well, as seen in the Table 3.7.

As illustrated in Figures 3.11 and 3.12, the graphical plots virtually overlap over the other, indicating that this design is polarization stabilized and shows comparable properties up to 30 degrees of oblique incidence. PFSS often use metallic patterns that are aligned in multilayer architectures that increase the intensity of the local electric field within the PFSS structure so that even with low incident energy, the local electric field strengths can exceed the breaking point created within the PFSS structure. The maximum field amplification factor (MFEF) is a factor that enables us to evaluate the extent of the increase in the intensity of the electric field within the PFSS compared to that of the incident electromagnetic wave [154] - [155]. The MFEF factor is calculated by dividing the highest amount of the electric field intensity lying within the PFSS by the net amount of the electric field strength possessed by the incident wave. It also used for the comparison of the relative power

Table 3.7: Resonant frequencies of operation at various angles of the incidence.

Inci-dent angle(θ)	f_1 (GHz)	f_2 (GHz)	Bandwidth (GHz)	% deviation of lower resonant frequency from 2.9 GHz	% deviation of upper resonant frequency from 5.38 GHz
0 °	2.9	5.38	2.48	0	0
5 °	2.89	5.37	2.48	0.34	0.18
10 °	2.89	5.36	2.47	0.34	0.37
15 °	2.88	5.34	2.46	0.68	0.74
20 °	2.87	5.30	2.43	1.03	1.48
25 °	2.87	5.26	2.39	1.03	2.20
30 °	2.86	5.24	2.38	1.37	2.60

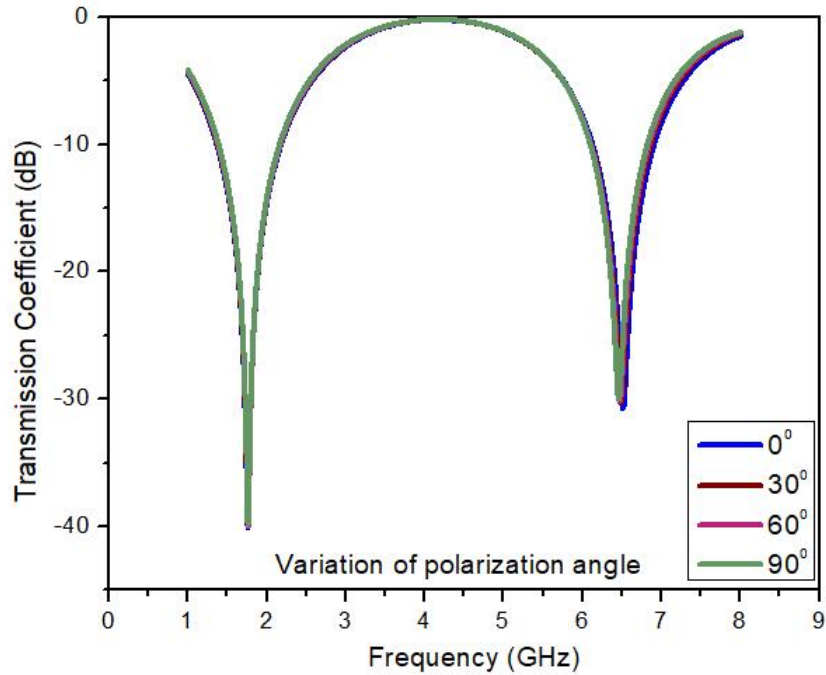


Figure 3.11: Response of DSLPFSS spatial filter at various polarization angles.

handling capacity of different PFSS types. The MFEF indicates power saturation for the PFSS, this factor has a higher ability to regulate peak power. Figure 10 depicts

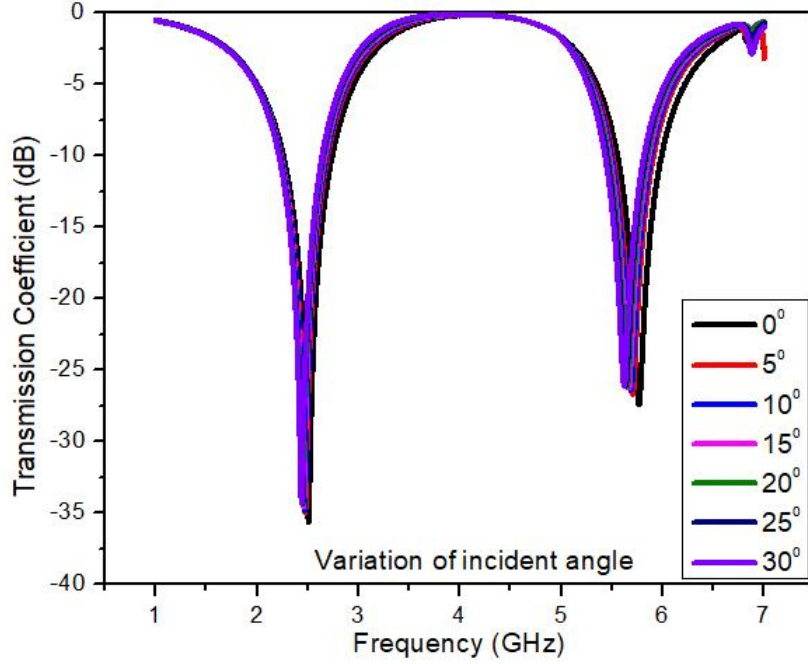


Figure 3.12: Response of DSLPFSS spatial filter at multiple incidence angles.

the calculation of the MFEF value for various frequency settings for the DSLPFSS. The normalized value of MFEF is around 37, which means that the intensity of the electric field within the DSLPFSS can be 37 times greater than the intensity of the electric field of the incoming wave in the FR1 sub-6 GHz 5G band as shown in the Figure 3.13. Hence, the proposed DSLPFSS can process a large amount of net microwave power.

3.5 DSLPFSS prototype and its measurements

PFSS have the crucial property of showing properties that correspond to those of a unit cell. The previous section illustrates the mathematical calculations of the parameters and their properties for a unit cell. The similar approach is used to create the 2x2 DSLPFSS matrix, which can be generalized to an NxN matrix, as shown in Figure 3.14. The output characteristics of the 2x2 DSLPFSS matrix, which is almost identical to that of the unit cell, are shown in Figure 3.15.

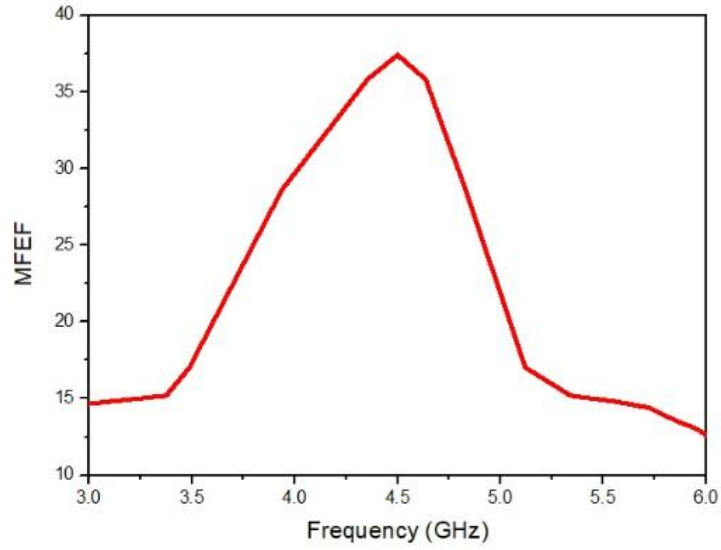


Figure 3.13: MFEF of the DSLPFSS.

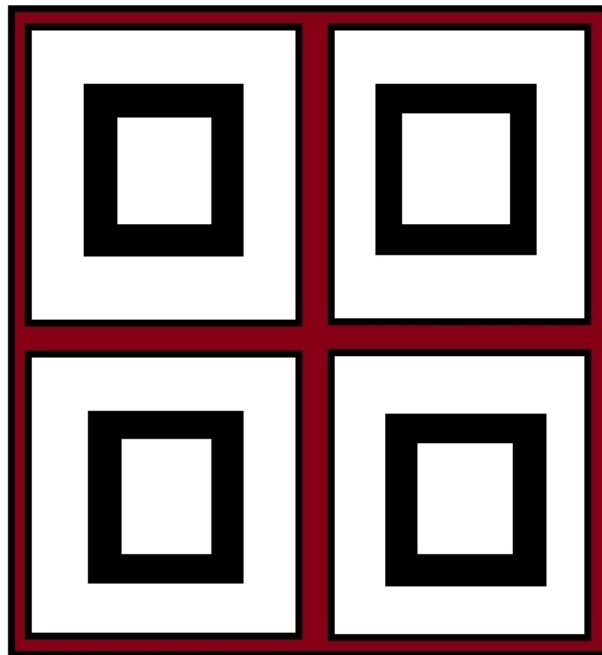


Figure 3.14: 2x2 array of DSLPFSS geometry.

The 2x2 matrix of a DSLPFSS structure is produced on a 60 mm x 60 mm FR4 substrate with a permittivity of 4.4 and a thickness of 1.6 mm. An array can be expanded to a size of $N \times N$, taking into account the dimensions of the unit cell. a 2x2 DSLPFSS is shown in Figure 3.16 and the electric field distribution is shown in Figure 3.17.

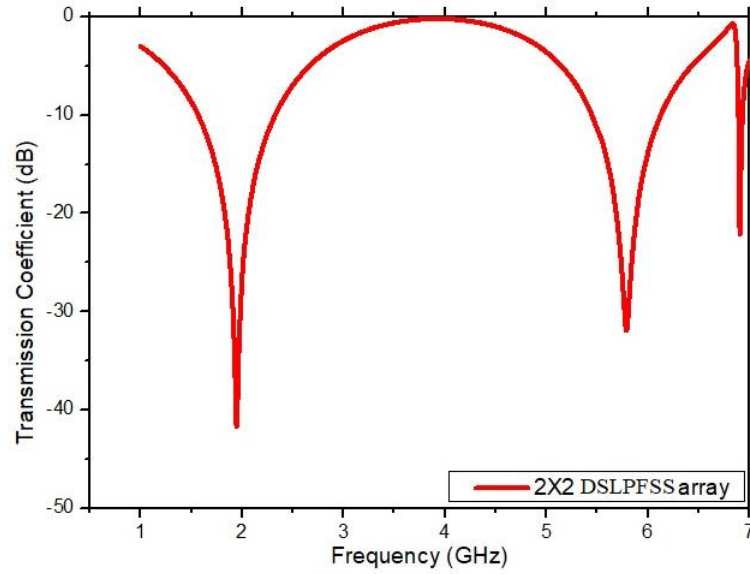


Figure 3.15: Spatial filtering response of DSLPFSS.

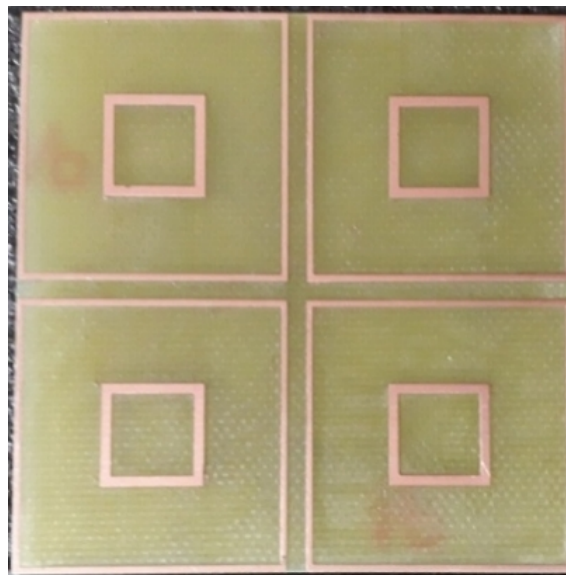


Figure 3.16: 2×2 array of DSLPFSS prototype.

3.6 DSLPFSS measurement results

The proposed design is validated by creating an experimental setup, as shown in Figure 13, to evaluate the transmission coefficient of the spatial filter based on DSLPFSS. Two horn antennas are required in the measurement setup in which the DSLPFSS is installed and the transmission coefficient is to be determined. A vector network analyzer (VNA) must be installed to provide the input excitation through

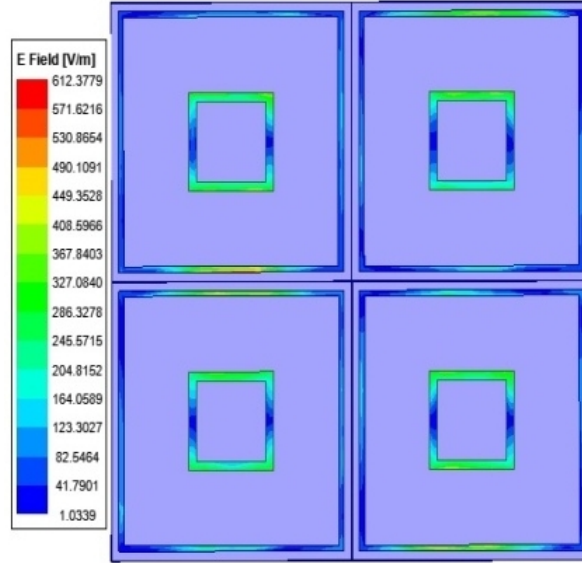


Figure 3.17: E-Field dispersion of 2×2 array of DSLPFSS.

the first input port. It is linked to the horn shaped radiator at the transmitter end with the help of coaxial cables, and the acquired radiations are collected by the receiver horn antenna, which is coaxially attached to the second output port of the VNA.

The processes followed for performing the measurements are divided into two sections, as listed below:

1. The net amount of power which is transferred between the radiating and the capturing horn antennas without inserting a DSLPFSS geometry between them is recorded in the first stage and it is utilized for calibration of the test environment.
2. The DSLPFSS geometry is then inserted between the transmitting and receiving antennas. The transmitted power is measured again, and the actual propagation is calculated by subtracting the two observed values.

The dimensions of the DSLPFSS are fixed in such a way that the -3dB bandwidth attains value of 2.96 GHz, spanning from 2630 MHz to 5590 MHz, which is inside the sub-6 GHz range.

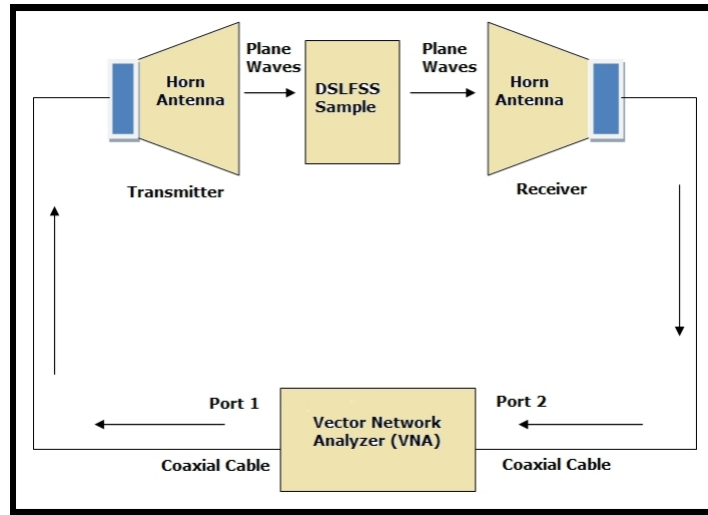


Figure 3.18: Testing and measurement set-up of the DSLPFSS.

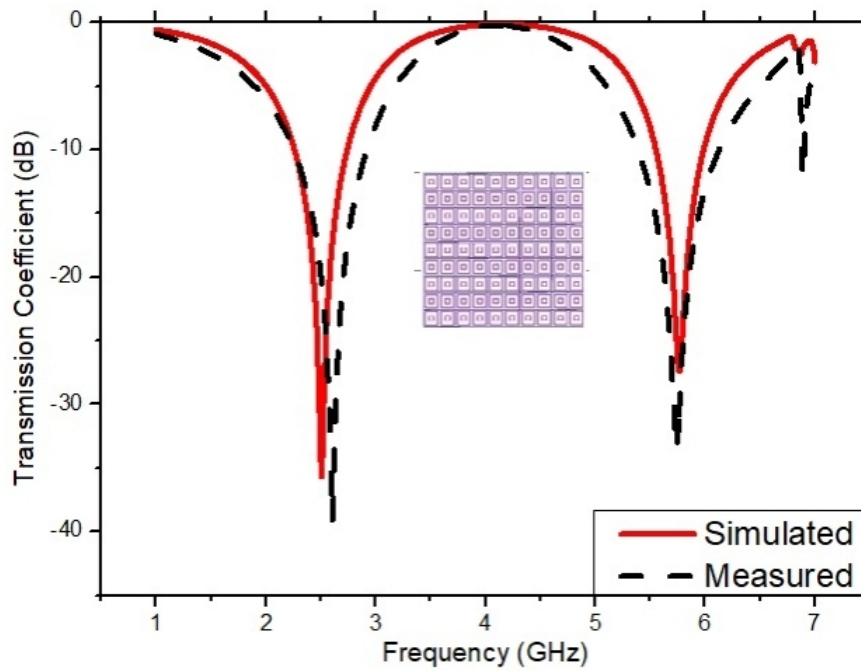


Figure 3.19: Comparison of the modeled and the experimental results of the 10x10 DSLPFSS array.

The results retrieved from the designed prototype in the free space environment circumstances are consistent with those obtained in the simulation, as shown in Figure 3.19.

3.7 Summary

This chapter presents the different designs of PFSS proposed for sub-6 GHz 5G frequency ranges. The basic design namely double square loop PFSS is formulated. The numerical modeling for this design by using the equivalent circuit modeling approach is completed. The transmission and reflection characteristics of the unit cell of double square loop PFSS designs is also investigated in the targeted sub-6 GHz frequency ranges. At last, the simulation and the measurement results of the proposed design is depicted and validated.

Chapter 4

Wideband Printed Patch Antennas for Sub-6 GHz 5G Applications

Printed patch antennas (PPAs) are the type of planar antennas that have been actively investigated and evolved over the last five decades. They have been popular among planar antennas and have been utilized in a variety of purposes in the cellular systems, both military and commercial. The future of PPAs is envisioned in the form of miniaturized structures and it is expected that these antennas should be able to operate in dynamic environment with variable characteristics. The design of the printed patch antennas (PPAs) is basically an application oriented. The advancements in wireless technology have demanded for tiny miniaturized antennas that may occupy lesser area while providing acceptable performance. The design of the antennas must be innovative and must be lighter as well as simple to fabricate. The PPA consists of a metallic transmitting patch produced on a dielectric substrate and supported by a metallic ground plane in its most basic form, and it may be found in reception devices for virtually all generations of mobile communications. Despite the numerous benefits, there is a significant drawback in the form of restricted bandwidth and low gain. Designing tiny wideband PPAs is exceedingly challenging because to the inherent narrow band characteristics. Various

techniques have been devised for improving the limited bandwidth of PPAs [155]-[160]. In the accessible literature, the researchers have recognized and examined the low bandwidth problem of the traditional PPA. This problem is targeted for the improvement in this design of the rectangular shape of the PPA. Rectangular PPA has several advantages, including being compact, cheap, and lightweight [161]. The FR1 band will be extremely helpful, according to current advances in the communication sector, especially with the introduction of 5G devices, since it will bridge the technological gap between existing 4G and 5G. The concepts discussed in this chapter are designed to function in the 5G new radio spectrum's FR1 band. These designs will mostly be employed in the sector of broadband communication, which will feature very reliable and low latency services that will need the usage of massive machine based technologies. To achieve the desired wideband response, the suggested solutions makes use of the partial ground plane and slotted patches.

4.1 Polygon slotted ground PPA

On the FR4 substrate, a partly polygon slotted ground PPA (PSGPPA) with a microstrip feed line is built, and measurements are conducted to verify the findings. The bandwidth of the PPA is enhanced by halving the size of the original ground plane along its major axis. In the partial half ground plane, an eighteen segment polygon shaped structure is carved [1]- [2].

The main design equations necessary for the formulation of the PPA are as follows:

The width (W) of the PPA is evaluated as:

$$W = \frac{c}{2f_r} \sqrt{\frac{2}{(\epsilon_r + 1)}} \quad (4.1)$$

Where, c denotes the speed of light in free space, ϵ_r indicates the value of dielectric constant of the substrate and f_r signifies the resonant frequency of operation.

An increase is visualized in the overall electrical dimensions along the length of the PPA by an amount of ΔL which is caused by the fringing effect. As a result, the extended length of the PPA is computed by using the following equation:

$$\frac{\Delta L}{h} = 0.412 \frac{(\epsilon_{reff} + 0.3) \left(\frac{w}{h} + 0.264\right)}{(\epsilon_{reff} - 0.258) \frac{w}{h} + 0.8} \quad (4.2)$$

Where ‘h’ denotes the height of the substrate and ϵ_{reff} indicates the effective dielectric constant of the structure. The overall length ‘L’ of the PPA is calculated as:

$$L = \frac{c}{2f_r \sqrt{\epsilon_{reff}}} - 2\Delta L \quad (4.3)$$

The dimensions of the basic PPA geometry are determined using the calculations given above. The design is simulated with HFSS software, and some of the parameters are adjusted with parametric sweep to guarantee that the transmission falls inside the required frequency band, which is between 3.3 GHz and 4.2 GHz. Figure 4.1 and Table 4.1 show the design procedures for generating the final suggested antenna geometries, respectively.

In this study, the brief analysis of the design geometry steps which are required to reach the finalized wideband antenna design is presented. The parametric analysis is performed and optimized dimensions are reported which gives the adequate values of the return loss and the bandwidth. The final iteration of the PPA is an ideal for operation in the sub-6 GHz 5G New Radio spectrum (NR) with exhibiting a wide bandwidth of 720 MHz. This PPA design also has the benefit of being less complicated, having a single layer design, and smaller in size. Initially, the traditional PPA design is built using the fundamental design equations, and then the partial ground plane idea is implemented. The conventional design of the PPA doesn’t radiate. So, the ground plane is gradually reduced and by reaching to exactly half of the dimension along one axis, the design starts radiating at 3.80 GHz. As reported in the Table 4.2, the bandwidth of the half ground plane PPA design is still not sufficient

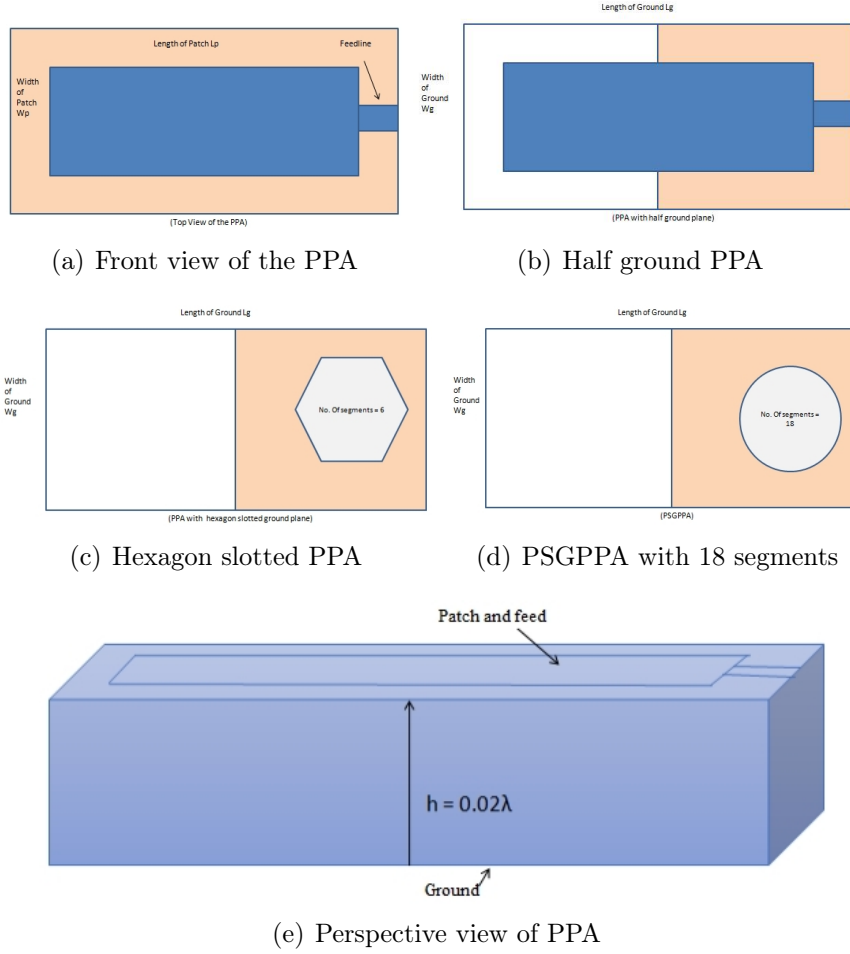


Figure 4.1: PPA design iterations

for utilizing this design in wideband applications. The structure is further changed by carving a hexagonal groove within the half grounded PPA design to increase the bandwidth of the half grounded PPA. The resulting design has a bandwidth of 500 MHz, making it ideal for use in wideband applications. The bandwidth is increased by increasing the number of segments in a polygon slot to eighteen. PSGPPA is the name given to the design that has a bandwidth of 720 MHz. The optimal values for the parameters are listed in Table 4.1, as follows:

Table 4.1: Dimensions of proposed PSGPPA (FR4 substrate with $h = 0.02\lambda$)

Parameters	L_p	W_p	W_f	L_f	L_g	W_g	No. of polygon segments
Dimension	0.46λ	0.20λ	0.006λ	0.02λ	0.25λ	0.35λ	18

4.2 Interpretation of the results for PSGPPA

The parametric optimizations of the dimensions are carried out for the PSGPPA design with an improved bandwidth. It is reported that for the hexagonal slotted PPA and PSGPPA, an adequate radiation performances are retrieved. The results are retrieved from the parametric analysis and are presented in the Table 4.2. The optimization of the antenna parameters is completed by using the parametric sweep option in HFSS for getting the radiation in the desired frequency bands of operation in sub-6 GHz 5G frequency range.

4.2.1 Reflection coefficient variation with design iterations

As shown in Figure 4.2, the parametric analysis is performed for all iterations of the PPA. Based on the formulated design equations as reported, a design of a basic PPA is proposed which resonates at 4.03 GHz. The only limitation of this design is its radiation which is limited to near field region with maximum value of -9.50 dB. The radiation characteristics are improved by reducing the dimensions of the ground plane is reduced along the length. It is also reported that as the dimensions are exactly reduced to half, the PPA design starts radiating. The reflection coefficient touches to maximum value of -33 dB which is quite good in terms of the radiation. The structure starts resonating at 3890 MHz with a bandwidth of nearly 0.25 GHz, which is not adequate to be used in wideband applications. Further, for increasing the bandwidth in the far field region of the proposed design structure, a polygon slot is engraved within the ground plane on which further iterations are being performed. The best results in terms of wide bandwidth are retrieved when the number of the segments is made 6 i.e. hexagon structure, thus making it as hexagonal slotted PPA. It is seen that by performing the above procedure, the reflection coefficient reaches to the maximum value of -13.35 dB which resonates at 3600 MHz with a wide bandwidth of about 0.5 GHz. Further, as the number of

the slot segments is gradually increases up to the value of 18, the antenna starts resonating at 3360 MHz with a bandwidth of 0.72 GHz and a maximum reflection coefficient of -31.15 dB. Figure 4.2 depicts a comparative study of the reflection coefficient data for all iterations. As we progress from one design to the next, a considerable improvement in operational bandwidth with good reflection coefficient indicative of far field radiation is reported. The final hexagonal slotted PPA designs have a broad bandwidth of 500 MHz and a highest amount of reflection coefficient of -13.35 dB at 3630 MHz. PSGPPA's other design has a 0.72 GHz bandwidth that ranges from 3280 MHz to 4000 MHz. At frequencies of 3410 MHz and 3830 MHz, the highest values of reflection coefficient are -26.17 dB and -31.15 dB, respectively. An exponential growth in the antenna's bandwidth is observed across multiple repetitions, according to the data in Table 4.2. The slot's position is critical while building the antenna, and once decided, increasing the number of segments of the engraved slot permits getting the antenna's broad band characteristics. The results of the parametric analysis are shown in Table 4.2.

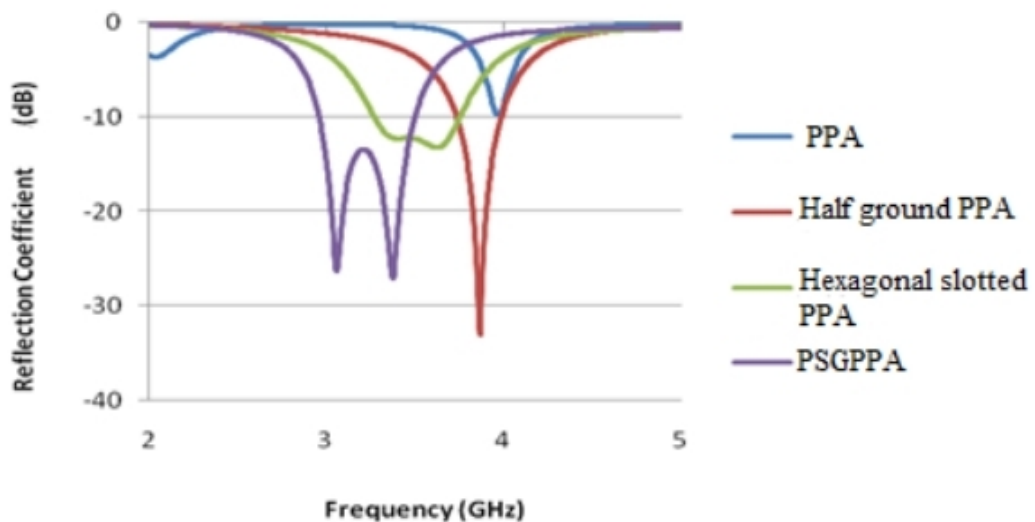


Figure 4.2: Comparative analysis of the output characteristics retrieved from all iterations.

The effect on the output characteristics by the variation of the feed width of the

Table 4.2: Parametric analysis of the results retrieved from the design iterations

Design iteration	Resonant frequency	Bandwidth	Reflection coefficient
PPA	4.02 GHz	30 MHz	-10.64 dB
Half ground PPA	3.88 GHz	250 MHz	-53 dB
Hexagonal slotted PPA	3.64 GHz	503 MHz	-14.56 dB
PSGPPA	3.42 GHz & 3.83 GHz	720 MHz	-26.17 dB & -31.15 dB

proposed PSGPPA design is elaborated in the Table 4.3.

Table 4.3: Effect on the output characteristics by the variation of the feed width of the PSGPPA.

Feed Width (W_f)	Resonant frequency	Bandwidth	Reflection coefficient
0.006 λ	3.42 GHz & 3.83 GHz	720 MHz	-26.17 dB & -31.15 dB
0.012 λ	3.69 GHz	650 MHz	-38.27 dB
0.019 λ	3.69 GHz	600 MHz	-38.15 dB
0.025 λ	3.66 GHz	550 MHz	-27.61 dB
0.032 λ	3.66 GHz	500 MHz	-22.51 dB
0.038 λ	3.66 GHz	480 MHz	-21.30 dB

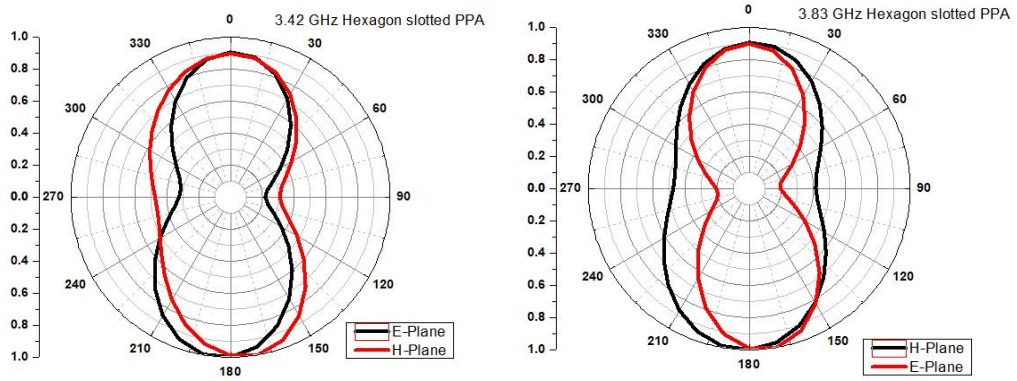
Hence, with a single layer structure and without much complexity of the design, the desired reflection coefficient along with the bandwidth is achieved. The output characteristics which are exhibited by the two proposed designs comprising of hexagon slotted PPA and PSGPPA are compared and reported in the Table 4.4.

4.2.2 Radiation intensity

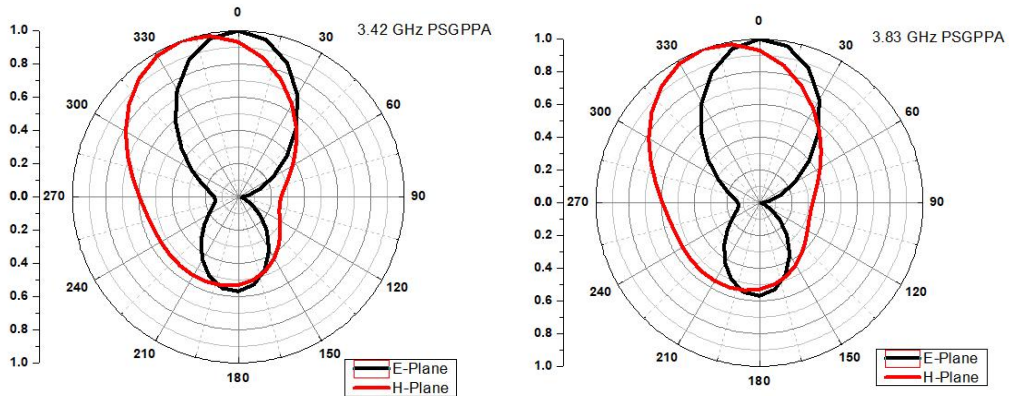
Radiation intensity is an essential statistic that defines the amount of energy emitted from the PPA. Figure 4.3 depicts the radiation patterns in the E and H planes for 3.42 GHz and 3.83 GHz resonating frequencies.

Table 4.4: Output characteristics of the hexagonal slotted PPA and PSGPPA.

Parameters	Hexagon slotted PPA	PSGPPA
Lower Cut off frequency (f_1)	3.250 GHz	3.280 GHz
Higher Cut off frequency (f_2)	3.750 GHz	4.000 GHz
Bandwidth	0.5 GHz	0.72 GHz
Reflection Coefficient	-13.35 dB	- 31.15 dB
Gain	2.2 dB	2.5 dB
Directivity	3.15 dB	3.21 dB
Radiation efficiency	81.03%	83.62%



(a) 3.42 GHz resonant frequency of hexagonal slotted PPA. (b) 3.83 GHz resonant frequency of hexagonal slotted PPA.



(c) 3.42 GHz resonant frequency of PSGPPA. (d) 3.83 GHz resonant frequency of PSGPPA.

Figure 4.3: Normalized radiation patterns for the wideband antenna designs comprising hexagon slotted PPA and PSGPPA

E-plane radiation efficiency pattern is depicted in red colour and H-plane radiation efficiency pattern is shown with green colour curve. The radiation pattern is

recovered after HFSS software simulations, with the highest gain reported to be 2.2 dBi at 3.42 GHz for hexagonal slotted PPA and 2.5 dBi at 3.83 GHz for PSGPPA. The E-plane radiation pattern depicts the "figure of eight," while the H-plane, omnidirectional radiation properties are depicted.

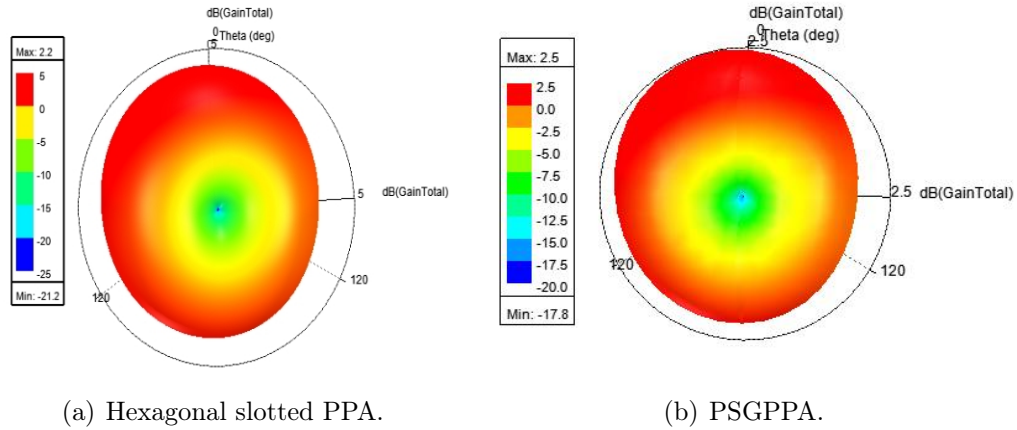


Figure 4.4: 3D polar plot depicting the gains exhibited by the two proposed designs

4.2.3 Gain and Efficiency

Figure 4.4 clearly illustrates that the gain and bandwidth of the PPA grow with iteration improvement, as demonstrated by hexagonal slotted PPA and PSGPPA. The design of PSGPPA offers an adequate gain and directivity which makes its feasibility to be utilized in the 5G applications. Also, the amount of radiation efficiency is nearly 80% which indicates that very less amount of radiation losses occurs during the process of the radiation as indicated in the Figure 4.5.

4.3 Experimental investigation of PSGPPA.

A PSGPPA design is presented in the preceding section and is modelled for the extraction of output radiation characteristics in the appropriate sub-6 GHz frequency range. To confirm these results, a fourth iteration of PSGPPA with a maximum bandwidth of roughly 720 MHz is built and evaluated using a vector network ana-

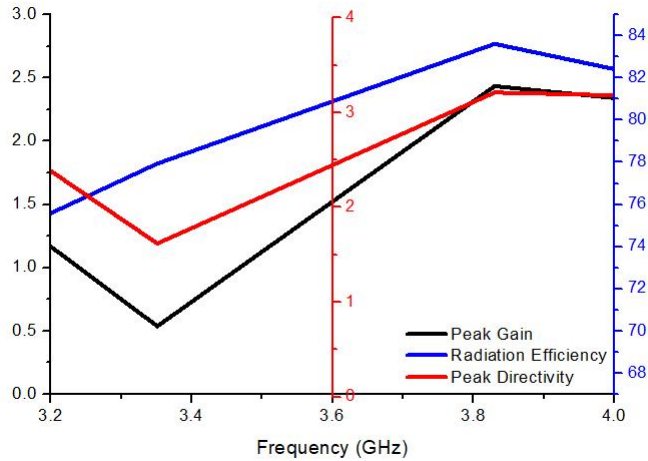


Figure 4.5: Graphical illustration of the gain (dB), directivity (dB) and the radiation efficiency (%) exhibited by the PSGPPA design.

lyzer (VNA). The MS2037C and its associated setup are used to evaluate antenna characteristics such as the reflection coefficient, radiation pattern, and gain. A MS2037C Network analyzer is used to measure the radiation properties. For antenna characterization, vector network analyzers, anechoic chambers, automated turn tables, and other critical technologies are used. MS2037C is a sophisticated Vector Network Analyzer (VNA) from Anritsu that can operate in both the time and frequency domains. The VNA is a microprocessor-based device that can precisely measure the scattering properties of two port networks. The network analyzer's built-in signal processing algorithms assist in sending and receiving data to the radiator before eventually showing the measured values in the form of graphical graphs. Furthermore, the anechoic chamber creates a "silent zone" free of any electromagnetic reflections. All antenna characterizations are carried out in an anechoic chamber to remove reflections from neighboring objects. It is a huge chamber in relation to the operating wave length, with microwave absorbers connected to the walls, ceiling, and floor to reduce EM reflections. Figure 4.6 is a picture of an anechoic chamber used to quantify and report radiation.

The absorbers connected to the walls are highly lossy at microwave frequencies. They have tapered shapes to provide proper impedance matching for the microwave

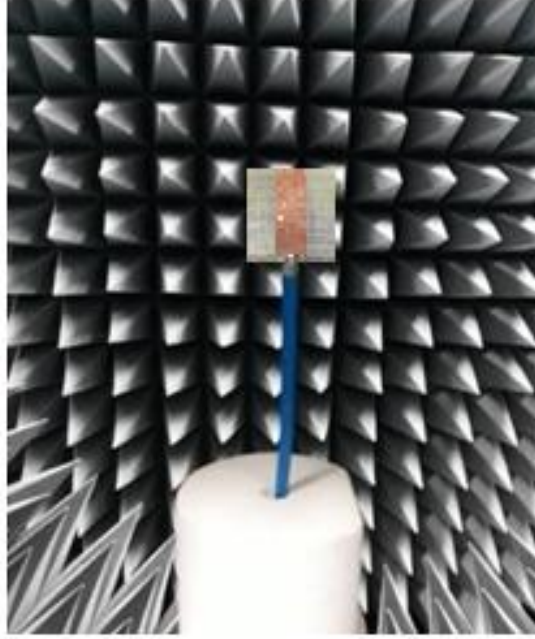


Figure 4.6: Photograph of an anechoic chamber used for measurements of the PPA designs.

power that impacts them. The room is protected from the ambient electromagnetic interferences by covering all of the walls and ceiling with aluminium sheet. The output characteristics which are used to determine the PPA properties are explained in this section. In practice, the VNA is linked to large length of the cables and connections. Each connection and cable will have their own set of losses. The device should be calibrated using accepted standards of open, short, and matched loads to get accurate scattering parameters. There are several calibration methods available on the VNA. Calibration methods such as single port and full two port are often used. The reflection coefficient, VSWR, and input impedance may all be described using the single port analysis approach. Figures 4.7(a) and 4.7(b) depicts the front and back view of the PSGPPA prototype that was built.

The experimental setup for extraction of the output characteristics of the PSGPPA is illustrated in the Figure 4.8 as shown below.

The PPA design is linked to either of the VNA's ports, and the VNA is set to the S_{11}/S_{22} mode, which produces the radiation characteristic. The calibration of the

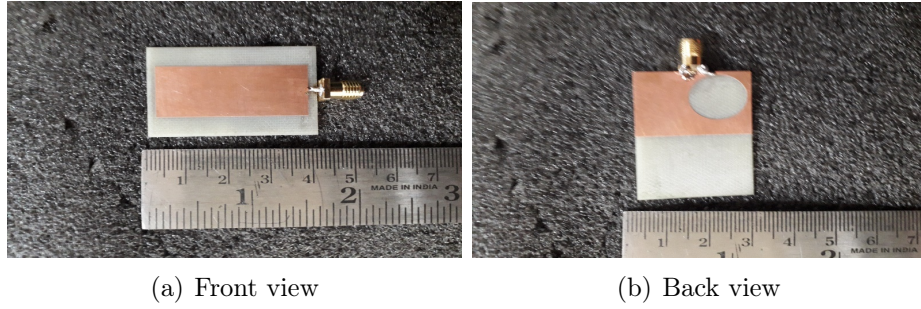


Figure 4.7: PSGPPA designed prototype

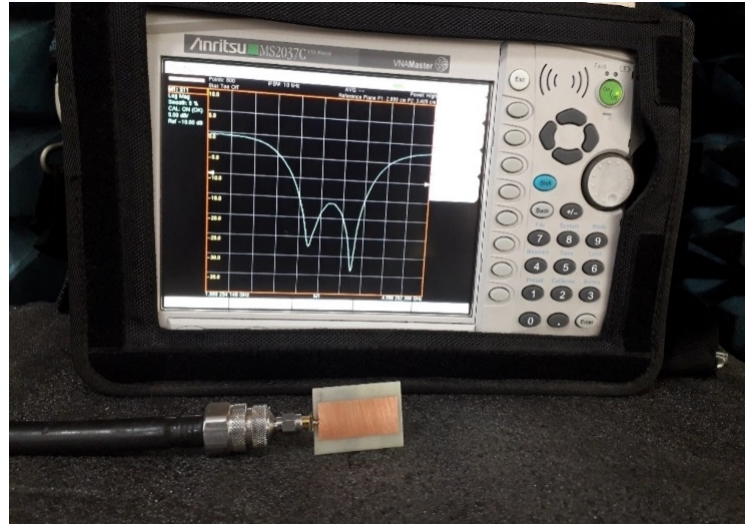


Figure 4.8: Measurement set-up for illustrating the output characteristics of the PSGPPA.

port cable is accomplished for the desired frequency range by employing typical open, short, and matched load circumstances. The simulated design's reflection coefficients are compared to the information received from the developed prototype, as shown in Figure 4.9. The simulated and measured results are clearly in accord with one another. Both curves' patterns coincide, confirming this concept and making it a viable contender for usage in sub-6 GHz frequencies.

The simulation and the measurement characteristics are compared in the Table 4 for the PSGPPA design. It clearly indicates that this design is best suitable for the targeted sub-6 GHz applications.

According to the results of the study presented in Table 4.5, the measured results are nearly comparable to the simulated findings, and the antenna thus constructed

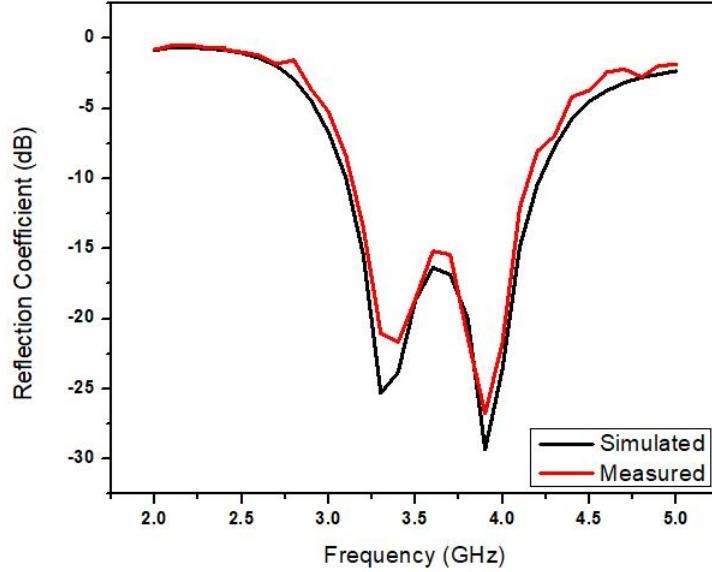


Figure 4.9: Comparative analysis of the output characteristics of the PSGPPA exhibiting a bandwidth of 720 MHz

Table 4.5: Comparison of the output characteristics retrieved from the simulation and the measurements for the proposed PSGPPA

Parameters	Simulated results	Measured results
Lower cut off frequency (f_L)	3.28 GHz	3.30 GHz
Higher cut off frequency (f_H)	4.00 GHz	3.98 GHz
Bandwidth	0.72 GHz	0.68 GHz
Min. reflection coefficient	-31.15 dB	- 26.98 dB

may be used for wideband applications in the sub-6 GHz 5G spectrum. This antenna design stands out in the sub-6 GHz 5G NR spectrum due to its single layer construction, minimal complexity, and small size.

4.4 U- slotted ground PPA (USGPPA)

In this section, the design of a U-slotted defected ground plane PPA (USGPPA) is presented and analyzed. The footprint of the USGPPA is displayed in the Figure 4.10. USGPPA's radiation element is engraved on the top side of a 1.6 mm thick FR4 dielectric substrate with a dielectric constant of 4.4 and a loss tangent of 0.02.

The readings are made and the dimensions are optimized using the transmission line model to get the desired performance. The simple structural formulae that are used to construct the novel proposed USGPPA are already illustrated in the equations (4.1) to (4.3).

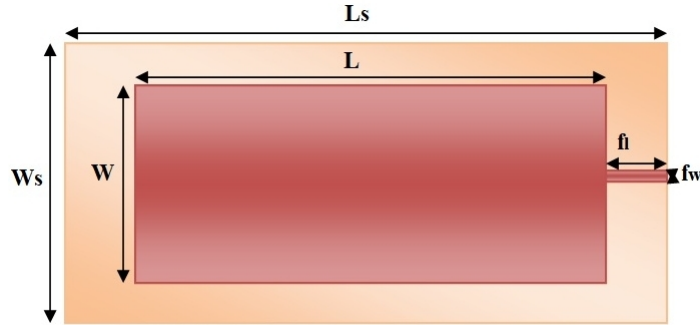


Figure 4.10: Design of a simple USGPPA.

By utilizing the parametric sweep optimization and from the generic formulae's as illustrated in the equations (4.1) to (4.3), the dimensions of the basic conventional PPA are determined. Initially, as shown in Figure 4.11(a), a conventional PPA with a complete ground is proposed and simulated. The bandwidth optimization is done by varying the length of the ground plane and varying it to a point in order to get the optimum solution, as depicted in Figure 4.11(b). In the next step, a U-slot is engraved within the ground plane and adjusted further for increasing the effective operating bandwidth as needed for the 5G applications. This geometry is illustrated in the Figure 4.11(c). Then the effect of inserting a U-slot is testified and compared with initial design of the conventional PPA.

The parametric specifications in terms of dimensions for USGPPA are defined in the Table 4.6.

In Table 4.6, all dimensions are given in terms of λ , which denotes the wavelength attained at the centre frequency within the spectrum's working range. A comparative analysis is presented in the Table 4.7 which presents the detail of the values obtained from the three design iterations for the output performance characteristics.

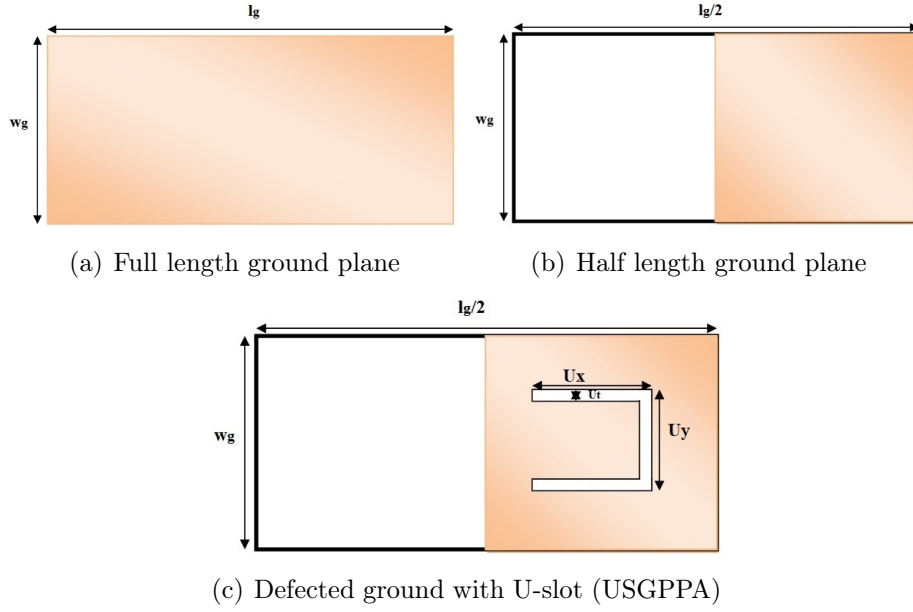


Figure 4.11: Modifications of the ground plane

Table 4.6: Parametric specifications of the USGPPA

Parameters	Dimensions
Length of patch (L)	0.46λ
Width of patch (W)	0.156λ
Length of substrate (L_s)	0.51λ
Height of substrate (h)	0.02λ
Length of feedline (f_l)	0.02λ
Width of feedline (f_w)	0.01λ
Length of ground plane (l_g)	0.51λ
Half ground length ($l_g/2$)	0.25λ
Half ground width (w_g)	0.51λ
U-slot x length (U_x)	0.20λ
U-slot y length (U_y)	0.20λ
U-slot thickness (U_t)	0.20λ

The outcome of this research clearly indicates that by inserting a U-slot, bandwidth augmentation is visualized for the proposed antenna design.

Table 4.7: Comparative analysis for the three iterations involved for making final proposed design of USGPPA.

Parameters	Full Ground	Half Ground	Defected Ground (U-slot)
Lower Cut off frequency (f_1)	Not Radiating	3.73 GHz	3.38 GHz
Higher Cut off frequency (f_2)	Not Radiating	4.12 GHz	4.28 GHz
Bandwidth	Not Radiating	390 MHz	900 MHz \uparrow
Peak gain	Not Radiating	4 dB	3.8 dB \downarrow
Peak directivity	Not Radiating	4.8 dB	4.55 dB

4.4.1 Interpretation of the results for USGPPA

The procedure adopted for analysis of the PSGPPA is again replicated for this design of USGPPA. The parametric optimizations of the dimensions are carried out and the best values are finalized for getting a design prototype. The U-slot helps to get an enhancement in the bandwidth of the antenna by adding an additional capacitance within the design. The bandwidth retrieved from the proposed design is sufficient for making it in use for the wide band applications in sub-6 GHz 5G applications. The output performance characteristics exhibited by this USGPPA are reported in the Table 4.8. Parametric sweep tool is utilized for getting the radiation in the desired frequency bands of operation in sub-6 GHz 5G frequency range.

4.4.2 Reflection coefficient response along the design iterations

The parametric analysis is used for all iterations of the PPA, as shown in Figure 4.11. The length of the ground plane is reduced along the major axis and the results are analyzed. It is reported that as the dimension of the ground plane along the

major axis is reduced to half of the value, the design starts radiating within the targeted band of operation but still the bandwidth is not sufficient. An U-slot is etched by maintaining the length of the ground plane to half of the value, and the results indicate that the bandwidth is raised to a sufficiently large value of 760 MHz. Figure 4.12 depicts a comparison of the reflection coefficient curves for the three design iterations. A considerable improvement in the value of the operational bandwidth is reported with good reflection coefficient indicative of far field radiation while moving across the design iterations. The final design of USGPPA exhibits a broad bandwidth of 760 MHz with a maximum value of reflection coefficient at -23.35 dB at a frequency of 4 GHz. According to the data reported in the Table 4.7, an exponential rise in the antenna's bandwidth is recorded throughout several repetitions. In the design of the proposed antenna, the position of the U-slot is a crucial consideration and once it is determined, and then broad band characteristics are retrieved. The graphical comparison as reported in the Figure 4.12 indicates that the USGPPA starts radiating at half ground structure, and subsequently the bandwidth is augmented by engraving a U-slot inside the half ground as visualized.

4.4.3 Radiation intensity

The amount of the radiations received at the distant point in the E-plane and the H-plane are measured in terms of the radiation intensity. It is an essential statistic that defines the amount of energy emitted from the USGPPA. E and H plane radiation patterns are recorded and illustrated in the Figure 4.13 for 4 GHz of resonating frequency.

Normalized radiation patterns in the E-plane and H-plane are compared for the USGPPA based on simulated and measured data. The E-plane radiation pattern displays the "figure of eight," but the H-plane radiation pattern retrieves omnidirectional radiation characteristics. Table 4.8 depicts the output characteristics obtained from the suggested design.

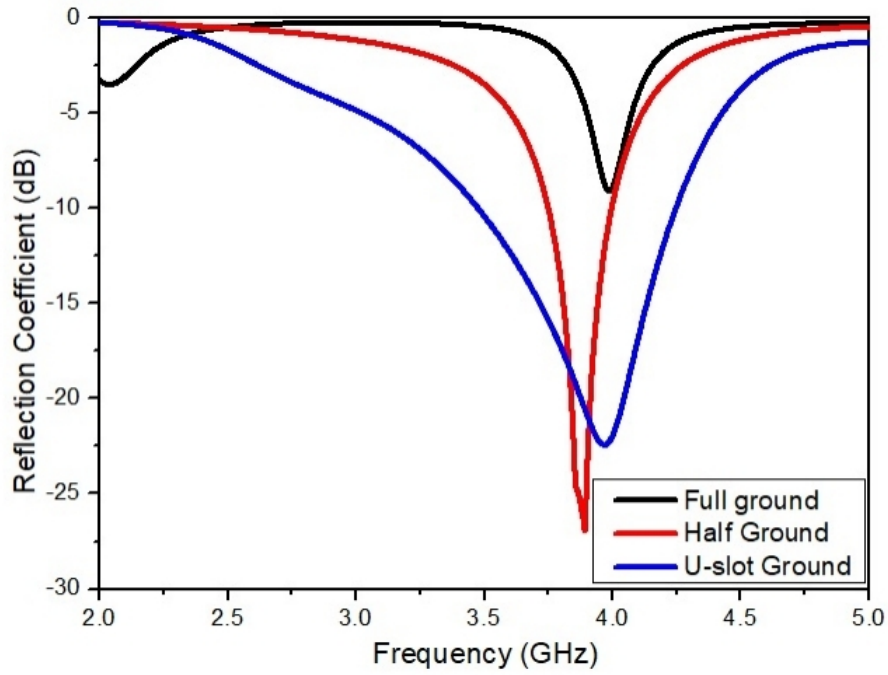


Figure 4.12: Comparative illustration of the reflection coefficients obtained from the three design steps consisting of complete ground plane, half ground plane and U-slot defected ground plane (USGPPA).

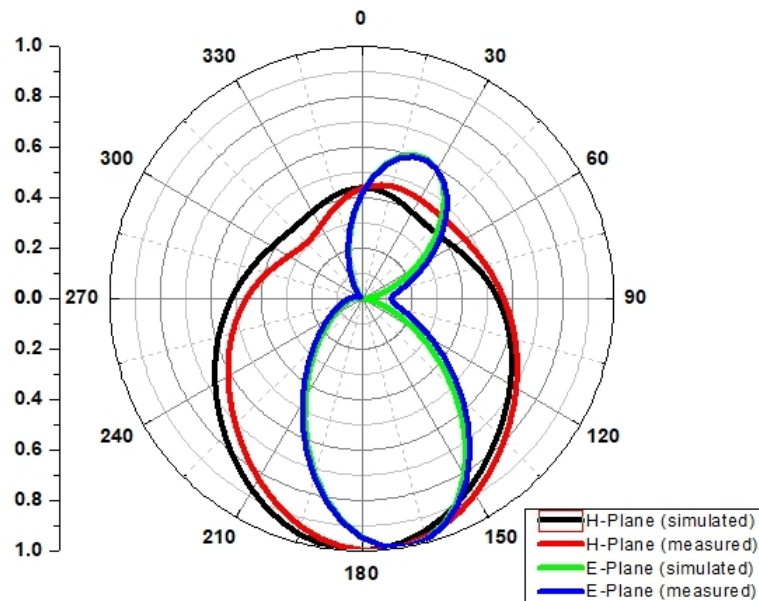


Figure 4.13: Normalized radiation patterns of the USGPPA in E-plane and H-plane at 4 GHz resonant frequency.

A 3-D polar plot of the gain exhibited by a USGPPA is illustrated in the Figure 4.14. A sufficiently large value of the gain of about 3.8 dB is retrieved from the proposed design which makes our design suitable.

Table 4.8: Output characteristics exhibited by USGPPA.

Parameters	Value
Lower Cut off frequency (f_1)	3.38 GHz
Higher Cut off frequency (f_2)	4.28 GHz
Bandwidth	900 MHz
Min. Reflection coefficient (dB)	-28.15 dB
Peak Gain	3.8 dB
Peak directivity	4.55 dB
Max. Radiation efficiency	87.6 %

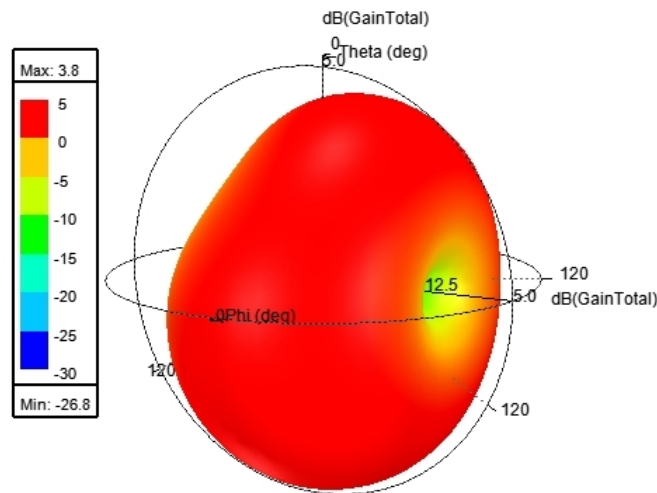


Figure 4.14: 3D polar plot depicting gains exhibited by USGPPA

4.4.4 Gain and Efficiency

The design of USGPPA offers adequate gain and directivity which makes its feasibility to be utilized in the 5G applications. Also, the amount of radiation efficiency is nearly 90% which indicates that very less amount of radiation losses occurs during the process of the radiation as indicated in the Figure 4.15.

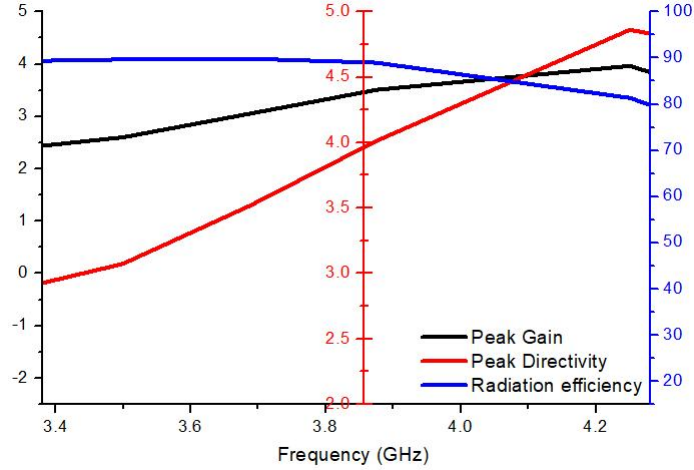


Figure 4.15: Graphical illustration of the gain (dB), directivity (dB) and the radiation efficiency(%) exhibited by the USGPPA design.

4.5 Experimental investigation for the USGPPA design.

In the preceding section, a design of the USGPPA is provided and is modeled for the extraction of output radiation characteristics in the desired sub-6 GHz frequency range. The validation of the proposed design is done by making a design prototype of USGPPA which exhibits maximum bandwidth of about 900 MHz. The MS2037C VNA and its associated setup are used to assess antenna characteristics such as the reflection coefficient, radiation pattern, and gain. A MS2037C Network analyzer is used to measure the radiation properties. Vector network analyzers, anechoic chambers, automated turn tables, and other essential technologies are utilized for antenna characterization. The prototype of the USGPPA is shown in the Figure 4.16.

A comparative analysis of the reflection coefficients which are retrieved from the modeled design and prototype is shown in the Figure 4.17. It is evident that the modeled and the experimental findings are in good agreement with one another. A perfect match is seen in the patterns followed by the results retrieved from the simulation and the measurement results, which makes it a strong contender for use

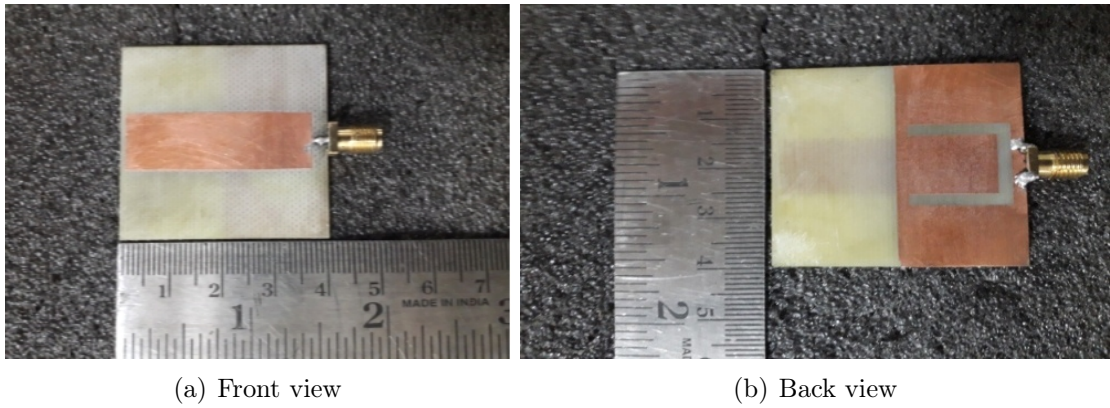


Figure 4.16: USGPPA prototype

in the sub-6 GHz frequencies.

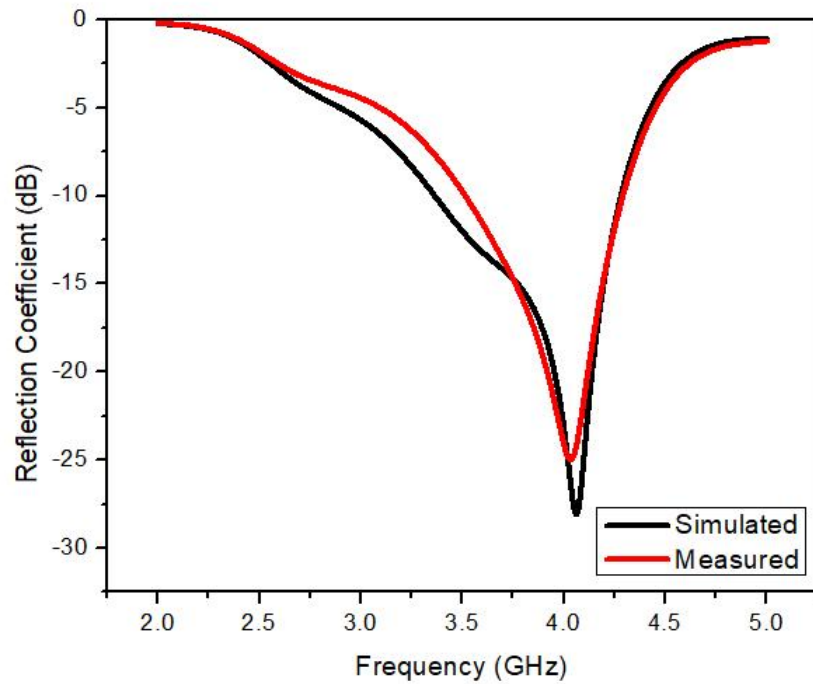


Figure 4.17: Comparative analysis of the output characteristics of the USGPPA retrieved from the simulation and experimental set-up.

The simulation and the measurement characteristics are compared in the Table 4.9 for the USGPPA design. It clearly indicates that this design exhibits good amount of gain and bandwidth which makes it best suitable for the targeted sub-6 GHz applications.

According to the analysis shown in the Table 4.9, the measured results are vir-

Table 4.9: Comparison of the output characteristics retrieved from the simulation and the measurements for the proposed USGPPA.

Parameters	Simulated results	Measured results
Lower cut off frequency (f_1)	3.38 GHz	3.48 GHz
Higher cut off frequency (f_2)	4.28 GHz	4.28 GHz
Bandwidth	900 MHz	800 MHz
Min. reflection coefficient (dB)	-28.15 dB	-26.18 dB
Gain	3.8 dB	3.6 dB

tually identical to the simulated findings, and the antenna so constructed may be utilized for the wideband applications in the sub-6 GHz 5G spectrum.

As a result of its single layer construction, low complexity, and tiny size, this antenna design stands out in the sub-6 GHz 5G NR band. The design holds viable with the originality and compactness compared to the existing designs is reported in the Table 4.10 as shown below.

Table 4.10: Comparison of USGPPA design with state of art literature for compactness in sub-6 GHz 5G NR range

Reference	Parameter			
	Patch size (mm × mm)	Bandwidth (GHz)	Resonant frequency (GHz)	Max. gain (dB)
[162]	54.5 × 22	2.6 - 6.0	4.03	~ 7
[163]	50 × 19.75	2.5 - 4.8	3.62	~ 2
[164]	47 × 19	3.2 - 5.1	2.52	~ 3
[165]	40 × 30	3.0 - 5.6	4.32	~ 2
Proposed PSGPPA design	36 × 16	3.3 - 4.0	3.83	~ 2.4
Proposed USGPPA design	36 × 12	3.38 - 4.28	4.00	~ 3.8

4.6 Summary

This chapter gives a brief description of the microstrip patch antenna designs formulated to operate in the sub-6 GHz 5G frequency ranges. Various techniques are included for enhancement of the bandwidth of the microstrip patch antennas by utilizing different shapes of the patches and defected ground geometries. The design, optimization, fabrication, and measurement of the two different conventional rectangular shaped microstrip patch antennas with different defected ground plane geometries are completed. The effect of inserting the various types of slots in form of polygon shaped and a U-shaped are discussed. This chapter is concluded with the comparison of the proposed work with the existing literature.

Chapter 5

Planar Frequency Selective Surface Based Printed Patch Antennas for Sub-6 GHz 5G Applications

In this chapter, the stacked designs comprising of a wideband PPA's (printed patch antennas) and the use of passive spatial filters in the form of PFSSs (planar frequency selective surfaces) are presented. The combination of the two structures in form of a stacked geometry (PPA with PFSS) is helpful for the enhancement of the gain and the directivity. The designs of the compact and miniaturized stacked geometries are illustrated which exhibits the gain and directivity augmentation. These filters help to mitigate the unwanted radiations from reaching the antenna aperture as they have an inherent capacity of passing only desired radiations while eliminating all interfering frequencies. This chapter presents the designs and analysis of the PFSS based PPA structures for operation in the sub-6 GHz 5G spectrum.

5.1 Introduction

Because of its small size, cheaper cost, and greater bandwidth, PPAs are a popular choice for use in sub-6 GHz frequency bands. However, one important disadvantage of using these PPAs is impedance mismatching, which happens when they are placed near metallic objects or electromagnetic equipment. Another drawback of PPAs is that they have limited gain and directivity at lower frequencies in the microwave spectrum. Figure 5.1 depicts a strategy for increasing the efficiency of the PPA by including a layer of PFSS that acts as a spatial filter when replaced in an electromagnetic radiation environment. PFSSs are made up of periodic arrays of conductive materials. When subjected to radio frequency electromagnetic radiations, only a subset of frequencies pass through PFSS, while the remainder are reflected.

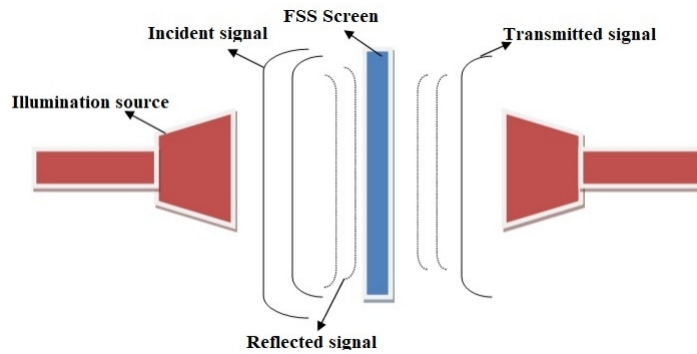


Figure 5.1: Illustration of PFSS based spatial filters in electromagnetic environment.

The PFSS may act as a spatial filter for plane waves and is used in broadband communications, radar systems, and high-performance applications. The characteristics of PFSSs have piqued the researchers' interest in creating and executing numerical synthesis for the stacked layer design consisting of PFSS-based PPA shapes for replacement in sub-6 GHz 5G devices. As shown in Figure 5.2, these stacked architectures are made up of PFSS structures that are incorporated as a superstrate over the antennas.

In this chapter, the designs of the PPA which are formulated in the chapter 4 are integrated with the DSLPFSS geometry of spatial filter as illustrated in the chapter

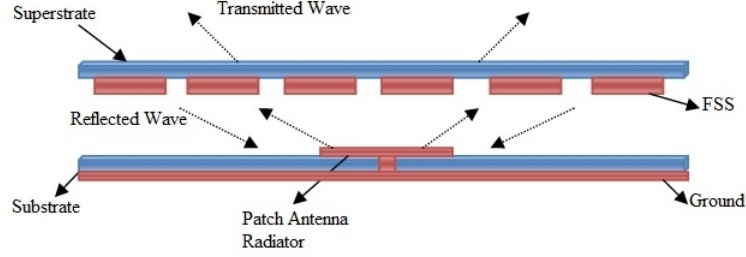


Figure 5.2: Incorporation of PFSS as a superstrate with PPAs.

3. The designs are simulated and validated by generating a design prototype and comparing measured results to modelled ones.

5.2 Design of DSLPFSS based PSGPPA

In this section, the PSGPPA geometry from Chapter 4 is coupled with the proposed DSLPFSS spatial filter as discussed in the Chapter 3. The layered design of DSLPFSS-PSGPPA exhibits the gain and directivity augmentation in comparison to the PSGPPA design with enhancement of the bandwidth. Initially, a conventional PPA design is constructed using standard design formulae's based on transmission line theory. The bandwidth of a standard PPA is insufficient for a wide range of operations and is increased by adding the concept of defected ground. The defected ground is created by reducing its dimensions along the major axis to half of the value and carving an eighteen segment polygon shaped groove within it. The results retrieved show that the bandwidth is enhanced at the expense of gain and directivity of the PSGPPA. To circumvent these constraints, a DSLPFSS is combined with PSGPPA in a layered design. The presented findings indicate that it is an excellent choice for improving the PPA's performance in terms of gain, directivity, and bandwidth. The stacked layer structure of the PSGPPA with DSLPFSS geometry is illustrated in the Figure 5.3 as given below.

The proposed design is divided into two parts: a DSLPFSS-based superstrate and a PSGPPA structure that serves as the radiating source. The compact geometry of

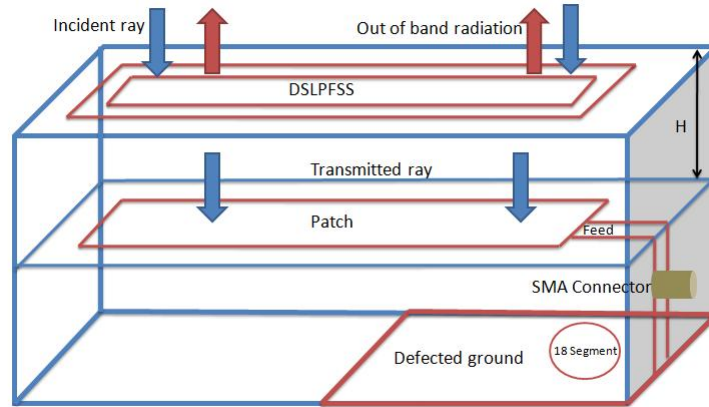


Figure 5.3: DSLPFSS based PSGPPA design.

the single layer DSLPFSS structure is positioned at a height of H above the radiating aperture. The DSLPFSS structure is designed to be placed as a superstrate in the direction of maximum radiation in order to improve the performance characteristics of the proposed structure. ANSYS HFSS software is used to optimize the proposed design, and the peripheral size of the DSLPFSS superstrate layer produced on the FR4 epoxy substrate is fixed at $0.5\lambda \times 0.5\lambda$. The power is sent to the DSLPFSS-based PSGPPA through a SMA connector, which is placed at a distance of $\lambda/30$ from the dielectric centre. The suggested final design geometry is produced by stacking the two layers such that one is on top of the other at a specified height, as shown in Figure 5.3. The DSLPFSS serves as a superstrate and is positioned directly above the radiating aperture. Previous chapters have previously illustrated the creation and analysis of the DSLPFSS and PSGPPA geometries. The PSGPPA and DSLPFSS structures are mounted on a 1.6 mm thick layered FR4 substrate. Transmission line feed is being used to inspire antenna design. In terms of dimensions, the information received from the layered geometry of the DSLPFSS-PSGPPA is described in Table 5.1 below:

Table 5.1: Structural configuration of the DSLPFSS-PSGPPA design.

Parameters	Dimension
Radiator length (l)	0.47λ
Radiator width (w)	0.20λ
Arm length of the square substrate (L_s)	0.50λ
Thickness of the substrate (t_s)	0.47λ
Length of feed (f_l)	0.02λ
Width of feed (f_w)	0.01λ
Ground length (l_g)	0.25λ
Ground width (w_g)	0.50λ
Periodicity of DSLPFSS (p)	0.50λ
Thickness of DSLPFSS outer loop (t_1)	0.06λ
Arm length of the DSLPFSS outer loop (s_1)	0.37λ
Thickness of the DSLPFSS inner loop (t_2)	0.05λ
Arm length of the DSLPFSS inner loop (s_2)	0.17λ
Distance between the PSGPPA and DSLPFSS (H)	0.03λ

5.3 Interpretation of the results for DSLPFSS-PSGPPA design

The parametric optimizations of the dimensions are carried out for the DSLPFSS-PSGPPA design. It is reported that an enhanced bandwidth is retrieved for the DSLPFSS-PSGPPA design with an adequate radiation performances. The results are retrieved from the parametric analysis and are presented in the Table 5.2. The optimization of the antenna parameters is completed by using the parametric sweep option in High Frequency Structure Simulator (HFSS). The analysis for orienting the radiation in the appropriate frequency ranges of operation in the sub-6 GHz 5G frequency range is finished. In the absence of a substrate, the ray tracing technique described in [166] is used to calculate the resonance for the DSLFSS along the

broadside direction. The following formula may be used to compute the resonating length using reflection phases and resonating frequencies:

$$S_{gap} = \frac{p\lambda}{2} + \left[\frac{\psi_{\Gamma}(frequency) + \phi_{\Gamma}(frequency)}{\pi} \right] \frac{\lambda}{4} \quad (5.1)$$

where p can take any integer value such as 1,2,3.....and so on, S_{gap} signifies the spacing in between the DSLPFSS and the ground, ψ_{Γ} represents the value of reflection phase of the DSLPFSS.

ϕ_{Γ} represents the value of the reflection phase exhibited by the ground plane and can be retrieved as:

$$\phi_{\Gamma} \approx \angle \frac{jZ_d \tan(\beta t_s) - Z_o}{jZ_d \tan(\beta t_s) + Z_o} \approx \pi - 2 \tan^{-1}(Z_d \tan(\beta t_s)/Z_o) \quad (5.2)$$

The terms Z_o and Z_d indicate the characteristic impedance's of the air and the dielectric substrate, respectively. The term t_s reflect about the effective dielectric thickness, and it helps to signify the dielectric phase constant.

Table 5.2: Comparison of the output characteristics retrieved from the simulation and the measurements for the proposed USGPPA.

Performance characteristics	Full ground	Half ground	PSGPPA	DSLPFSS PSGPPA
Lower cut off frequency (f_1)	NR	3.75 GHz	3.30 GHz	3.20 GHz
Higher cut off frequency (f_2)	NR	4.15 GHz	4.00 GHz	3.95 GHz
Bandwidth	NR	0.4 GHz	0.7 GHz	0.75 GHz ↑
Fractional bandwidth	NR	17.73 %	19.16 %	20.96 %
Gain	NR	4.12 dB	2.5 dB	5.5 dB ↑
Directivity	NR	5.21 dB	3.21 dB	6.2 dB ↑
Radiation efficiency	NR	80.66%	83.63%	87.32% ↑

Table 5.2 indicates that the bandwidth is increased as well as augmentation of the gain and directivity values are experienced. The results show that this proposed design is a feasible small structure for usage in high performance wideband applications in the sub-6 GHz 5G spectrum.

5.3.1 Reflection coefficient variation with design iterations

The comparative analysis is carried out for all the design iterations of the PPA and the stacked geometry as visualized in Figure 5.4. The design of a basic conventional PPA as proposed in the earlier chapter resonates at 4.03 GHz. The only limitation of this design was in form of its radiation which is limited to near field region with maximum value of - 9.50 dB. By decreasing the size of the ground plane throughout its length, the radiation properties are enhanced. It is also stated that when the dimensions are perfectly cut in half, the PPA pattern begins to radiate. The reflection coefficient touches to maximum value of -33 dB which is quite good in terms of the radiation. The structure starts resonating at 3890 MHz with a bandwidth of nearly 0.25 GHz, which is not adequate to be used in wideband applications. Further, for increasing the bandwidth in the far field region of the proposed design structure, a polygon slot is engraved within the ground plane on which further iterations are being performed. The best results in terms of wide bandwidth are retrieved when the number of the segments is set up to the value of 18. The antenna starts resonating at 3360 MHz with a bandwidth of 0.72 GHz and a maximum reflection coefficient of -31.15 dB. As the DSLPFSS layer is placed as a superstrate above the radiating PSGPPA structure, the unwanted radiations are mitigated. It helps to increase the overall gain and the directivity of the radiating stacked structure along with maintaining a wide bandwidth. The stacked structure resonates with centre frequency of 3750 MHz with a maximum reflection coefficient of -33 dB. The comparative study of the reflection coefficient curves retrieved from all the iterations is illustrated in the Figure 5.4. The DSLPFSS-PSGPPA design exhibits a broad bandwidth of 0.75 GHz

which makes it suitable for wideband applications. According to the data reported in the Table 5.2, a sufficient amount of large bandwidth is maintained by the designs of the PSGPPA and the stacked geometry. The distance of the DSLPFSS layer as a superstrate is crucial while constructing the stacked geometry. The more nearby is the DSLPFSS towards the PSGPPA, the more interference is experienced by the radiator. Also, if the distance of the superstrate is increased, the losses further increases which deteriorate the performance. Hence, the distance of the superstrate above the PSGPPA must be carefully fixed.

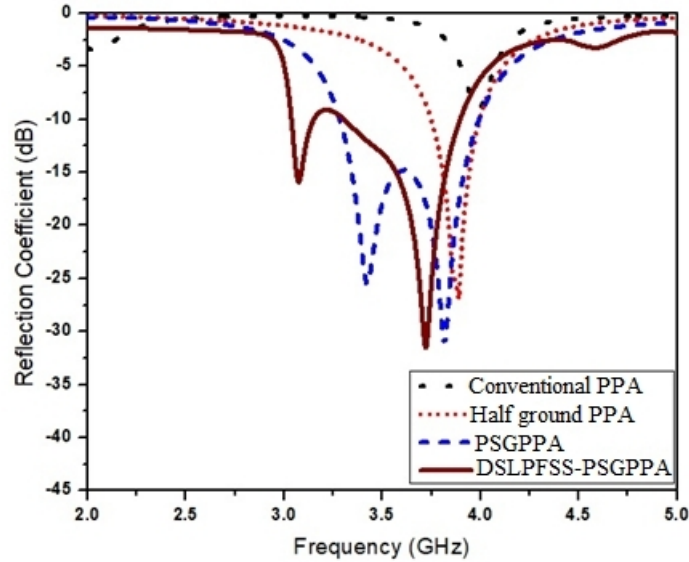


Figure 5.4: Comparison of the radiation region covered by the various designs in terms of the reflection coefficient response versus frequency.

5.3.2 Radiation intensity

The quantity of energy released by the PPA is described by radiation intensity, which is a significant measure. Figure 5.5 depicts a comparison of the radiation patterns in the E and H planes for the design of stacked geometry of DSLPFSS-based PSGPPA at 3.75 GHz resonating frequency, respectively. Figure 5.5 illustrates the observed radiation patterns in the E-plane and H-plane for the PSGPPA designs with and without the DSLPFSS superstrate. The model demonstrates a considerable

difference in both the main beam and the inner lobes. When compared to the PSGPPA design, the proposed device improves gain by 3 dB with a single DSLPFSS superstrate. The design structure has dumbbell-shaped omnidirectional radiation patterns in the E-plane and H-plane.

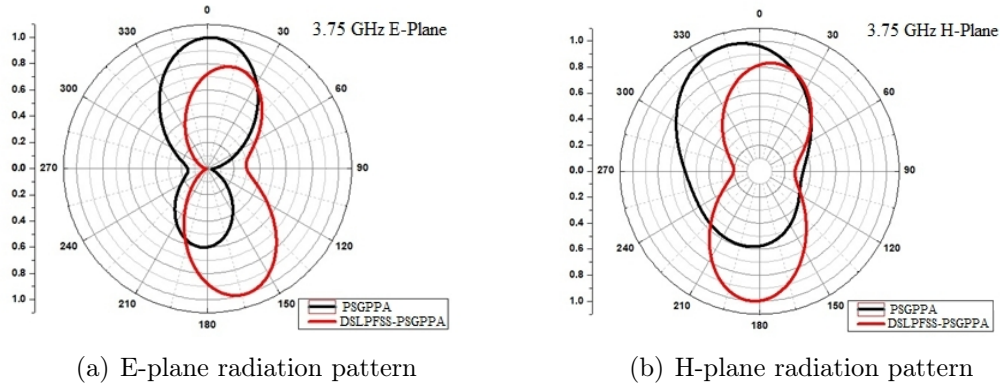


Figure 5.5: Comparative analysis of the radiation patterns retrieved from the PSGPPA with and without incorporation of the DSLPFSS superstrate at the 3.75 GHz resonant frequency

The radiation pattern is recovered after HFSS software simulations, with the highest gain reported to be 5.5 dBi at 3.75 GHz for DSLPFSS-PSGPPA.

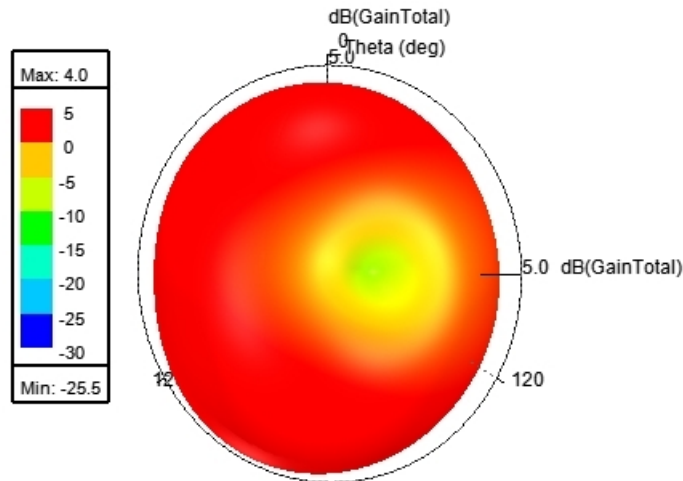


Figure 5.6: 3D polar plot depicting the gains exhibited by of DSLPFSS-PSGPPA.

5.3.3 Gain and Efficiency

The gain of a printed patch antenna is its capacity to transmit more or less in any direction. In reality, the printed patch's spherical shape radiates evenly in all directions, making it an isotropic antenna. Although, it does not exist in reality but it is utilized to compare the gain of actual antennas. In addition, an antenna's efficiency is defined as the ratio of power supplied to power radiated by the printed patch antenna. The bulk of the power present at the input is radiated out through a high efficiency antenna. Also, the majority of the power is absorbed or reflected in a low efficiency antenna owing to impedance mismatch. Figure 5.6 clearly shows that the gain of the PSGPPA increases by the substitution of DSLPFSS as a superstrate as illustrated by stacked geometry. The design of DSLPFSS-PSGPPA offers an enhanced gain and directivity along with bandwidth augmentation which makes it feasible to be utilized in the 5G applications. Also, the amount of radiation efficiency is nearly 85% which indicates that very less amount of radiation losses occurs during the process of the radiation as indicated in the Figure 5.7 .

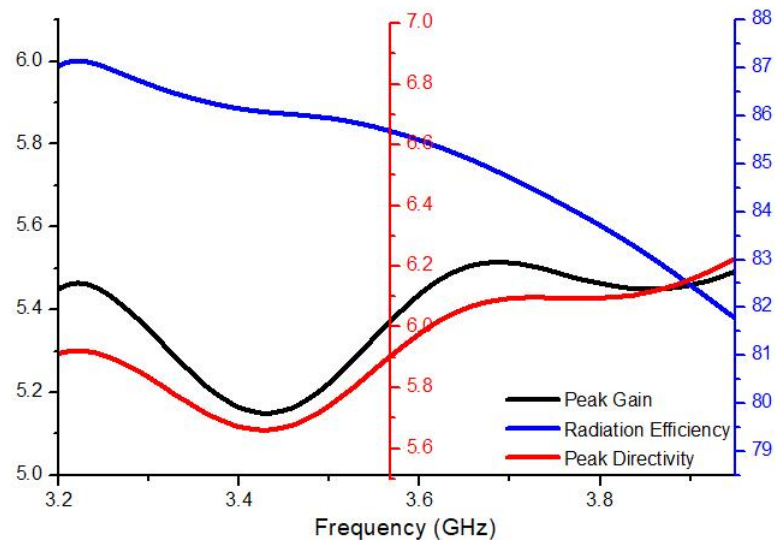


Figure 5.7: Graphical illustration of the gain (dB), directivity (dB) and the radiation efficiency (%) exhibited by the DSLPFSS-PSGPPA design.

The distance between the PSGPPA radiator and the DSLPFSS structure plays a

crucial part in obtaining spatial filtering of the unwanted signals. The distance which is denoted by H is optimized by using the parametric analysis, and the variance in the results is reported in form of variation in the output characteristics. The radiation behavior of the stacked geometry is reported in the Figure 5.8 by varying the distance of the DSLPFSS superstrate. Going beyond $H = 0.03\lambda$, narrows the bandwidth which is undesirable. The ideal distance between the PSGPPA design and the DSLPFSS superstrate is determined by the values at which a sufficient improvement in gain and directivity may be achieved along with the bandwidth and it comes out to be $H = 0.03\lambda$.

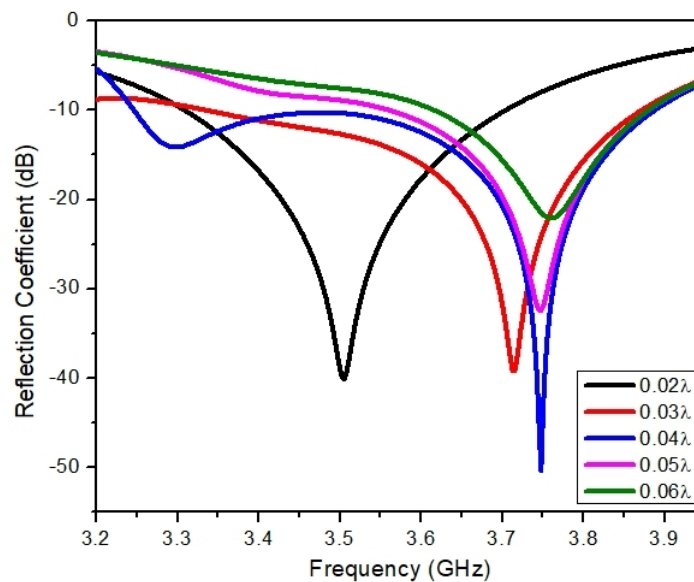


Figure 5.8: Response of the reflection coefficient (dB) with respect to effective height between PSGPPA and DSLPFSS superstrate for the stacked design.

Figure 5.9 and Figure 5.10 indicate that the gain and directivity of the stacked design is varied by varying the height of the DSLPFSS superstrate above the PSGPPA. It is clearly visible that by keeping DSLPFSS structure at a distance of 0.03λ , it is able to retrieve an adequate wide bandwidth and high gain up to 5dB maximum value.

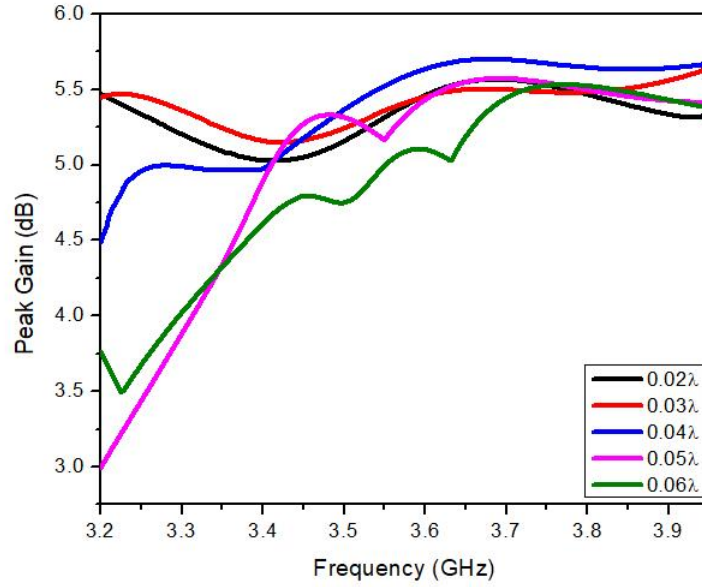


Figure 5.9: Variation in the gain of the stacked design by placing DSLPFSS superstrate at different distance above PSGPPA.

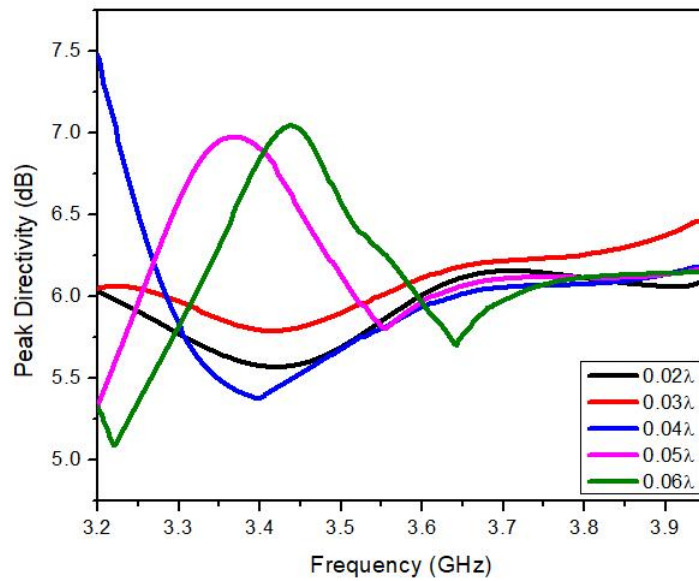


Figure 5.10: Variation in the directivity of the stacked design by placing DSLPFSS superstrate at different distances above the PSGPPA.

5.4 Experimental investigation of the stacked DSLPFSS-PSGPPA design.

In the preceding section, a design of the DSLPFSS-PSGPPA is provided and is modeled for the extraction of output radiation characteristics in the desired sub-6

GHz frequency range. To validate these results, a prototype is formulated of the DSLPFSS-PSGPPA geometry, and the measurements are performed by using vector network analyzer (VNA). The MS2037C and accompanying setup are used to test antenna parameters such as reflection coefficient, radiation pattern, and the gain. The radiation characteristics are measured by using a MS 2037C Network analyzer. Vector network analyzers, anechoic chambers, automated turn tables, and other essential technologies are utilized for antenna characterization. MS 2037C is a powerful Vector Network Analyzer (VNA) from Anritsu which has a capability of operation in both the time domain and the frequency domain. The VNA is a microprocessor-based device that can precisely measure the two port network characteristics as scattering parameters. The network analyzer's built-in signal conditioning algorithms assist in sending and receiving data to the radiator before eventually showing the measured values in the form of graphical graphs. In addition, the anechoic chamber provides a "quiet zone" devoid of electromagnetic reflections. All antenna characterizations are carried out in an anechoic chamber to remove reflections from neighboring objects. It's a massive room in comparison to the operational wave length, with microwave absorbers attached to the walls, ceiling, and floor to decrease EM reflections. Figure 5.11 illustrates the orientation of the DSLPFSS layer over the PSGPPA geometry.

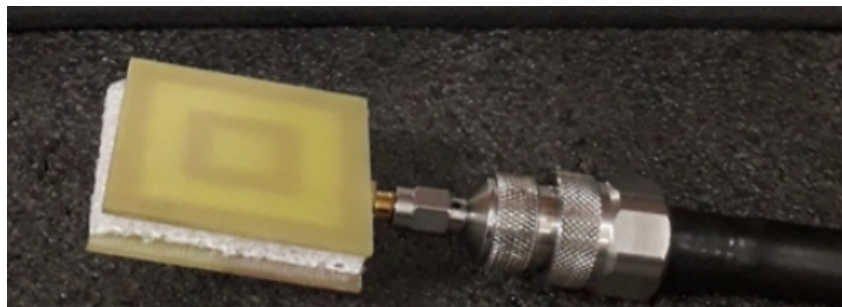


Figure 5.11: Orientation of the DSLPFSS layer over the PSGPPA geometry

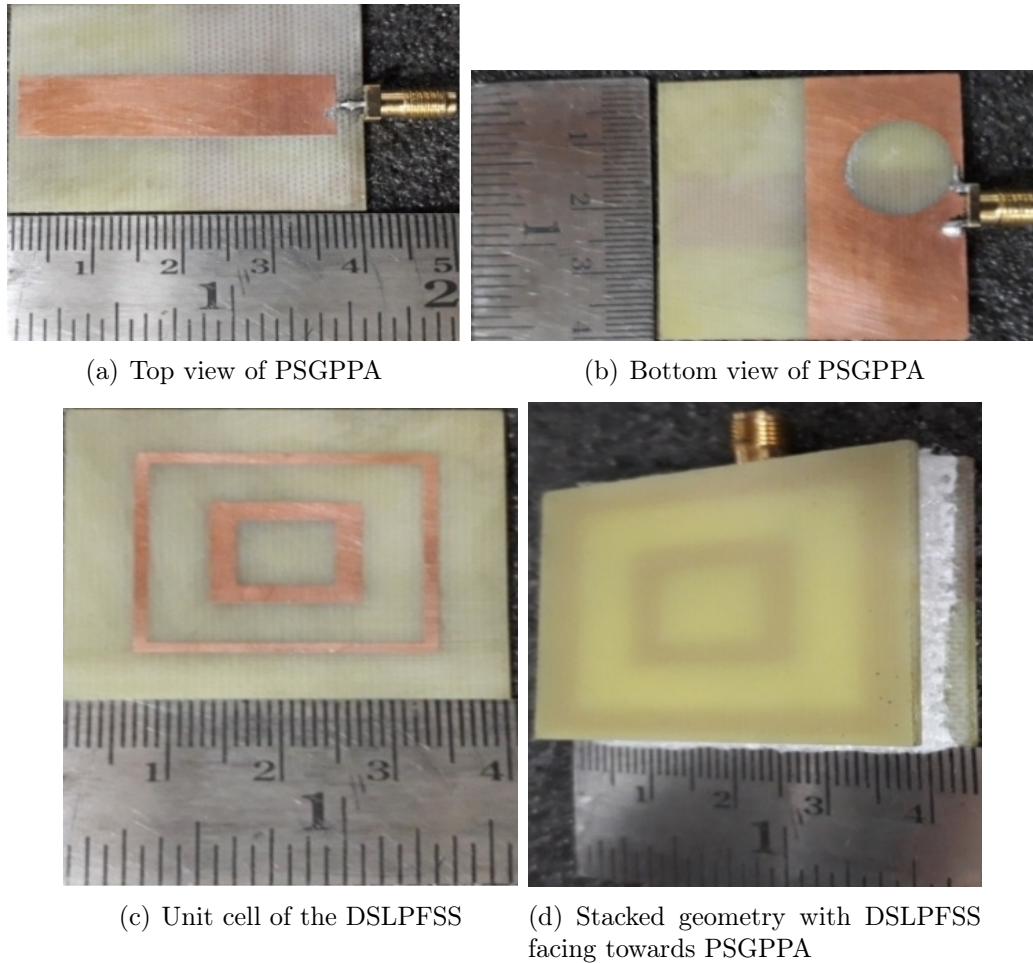


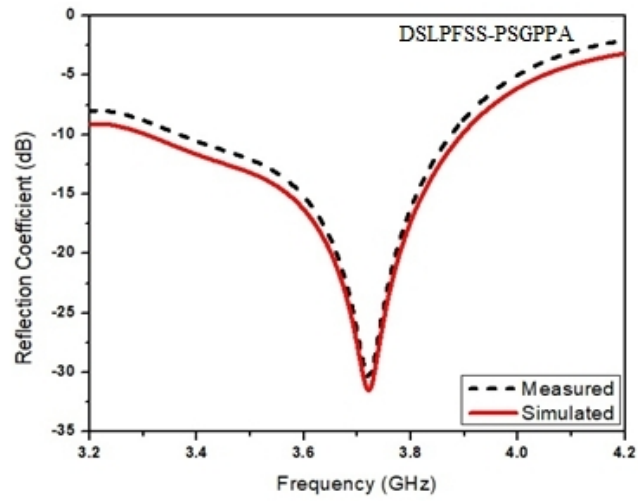
Figure 5.12: Illustration of the design prototypes of PSGPPA and DSLPFSS

5.5 Validation of measured results with simulation

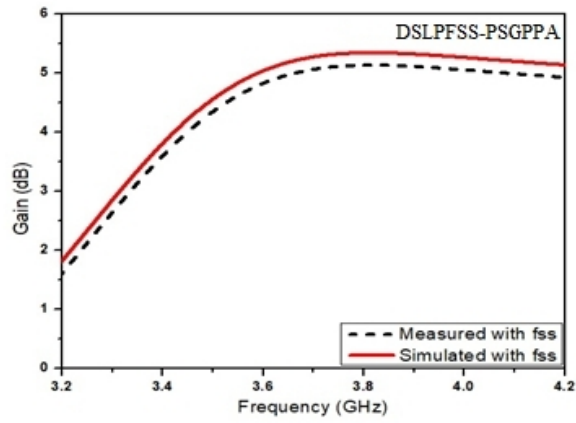
The measured findings are compared with the simulated results in terms of graphical plots of output characteristics such as reflection coefficient, gain, and directivity as shown in the Figure 5.13. The measured results are almost identical to the modelling results as reported for the stacked design of the DSLPFSS - PSGPPA.

The performance parameters are validated by evaluating the output performances of the constructed designed stacking antenna with the modeled design structure, as shown in Table 5.3.

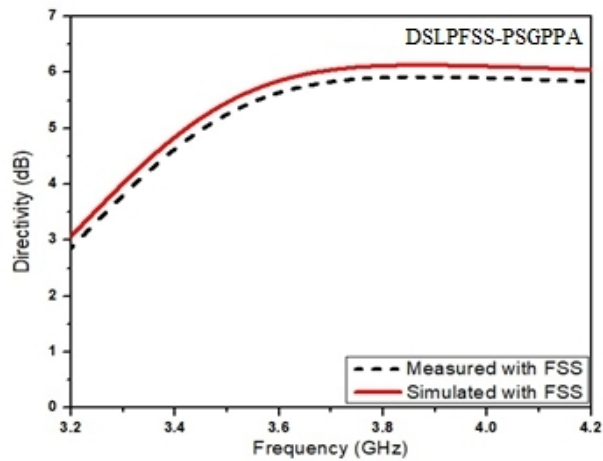
As a result, the double layered stacked architecture of PSGPPA with DSLPFSS has the benefit of being compact and exhibiting superior performance for broadband applications.



(a) Reflection coefficient



(b) Gain



(c) Directivity

Figure 5.13: Validation of the results retrieved from the experimental set-up and through modeling

Table 5.3: Experimental results compared with modeled design for DSLPFSS-PSGPPA.

Parameters	Modeled value (Stacked design)	Experimental value (Stacked design)
Lower cut off frequency (f_1)	3.20 GHz	3.22 GHz
Higher cut off frequency (f_2)	3.95 GHz	3.93 GHz
Bandwidth	750 MHz	710 MHz
Fractional bandwidth	20.97%	19.86%
Maximum gain	5.5 dB	5.3 dB
Maximum directivity	6.2 dB	5.9 dB

5.6 Design of DSLPFSS based USGPPA

In this section, the USGPPA geometry mentioned in Chapter 4 is combined with the proposed DSLPFSS spatial filter, which was described in Chapter 3. The DSLPFSS shape is created in an upside-down position, with the printed edge facing outwards. The effect of reversing the DSLPFSS geometry's orientation is visualised and reported. In comparison to the design of the USGPPA, the layered design of the DSLPFSS-USGPPA exhibits the gain and directivity augmentation with a sufficient increase in the bandwidth. Initially, a typical PPA is built in the n77 and n78 frequency bands of the sub-6 GHz 5G microwave spectrum. A standard PPA's bandwidth is insufficient for a wide range of operations. The defective ground is made by decreasing the dimensions along the primary axis to half the value and cutting a U-slot groove inside it. The experimental results obtained from the experimental setup show that the bandwidth is increased at the expense of the gain and directivity of the USGPPA's. In order to overcome these limitations, a DSLPFSS is combined with USGPPA in a layered design. According to the findings, it is an

excellent choice for improving the PPA's performance in terms of active parameters such as gain, directivity, and bandwidth. The footprint of the USGPPA's stacked layer structure with DSLPFSS geometry is depicted in Figure 5.14 below.

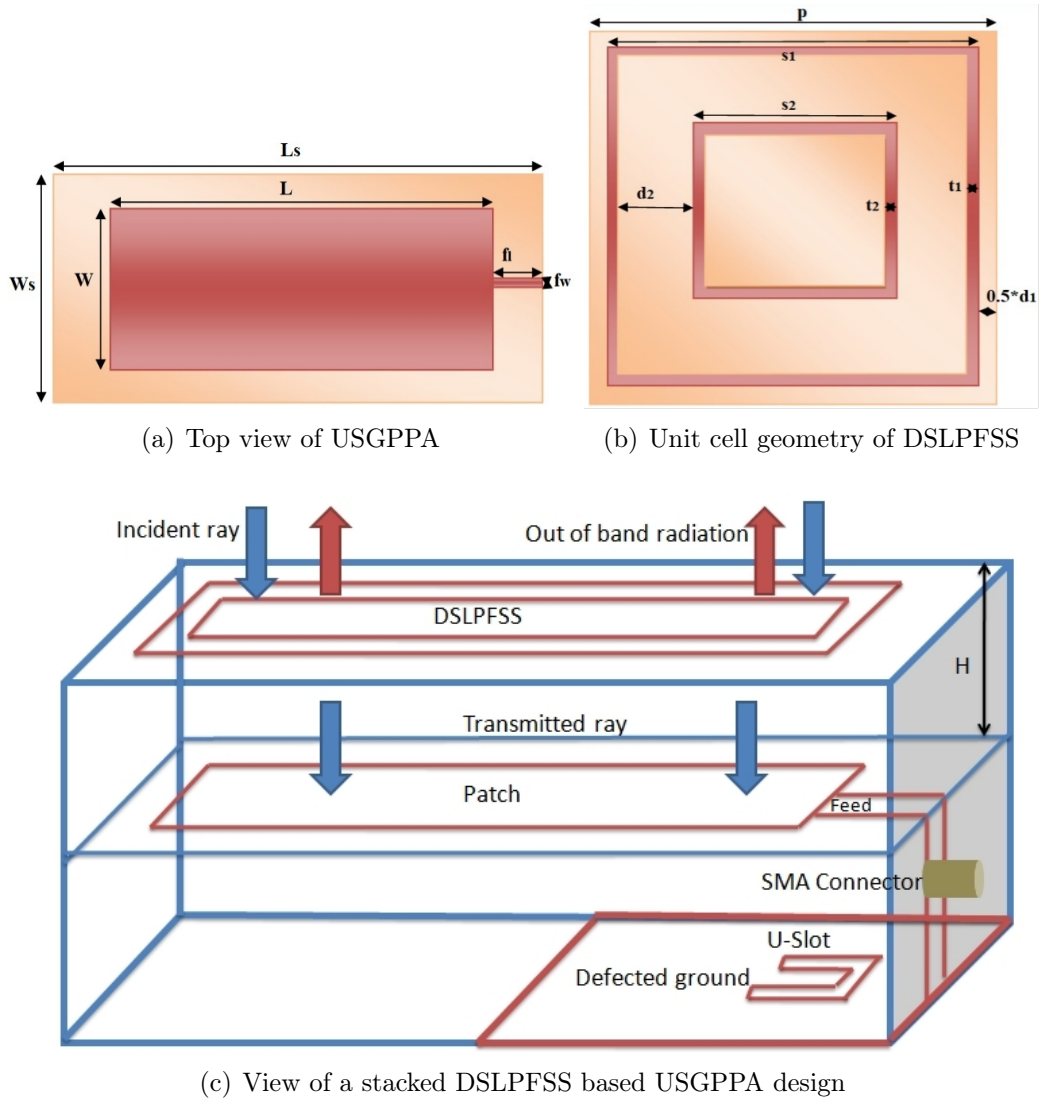


Figure 5.14: Proposed designs of USGPPA and DSLPFSS

Figure 5.14 depicts the recommended stacking shape of a high performance DSLPFSS-USGPPA structure. The proposed design is divided into two parts: a DSLPFSS-based superstrate and a USGPPA structure that serves as the radiating source. The compact geometry of the single layer DSLPFSS structure is positioned at a height of H above the radiating aperture. The DSLPFSS structure is designed to be placed as a superstrate in the direction of maximum radiation in order to improve the performance characteristics of the proposed structure. ANSYS HFSS

software is used to optimize the proposed design, and the peripheral size of the DSLPFSS superstrate layer produced on the FR4 epoxy substrate is fixed at $0.5\lambda \times 0.5\lambda$. The radiation energy is delivered to the DSLPFSS-based PSGPPA through a SMA connector located at $\lambda/30$ from the dielectric centre. The suggested final design geometry is produced by stacking the two layers such that one is on top of the other at a specified height H , as shown in Figure 5.14 (c). The DSLPFSS is substituted as a superstrate and is placed just above the radiating aperture such that the printed side faces outwards. The design and analysis of the DSLPFSS and USGPPA geometries have been already demonstrated in previous chapters. The USGPPA and DSLPFSS structures are placed on a 1.6 mm layered FR4 substrate. To stimulate the antenna design, transmission line feed is being employed. The information retrieved from the stacked geometry of the DSLPFSS-USGPPA in terms of the dimensions is described in the Table 5.4 as given below.

In the Table 5.4, all the dimensions are given in terms of λ , which indicates the wavelength acquired at the operating range's centre frequency.

5.6.1 Reflection coefficient variation with design iterations

A statistical comparison is performed for the acquired results in respect of the reflection coefficient behavior. The variations are indicated for all the design iterations consisting of complete ground, half ground, and a deficient ground consisting of a U-slot is depicted in the Figure 5.15. The graphical plot shows that the USGPPA begins to radiate at a half ground structure, and the bandwidth is then increased by engraving a U-slot inside the half ground, as shown in Figure 5.15.

The further enhancement of the bandwidth is completed by placing the DSLPFSS as a superstrate above the designed USGPPA geometry. The bandwidth of the operation increases as the DSLPFSS layer is placed as a superstrate above the radiating aperture. The impedance bandwidth of designed USGPPA without DSLPFSS is 0.76 GHz (3.48 GHz-4.24 GHz) whereas with the presence of it the value is increased to

Table 5.4: Geometrical configuration of the DSLPFSS with USGPPA.

Parameters	Dimension
USGPPA length (l)	0.46λ
USGPPA width (w) (w)	0.15λ
Arm length of the square substrate (L_s)	0.51λ
Distance of DSLPFSS from USGPPA	0.07λ
Thickness of the substrate (t_s)	0.02λ
Length of feedline (f_l)	0.02λ
Width of feedline (f_w)	0.01λ
Ground plane length for USGPPA (l_g)	0.25λ
Ground plane width for USGPPA (w_g)	0.51λ
U-slot x length (U_x)	0.20λ
U-slot y length (U_y)	0.20λ
U-slot thickness (U_t)	0.02λ
Periodicity of DSLPFSS (p)	0.51λ
Thickness of outermost loop of DSLPFSS (t_1)	0.03λ
Arm length of the outermost loop of DSLPFSS (s_1)	0.35λ
Thickness of the innermost loop of DSLPFSS (t_2)	0.06λ
Arm length of the innermost loop of DSLPFSS (s_2)	0.18λ
Distance of the DSLPFSS above the USGPPA (H)	0.07λ

1.03 GHz (3.20 GHz-4.23 GHz). The increased bandwidth with DSLPFSS gives an added advantage. The height between the radiator and the DSLPFSS is optimized to 0.07λ for ensuring the maximum impedance bandwidth. The impedance bandwidth is increased to 25%, which makes its suitable for wide band applications. The comparison of the impedance bandwidth is extracted from the graph of reflection coefficient with respect to frequency and is illustrated in the Figure 5.16.

The parameters of the ground plane for the intended USGPPA design are adjusted over iterations, and Figure 5.13(a) clearly shows that the bandwidth of the suggested USGPPA design has increased. Previous research and literature indicate

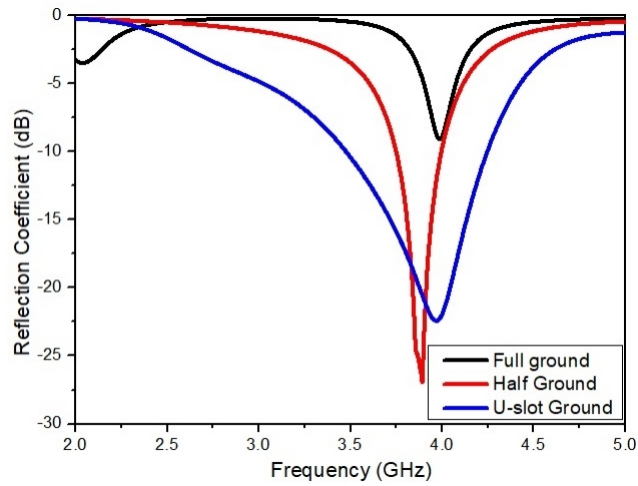


Figure 5.15: Comparative illustration of the reflection coefficients obtained from the three design iterations for making USGPPA.

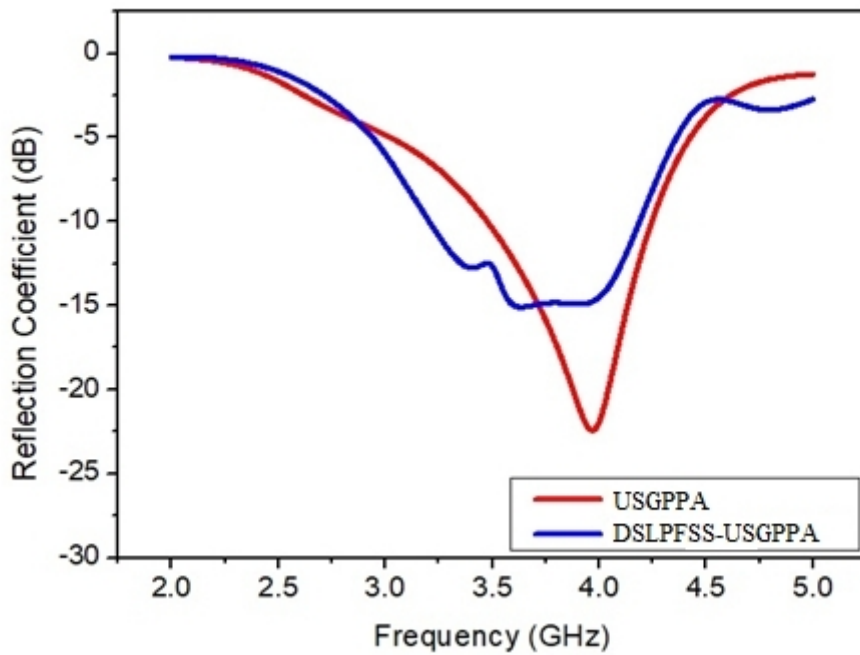


Figure 5.16: Comparative analysis of the impedance bandwidth retrieved from the geometry of USGPPA with and without DSLPFSS reflector.

that lowering the gain is likely to increase the value of the bandwidth. As a consequence, a sufficiently high value of each of these characteristics is required for the construction of an effective patch radiator, which would be used in a broad range of 5G enabled devices. Furthermore, while optimizing the dimensions, the overall

aperture area of the radiator is a significant parameter that must be addressed. The values of the output performance attributes derived from all the design iterations is illustrated in the Table 5.5. It clearly shows that bandwidth augmentation is depicted for the proposed antenna design by introducing a U-slot and the gain is increased on placement of DSLPFSS as a superstrate.

Table 5.5: Comparative analysis of the output performance parameters retrieved from the design iterations comprising of full ground, half ground, U-slot defected ground and with DSLPFSS-USGPPA.

Performance characteristics	Full ground	Half ground	Defected ground (U-slot)	DSLPFSS USGPPA
Lower cut off frequency (f_1)	Not radiating	3.73 GHz	3.48 GHz	3.20 GHz
Higher cut off frequency (f_2)	Not radiating	4.12 GHz	4.24 GHz	4.23 GHz
Bandwidth	Not radiating	390 MHz	760 MHz	1030 MHz ↑
Fractional bandwidth	Not radiating	9.93 %	19.68 %	27.72 % ↑
Gain	Not radiating	3.8 dB	3.3 dB	5 dB ↑
Directivity	Not radiating	4.4 dB	3.8 dB	6.3 dB ↑
Radiation efficiency	Not radiating	83.61%	83.42%	86.23% ↑

5.6.2 Gain and Efficiency

As per the data retrieved from the graphical representation presented in the Figure 5.16 and the values of the output characteristics as reported in the Table 5.6, an augmentation is reported in all the output characteristics. The peak gain and peak directivity of USGPPA geometry with and without the incorporation of the DSLPFSS layer are shown in the Figure 5.17 and the Figure 5.18 respectively. The peak gain and directivity of the USGPPA comes out to be 3.3 dBi and 3.8 dBi.

When the DSLPFSS is introduced above the radiator, the net amount of the gain of the stacked geometry is improved to 5.4 dBi and directivity reaches the value of 6.5 dBi. So, there is a gain improvement of 2.1 dBi and directivity improvement of 2.7 dBi.

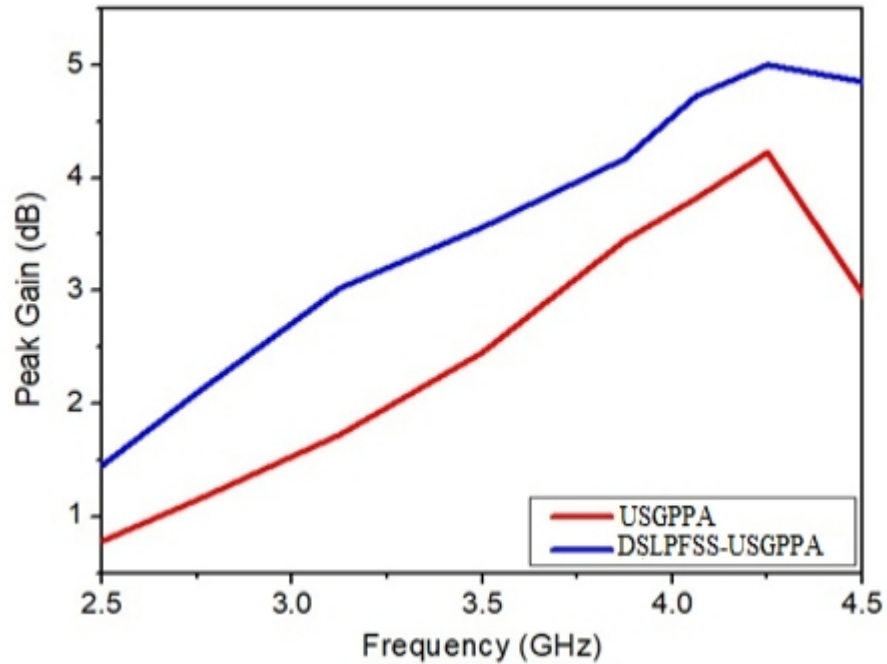


Figure 5.17: Comparison of the maximum gain of the USGPPA with and without the DSLPFSS.

Also, the amount of radiation efficiency is nearly 86% which indicates that very less amount of radiation losses occurs during the process of the radiation as indicated in the Figure 5.19.

5.6.3 Radiation intensity

The radiation patterns of the USGPPA with and without DSLPFSS are illustrated in the Figure 5.20. The radiation patterns are reported at 3.6 GHz, 3.8 GHz and 4.0 GHz of resonant frequency. An omnidirectional radiation pattern is visualized in the E-plane and the bidirectional radiation pattern is seen in the H-plane. It is clearly visible that the radiation patterns become more directional with the introduction of

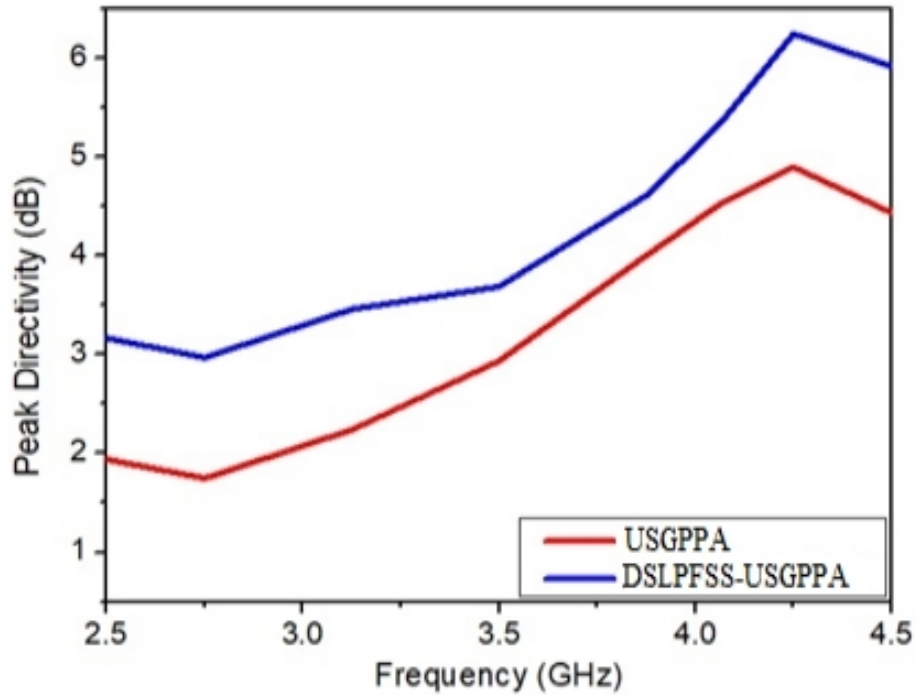


Figure 5.18: Comparison of the maximum directivity of the USGPPA with and without the DSLPFSS.

the DSLPFSS.

5.7 Parametric analysis of the height of stacked geometry

Practical applications necessitate a wideband output with acceptable gain and directivity characteristics. The proposed design of the DSLPFSS helps in enhancing the gain and directivity of the USGPPA structure when applied as a superstrate with the antenna. The DSLPFSS geometry is positioned as a superstrate in the stacked antenna design to allow it to pass only necessary radiations while blocking or scattering the out of band radiations. As the frequency of the incident signal is increased, it leads to enhancement in the phase of the antenna's radiated wave oriented towards the DSLPFSS. It is to be taken into account that the phase of the

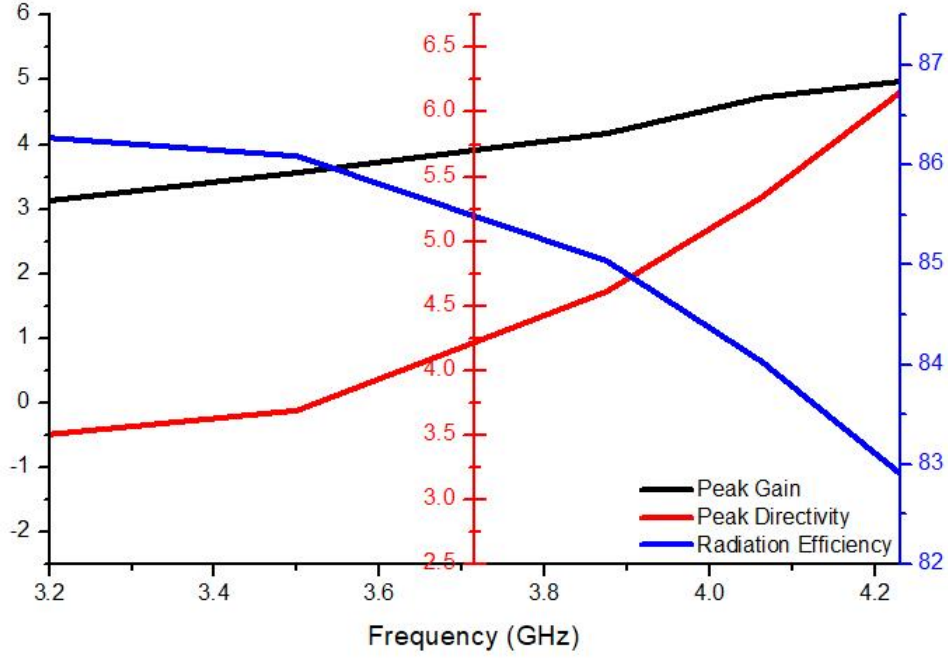
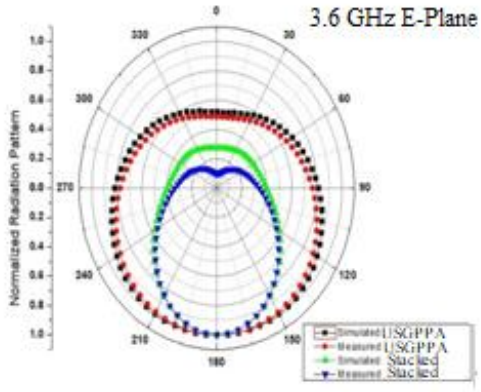


Figure 5.19: Graphical illustration of the maximum gain (dB), maximum directivity (dB) and the radiation efficiency (%) exhibited by the DSLPFSS-USGPPA design.

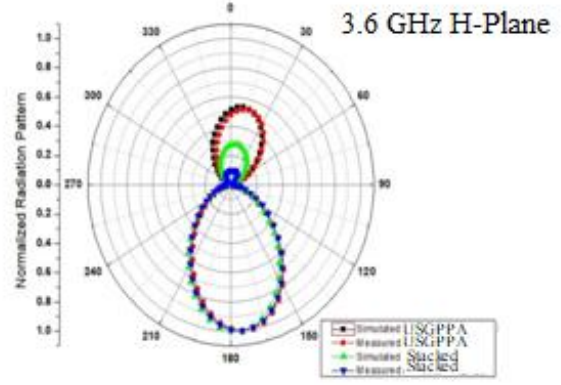
reflected waves from the DSLPFSS must decrease with the increase in frequency for ensuring constructive interference at the patch radiator plane. The distance at which the DSLPFSS structure is placed as a superstrate above the rectangular patch radiator plane is an important factor for evaluating the condition of the constructive interference. The value of the distance at which DSLPFSS is placed above the USGPPA is approximated by the following standardized equation equation (5.3):

$$\Gamma_{FSS} - 2\beta H = 2m\pi \text{ where } m = -, -, -, -2, -1, 0, 1, 2, -, -, - \quad (5.3)$$

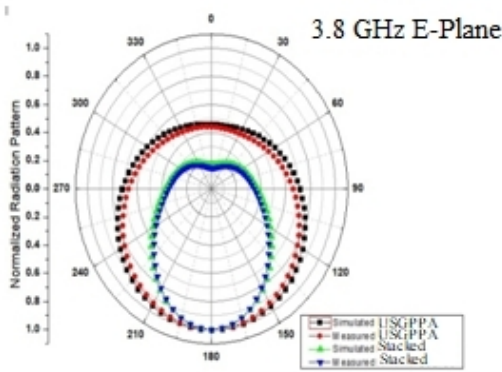
Γ_{FSS} denotes the reflection phase introduced by the DSLPFSS, 'H' signifies the value of the distance between the FSS reflector and the antenna, and the parameter β denotes the propagation constant of free space. In the absence of a substrate, the ray tracing method is used to calculate the resonance in the broadside direction. It is also feasible to calculate the estimated distance between DSLPFSS and the USGPPA radiator, which may be expressed in terms of reflection phase coefficients



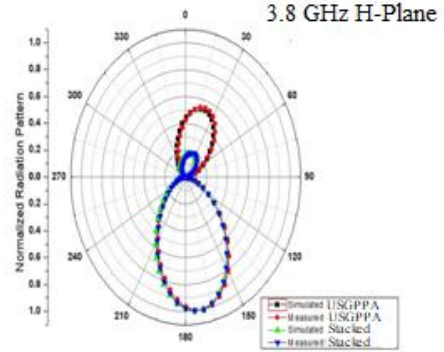
(a) 3.6 GHz E-Plane



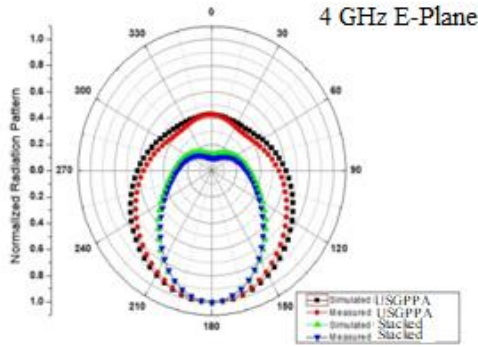
(b) 3.6 GHz H-Plane



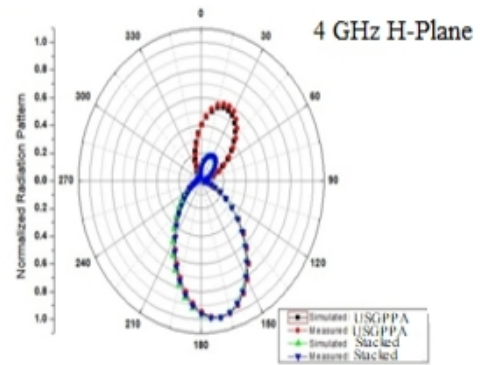
(c) 3.8 GHz E-Plane



(d) 3.8 GHz H-Plane



(e) 4 GHz E-Plane



(f) 4 GHz H-Plane

Figure 5.20: Graphical illustration of the radiation patterns for the USGPPA with and without DSLPFSS

and the wavelengths at the resonating frequencies as in equation (5.4):

$$D_{airgap} = \frac{N\lambda}{2} + \left[\frac{\Delta_{\lambda}(frequency) + \beta_{\lambda}(frequency)}{\pi} \right] \frac{\lambda}{4} \quad (5.4)$$

where N attains any integer number such as 1,2,3..... and so on, D_{airgap} represents the distance in between the DSLPFSS and the ground plane, Δ_λ signifies the value of the reflection phase coefficient of the DSLPFSS and can be derived from Figure 5.21, whereas β_λ denotes the reflection phase coefficient of the ground plane and may be obtained as:

$$\beta_\lambda \iff \angle \frac{jZ_d \tan(\psi t_s) - Z_o}{jZ_d \tan(\psi t_s) + Z_o} = \pi - 2 \tan^{-1}(Z_d \tan(\psi t_s)/Z_o) \quad (5.5)$$

where the terms Z_o indicates the value of the free space, Z_d denotes the values of the characteristic impedance inside a dielectric substrate respectively, t_s signifies the thickness of the dielectric substrate and ψ denotes the phase constant of the dielectric substrate. The reflection coefficient (Γ) for the unit cell of the DSLPFSS geometry at the resonance condition is depicted in the The height of the DSLPFSS structure which is placed as a superstrate above the USGPPA is optimized by performing parametric analysis and the variation in the results are reported as extracted from the stacked design. The enhancement in the output performance characteristics of the USGPPA design by variation of the effective distance (H) at which the DSLPFSS layer is placed is illustrated in the Figure 22. It is clearly visualized that a wide bandwidth of more than 500 MHz is achieved by going beyond $H = 0.064\lambda$. The optimal distance between the USGPPA design and the DSLPFSS superstrate is fixed and is based upon the values at which an adequate increase in the gain and directivity is experienced and comes out to be $H = 0.077\lambda$. . It is extracted that the reflection coefficient attains value of less than 0.6 in the frequency band ranging from 3.3 GHz to 5 GHz. Hence, these double square loops metallic patterns engraved on a dielectric substrate will act as transmitters in the desired band and reflectors in out of band frequencies.

The height of the DSLPFSS structure which is placed as a superstrate above the USGPPA is optimized by performing parametric analysis and the variation in

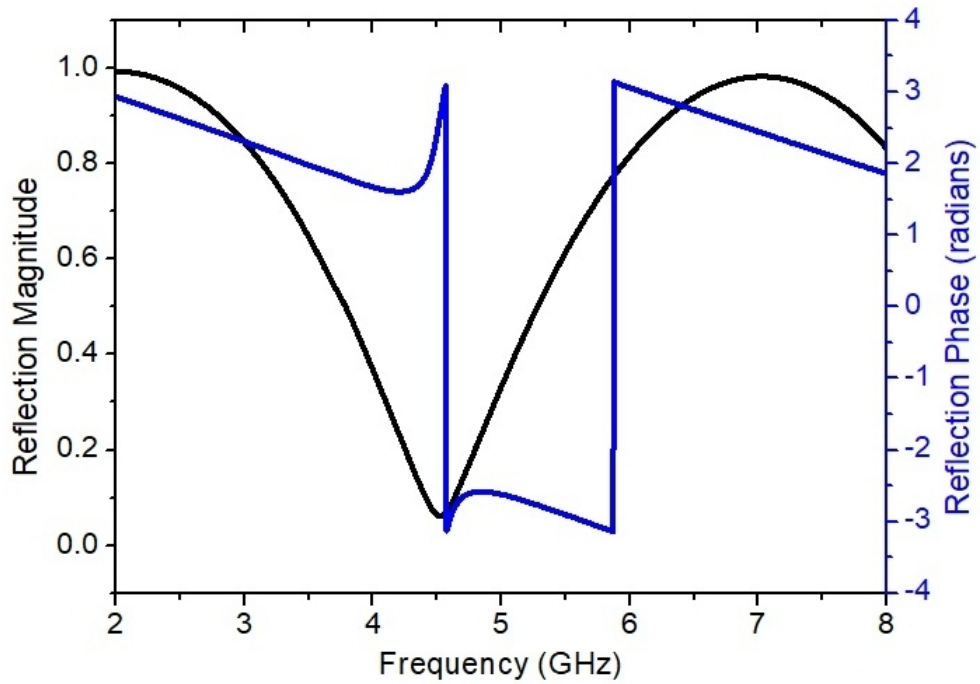


Figure 5.21: Net Magnitude and phase of the reflection coefficient for the unit cell of DSLPFSS.

the results are reported as extracted from the stacked design. The enhancement in the output performance characteristics of the USGPPA design by variation of the effective distance (H) at which the DSLPFSS layer is placed is illustrated in the Figure 5.22. It is clearly visualized that a wide bandwidth of more than 500 MHz is achieved by going beyond $H = 0.064\lambda$. The optimal distance between the USGPPA design and the DSLPFSS superstrate is fixed and is based upon the values at which an adequate increase in the gain and directivity is experienced and comes out to be $H = 0.077\lambda$.

Figure 5.23 and Figure 5.24 indicate that the gain and directivity of the stacked design is varied by varying the height of the DSLPFSS superstrate above the USGPPA. It is clearly visible that by keeping DSLPFSS structure at a distance of $H = 0.07\lambda$, it is able to retrieve an adequate wide bandwidth and high gain up to 5dB maximum value.

Another important characteristic of the USGPPA is its directivity. The directivity of the proposed USGPPA design attains value of 3.8 dB (reference) as reported.

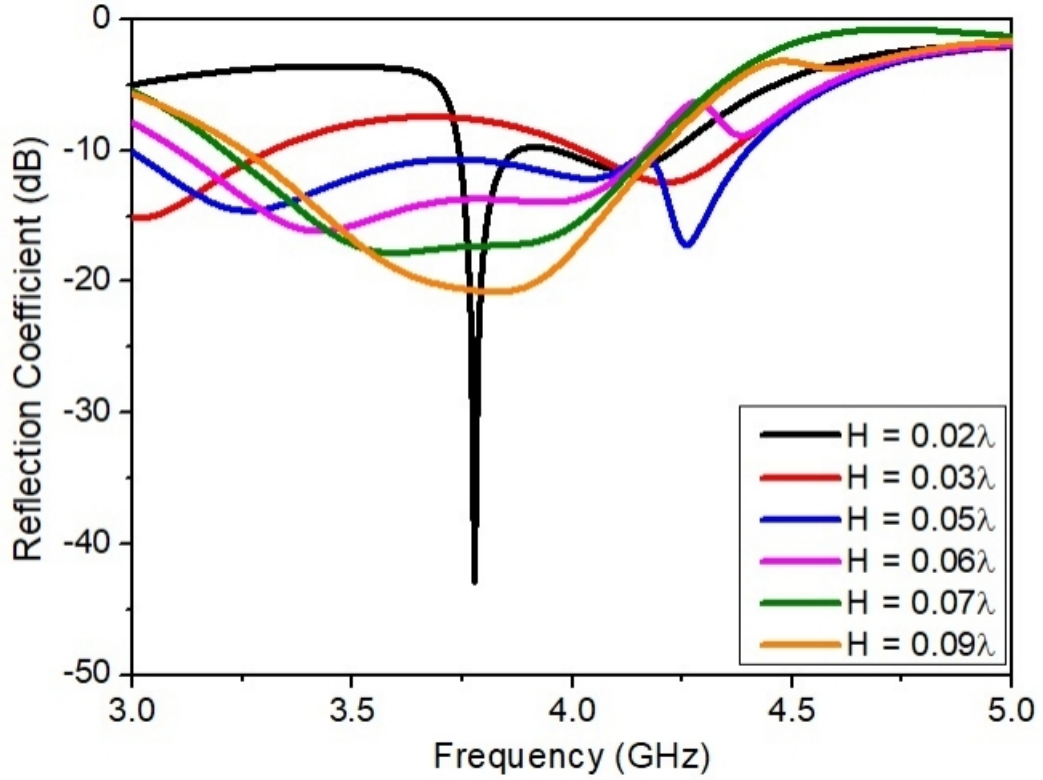


Figure 5.22: Reflection coefficient response with respect to effective height between USGPPA and DSLPFSS superstrate for the stacked design.

The distance of the DSLPFSS superstrate is varied from the USGPPA and the variation in the directivity value from the reference is reported. The distance between the DSLPFSS and the USGPPA which is denoted as H is fixed to a value of 0.07λ for retrieving a wide bandwidth with adequate increase in the gain and directivity within the sub-6 GHz frequency spectrum. The variation in the values of directivity over the full frequency sweep by adjusting the distance of the DSLPFSS is illustrated in Figure 5.24.

5.8 Experimental investigation of the stacked DSLPFSS

USGPPA design

The DSLPFSS-USGPPA is designed and modeled in the preceding section for the extraction of output radiation parameters in the appropriate sub-6 GHz frequency

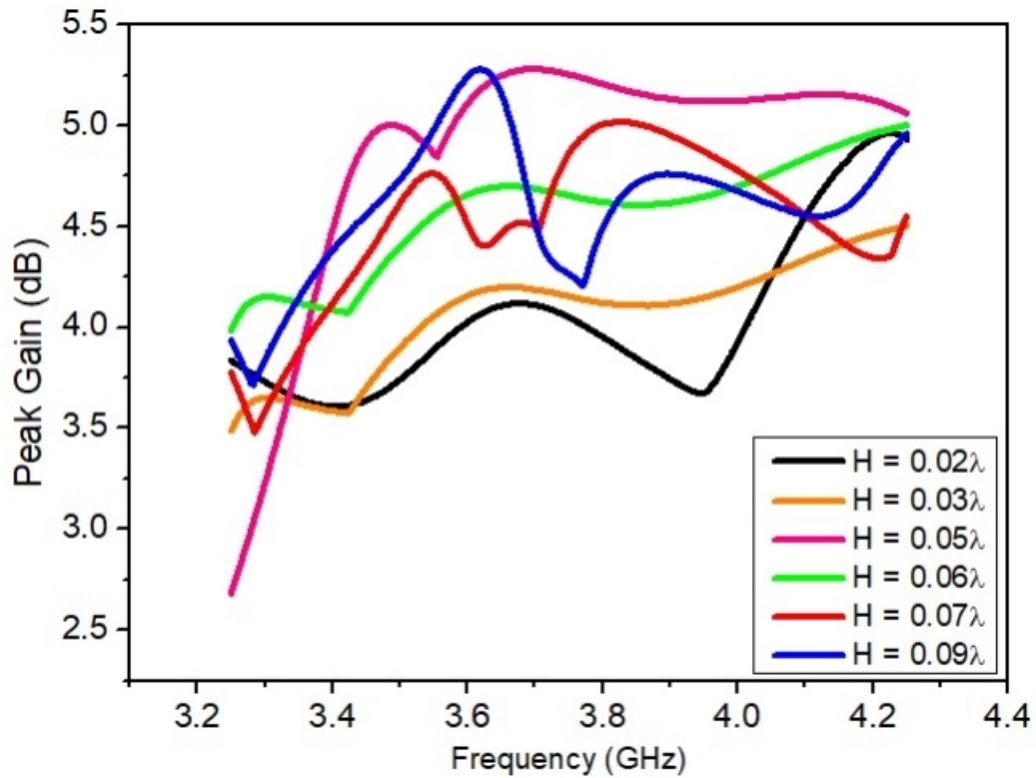


Figure 5.23: Variation in the gain of the stacked design by placing DSLPFSS superstrate at different distance above USGPPA.

range. To verify these findings, a prototype of the DSLPFSS-USGPPA geometry is created, and measurements are taken with a vector network analyzer (VNA). Antenna characteristics like as reflection coefficient, radiation pattern, and gain are tested with the MS2037C and its associated setup. A MS 2037C Network analyzer is used to measure the radiation properties. Antenna characterization is done via vector network analyzers, anechoic chambers, automated turn tables, and other important technologies. Anritsu's MS 2037C is a powerful Vector Network Analyzer (VNA) with the capacity to operate in both the time and frequency domains. The VNA is a microprocessor-based device that can measure the two port network characteristics as scattering parameters with pinpoint accuracy. The built-in signal conditioning techniques in the network analyzer aid in delivering and receiving data to the radiator before displaying the measured values as graphical graphs. The anechoic chamber also produces a "quiet zone" that is devoid of electromagnetic re-

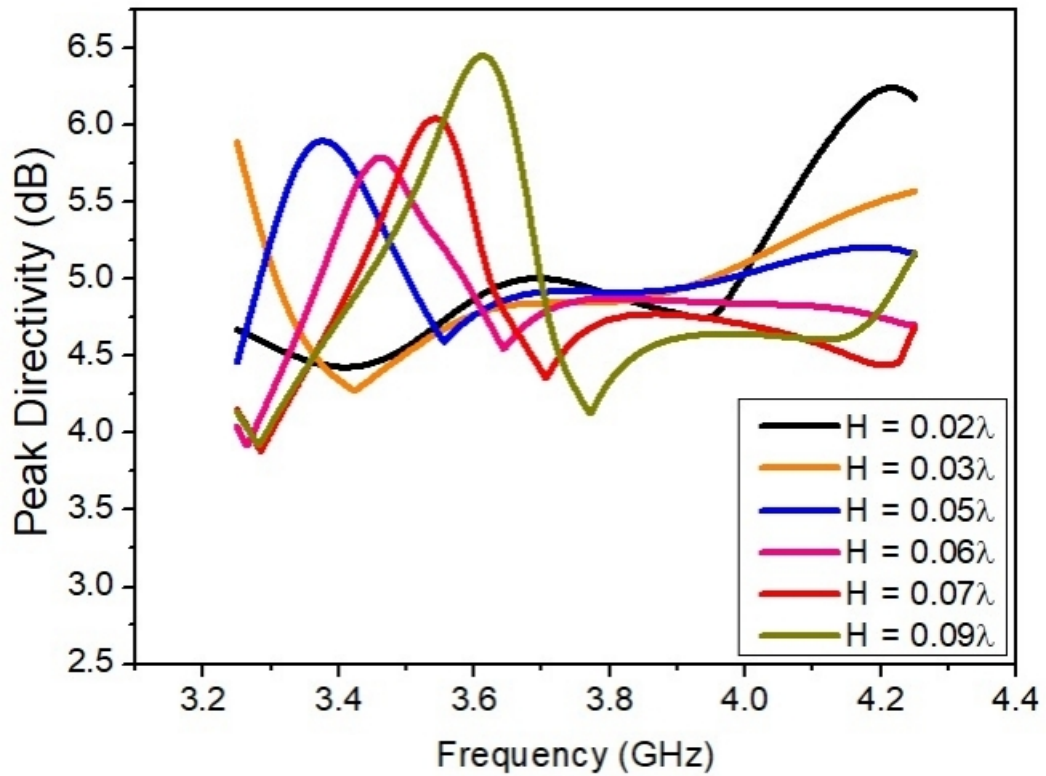


Figure 5.24: Variation in the directivity of the stacked design by placing DSLPFSS substrate at different distances above the USGPPA.

flections. To eliminate reflections from nearby objects, all antenna characterizations are performed in an anechoic room. It's a big room in terms of operational wave length, with microwave absorbers on the walls, ceiling, and floor to decrease EM reflections. Figure 5.25 shows the orientation of the DSLPFSS over the USGPPA.

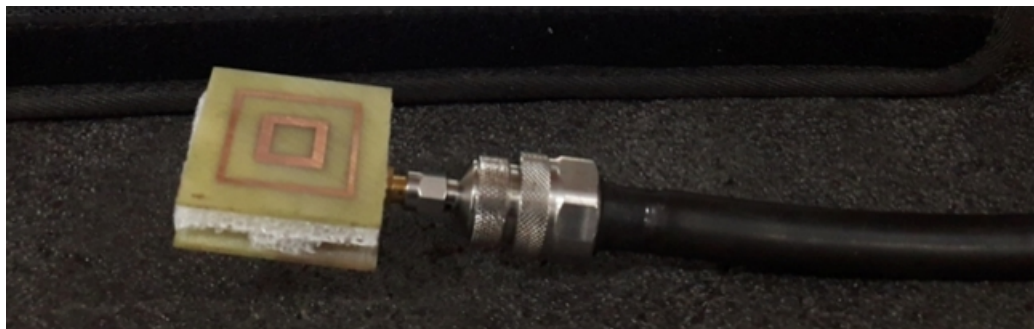


Figure 5.25: Orientation of the DSLPFSS over the USGPPA geometry

The VNA is really linked to a large number of cables and connections. Each cable and connector will have its own set of losses. To get correct scattering parameters,

the instrument should be calibrated using established standards of open, short, and matched loads. On the VNA, there are various calibration methods accessible. Single port and complete two port calibration techniques are often utilized. The reflection coefficient, VSWR, and input impedance may all be described using the single port analysis approach. The fabricated prototype of the DSLPFSS-USGPPA is shown in the Figure 5.26. Figure 5.26(a), 5.26(b), and 5.26(c) are showing the USGPPA top view, USGPPA bottom view, and DSLPFSS top view. The stacked geometry is illustrated in the Figure 5.26(d) made by the combination of DSLPFSS with the USGPPA.

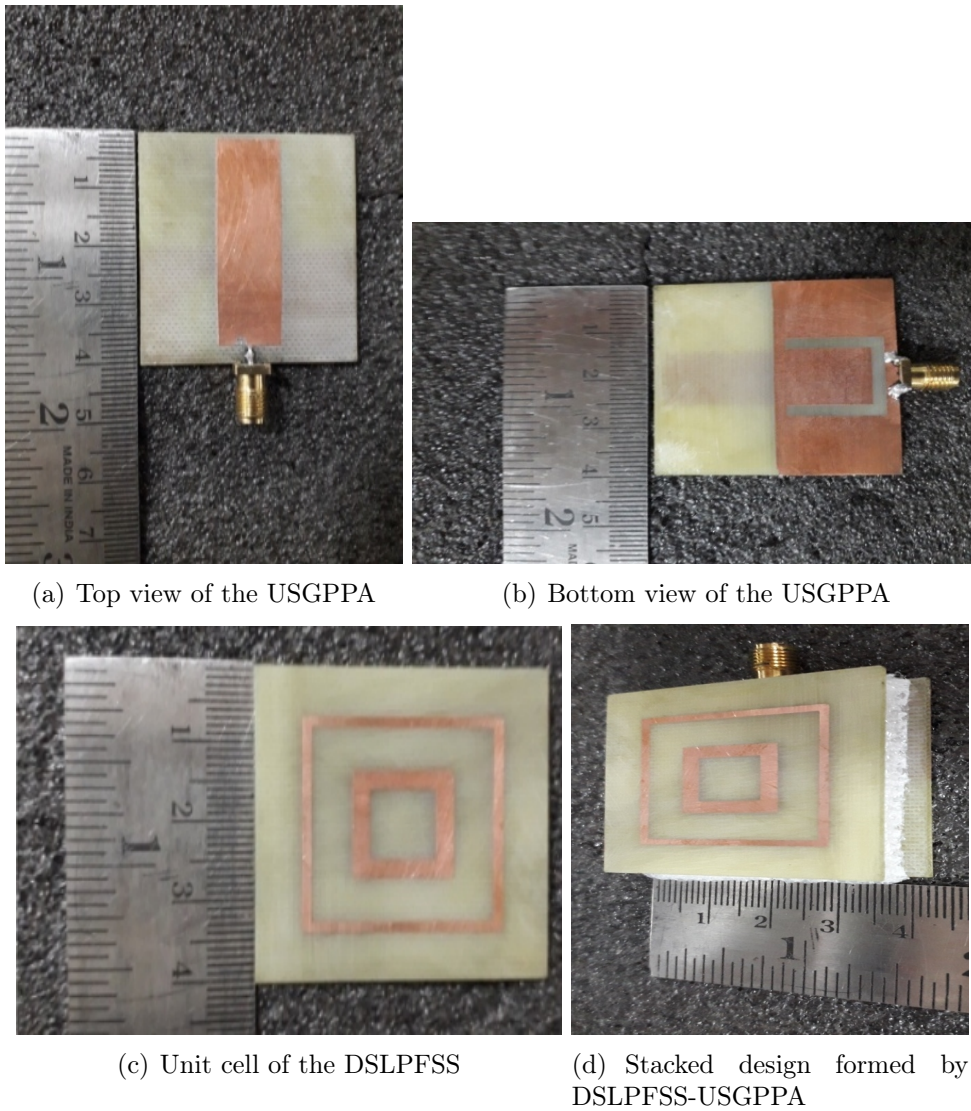


Figure 5.26: Prototypes of the proposed design

5.9 Validation of measured results with design simulation

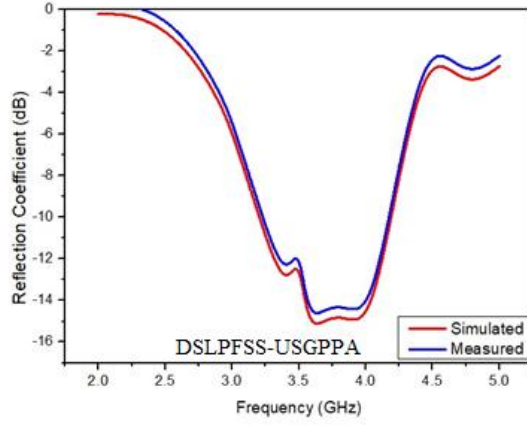
The measured results are compared to the predicted results using graphical representations of output parameters such as reflection coefficient, gain, and directivity, and it is illustrated in Figure 5.27. The measured findings are nearly comparable to the modelling results published for the DSLPFSS - USGPPA's stacked architecture.

The measurements of the fabricated designed stacked antenna are reported in the Table 5.6, and the comparison with the simulation results here validates our design.

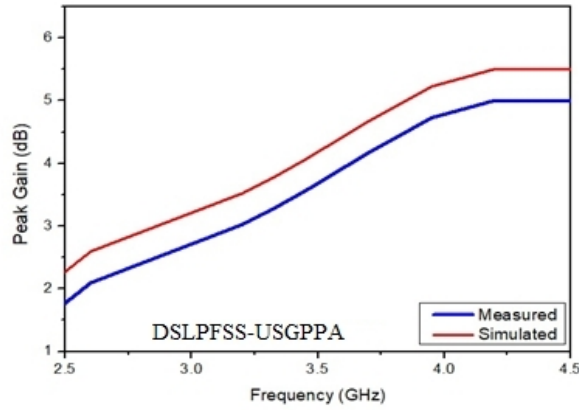
Table 5.6: Comparison of simulated and measured results of stacked geometry of USGPPA with DSLPFSS.

Output characteristics	Simulated results (Stacked design)	Measured results (Stacked design)
Lower cut off frequency (f_1)	3.20 GHz	3.22 GHz
Higher cut off frequency (f_2)	4.23 GHz	4.17 GHz
Bandwidth	1030 MHz	950 MHz ↓
Maximum gain	5.4 dB	5.0 dB ↓
Maximum directivity	6.5 dB	5.6 dB ↑

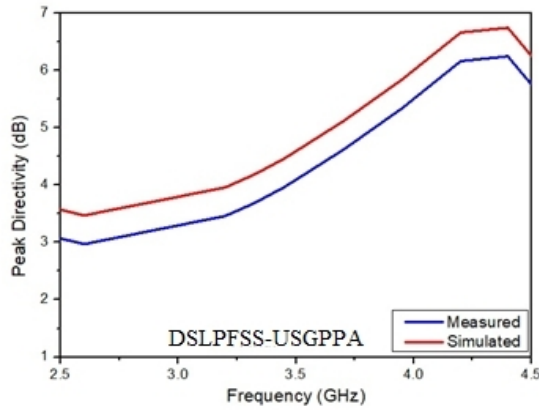
As a consequence, the USGPPA with DSLPFSS dual layer stacked architecture is compact and exhibit adequate characteristics for wideband applications at sub-6 GHz 5G applications, which is a great outcome of this design.



(a) Reflection coefficient



(b) Gain



(c) Directivity

Figure 5.27: Validation of the results retrieved from the experimental set-up and through modeling.

5.10 Comparison with existing research

In contrast to past comparable research, Table 5.7 demonstrates the relevance of the proposed designs i.e. “DSLPFSS-PSGPPA” and “DSLPFSS-USGPPA”. When

compared to alternative designs, it is clear that the recommended design provides the best performance in terms of the gain while maintaining the compactness in the desired frequency range.

Table 5.7: Performance comparison of the proposed compact “DSL PFSS-PSGPPA” and “DSL PFSS-USGPPA” with the state-of-art literature.

Reference	Patch size	FSS size	No. of FSS layer	Operating band (GHz)	Peak gain (dBi)	Fractional bandwidth
[167]	$0.61\lambda \times 0.42\lambda$	$0.24\lambda \times 0.21\lambda$	1	2.45	4.92	5.51%
[168]	$0.22\lambda \times 0.18\lambda$	$0.61\lambda \times 0.61\lambda$	1	2.2 - 2.44	5.2	10.34%
[169]	$1.87\lambda \times 0.13\lambda$	$0.46\lambda \times 0.46\lambda$	1	27.5 - 28.4	5	3.22%
[170]	$0.72\lambda \times 0.37\lambda$	$0.16\lambda \times 0.16\lambda$	2	2.4 - 2.7	4.46	5.18%
[171]	$0.41\lambda \times 0.33\lambda$	$0.12\lambda \times 0.05\lambda$	1	2.3 - 2.66	4.78	14.69%
DSL-PFSS-PS-GPPA	$0.47\lambda \times 0.20\lambda$	$0.50\lambda \times 0.50\lambda$	1	3.2 - 3.95	5.5	20.97%
DSL-PFS-US-GPPA	$0.50\lambda \times 0.50\lambda$	$0.50\lambda \times 0.50\lambda$	1	3.20 - 4.23	5.4	27.72%

5.11 Summary

This chapter presents the design, parametric optimization, fabrication, and measurement of the stacked designs composed of PPA and the PFSS geometries. The PPA’s designed in the chapter 4 are combined with the PFSS designs proposed in the chapter 3. The distance between the two geometries comprising of PFSS and PPA is optimized by choosing the best suitable value at which both the gain and bandwidth attain the maximum values. The fabrication is completed in the computerized mechanical etching PCB fabricator. Vector network analyzer (VNA) is used for measuring the reflective behavior of the stacked designs and for providing

the validation of the simulated results. Parametric analysis is also conducted and presented in this chapter to validate the converged design. This chapter is concluded with the comparison of the proposed work with the existing literature.

Chapter 6

Conclusion and Future Research

6.1 Conclusion

This chapter summarizes the main points of this thesis, as well as the primary findings drawn from the numerical and experimental analyses are presented. A double square loop planar frequency selective surface is designed and numerically synthesized for operation as a spatial filter when integrated with the antenna. A planer frequency selective surface consisting of double square loop structures and having a periodicity value of 0.55 is presented. The numerical analysis is presented for approximating the dimensions of the designed double square loop frequency selective surface geometry depending upon the range of the frequencies for which the filtering phenomenon is required. The effect of the variation of the dimensions of both square loops on the output performance characteristics is reported. Equivalent circuit analysis is performed for characterization of the filtering behavior of the frequency selective surface. A generic approach is being presented to evaluate the equivalent circuit parameters from the physical dimensions and vice-versa. Also, the effect of the variation of the incident and the polarization angle is studied on the double square loop frequency selective surface. The proposed design of DSLPFSS offers angular stability and polarization insensitive behavior. Maximum power han-

ding in form of maximum field enhancement factor is also reported for the proposed design of DSLPFSS. The normalized value of MFEF is around 37, implying that the electric field intensity within the DSLPFSS is possibly 37 times greater than the electric field intensity of the incoming wave in the 5G sub-6 GHz FR1 band. The results retrieved indicate that the planned DSLPFSS has the capability of managing a large amount of net microwave power. The prototype of the 2x2 array of DSLPFSS is fabricated and tested by using an experimental setup. The results retrieved from an experimental set-up are in line with the results exhibited by the modeled geometry which validates our design.

The antenna designs in form of printed patch geometries with defected ground are illustrated. Two different designs of defected ground with a polygon-shaped slot and a U-shaped slot are described. In the first case, a polygon slot is engraved within the ground plane and thus making the design a polygon slotted ground printed patch antenna. The design iterations are presented indicating a conventional ground shaped PPA, a hexagonal slotted PPA and 18 segment slotted PPA. The PSGPPA offers a compact design offering the dimensions of $0.46\lambda \times 0.20\lambda$. The proposed design of 18 segment PSGPPA offers a wide bandwidth of 720 MHz with a gain of 2.5 dB. The design of PSGPPA exhibits a radiation efficiency of 83.62% which makes it the best candidate for use in the sub-6 GHz 5G spectrum. Another design of the USGPPA is proposed, having the dimensions of $0.46\lambda \times 0.15\lambda$ which makes it also a compact structure. The design of the USGPPA offers a wide bandwidth of 900 MHz with a gain of 3.8 dB. The radiation efficiency offered by the proposed USGPPA structure comes out to be 87.6% which justifies its feasibility in the sub-6 GHz 5G spectrum. It is seen that as the bandwidth is increased across the design iterations of the PPA, the active parameters such as gain and directivity tend to reduce. Hence, to overcome this slight decrease in the active parameters such as gain and directivity, there is a need to employ the spatial filters with the PPAs.

The geometries of the frequency selective surface are integrated with the designed

patch radiators for removing the out-of-band radiations which in turn increases the net output characteristics. An enhancement in the bandwidth with gain and directivity augmentation is experienced when an antenna is integrated with frequency selective surface, which is the need of the current world. The two stacked designs of frequency selective surface based patch antenna radiators are reported with different orientations of the frequency selective surface. The effect of reversing the orientations of the frequency selective surface on the output characteristics is also reported. In the first stacked design, DSLPFSS is stacked with Polygon shaped ground printed patch antenna (PSGPPA). The fractional bandwidth has been increased from 19.17% to 20.97% whereas an enhancement in the gain is reported from 2.5 dB to 5.5 dB upon placing DSLPFSS as a superstrate on PSGPPA. A sharp increase in the directivity is reported from 3.21 dB to 6.2 dB with a rise in the radiation efficiency from 83.62% to 84.71%. In the second stacked antenna design, the DSLPFSS is added as a superstrate by reversing its orientation with the U-slotted ground printed patch antenna. The fractional bandwidth experiences an increase from 19.68% to 27.72% with an enhancement in the value of gain from 3.3 dB to 5.4 dB. Further, the other parameters such as directivity experience an increase from 3.8 dB to 6.5 dB with a rise in the value of the radiation efficiency from 83.42% to 86.23% respectively. Thus it is concluded that planar frequency selective surface can increase the output characteristics to an extent for making the patch antenna design feasible to be utilized in the sub-6 GHz 5G applications.

6.2 Suggestions for future research

In the present thesis, while designing the geometries of the planar frequency selective surfaces, only one basic symmetrical shape in form of a square loop is considered. Many other symmetrical shapes in form of circular ring geometries, Jerusalem cross structure, and a folded dipole may be considered. The effect of the incorporation

of the planar frequency selective surface as a superstrate with the printed patch antenna designs is analyzed and reported. The placement of these frequency selective surface based spatial filters in form of the substrates may also be analyzed and the performance variations may be recorded. The proposed stacked designs have prioritized only the transmission properties of frequency selective surface based spatial filters whereas the absorption behaviors may also be looked into in the future course of work.

Bibliography

- [1] Balanis, C.A.(2005),*Antenna Theory: Analysis and Design*,John Wiley and Sons, New Jersey, USA.
- [2] Garg, R., Bhartia, P., Bahland, I., Ittippiboon, A., (2001), *Microstrip antenna design handbook*, Norwood, MA:Artech House.
- [3] Pozar, D.M.,(1992), *Microstrip antennas*, Proc. IEEE, vol. 80, pp.79-91.
- [4] Kraus, J. D., Marhefka, R. J., (2002), *Antennas for all applications*, Book McGrawHill.
- [5] A white paper on “Enabling 5G in India” (2019). <https://tra.gov.in/sites/default/files/White Paper22022019.pdf>
- [6] Munk, B. A., (2000), *Frequency selective surfaces: Theory and Design*, Wiley: New York.
- [7] Wu, T. K., (1995), *Frequency selective surfaces and grid arrays*, Wiley: New York.
- [8] Sui, S., Ma, H.,Wang, J., et. al.,(2019), A hybrid encoding method for frequency selective surface optimization design with angular stability property, *Appl. Phys. A*, vol. 125, pp. 718.
- [9] Liu, H. T., Cheng, H. F., Chu, Z. Y., Zhang, D. Y., (2007), Absorbing properties of frequency selective surface absorbers with cross-shaped resistive patches, *Material Design*, vol. 28, pp. 2166–2171.
- [10] Singh, D., Kumar, A., Meena, S., Agrawal, V., (2012), Analysis of frequency selective surfaces for radar absorbing materials, *Progress Electromagnetics Research B*, vol. 38, pp. 297–314.
- [11] Kohlgraf,D. C.,(2005), *Design and testing of a frequency selective surface based wide-band multiple antenna system*, PhD. Thesis, The Ohio State University, USA.
- [12] Li, L., Chen, Q., Yuan, Q., Sawaya, K., Maruyama, T., Furuno, T.,Uebayashi, S., (2011), Frequency selective reflect-array using crossed-dipole elements with square loops for wireless communication applications, *IEEE Trans. on Antennas and Propagation*, vol. 59, no. 1, pp. 89-99.

- [13] Araujo, G. L. R., Campos, A. L., Martins, A. M., (2015), Improvement of the equivalent circuit method for analysis of frequency selective surfaces using genetic algorithms and rational algebraic models, *Progress In Electromagnetics Research Letters*, vol. 55, pp. 67-74.
- [14] Ranga, Y., Matekovits, L., Weily, A. R., Esselle, K. P., (2013), A low-profile dual-layer ultra-wideband frequency selective surface reflector, *Microwave and Optical Technology Letters*, vol. 55, no. 6, pp. 1223-1227.
- [15] da Silva Segundo, F. C. G., Campos, A. L. P. S., (2015), Compact frequency selective surface with dual band response for WLAN applications, *Microwave and Optical Technology Letters*, vol. 57, no. 2, pp. 265-268.
- [16] Necibi, O., Hamzaoui, D., Vuong, T. P., Gharsallah, A., (2015), A novel RFID-HIS-PRS reader antenna for the millimeter wave band 30 GHz, *Microwave and Optical Technology Letters*, vol. 57, no. 8, pp. 1835-1842.
- [17] Garcia, P. G., Alvarez, J. P. F., (2015), Floquet-Bloch theory and its application to the dispersion curves of non-periodic layered systems, *Mathematical Problems in Engineering*, vol. 2015, Article ID 475364, 12 pages.
- [18] Costa, F., Monorchio, A., Talarico, S., Valeri, F. M., (2008), An active high impedance surface for low profile tunable and steerable antennas, *IEEE Antennas Wireless Propag. Lett.*, vol. 7, pp. 676-680.
- [19] Munk, B. A., Burrell, G. A., (1979), Plane wave expansion for arrays of arbitrary oriented piecewise linear elements and its application in determining the impedance of single linear antennas in a lossy half space, *IEEE Trans. on Antennas and Propagation*, vol. 27, pp. 331 -343.
- [20] Tsao, C. H., Mittra, R., (1984), Spectral-domain analysis of frequency selective surfaces comprises of periodic arrays of cross dipoles and Jerusalem crosses, *IEEE Trans. on Antennas and Propagation*, vol. 32, pp. 478 -486.
- [21] Cwik, T. A., Mittra, R., (1987), Scattering from a periodic array of free standing arbitrarily shaped perfectly conducting or resistive patches, *IEEE Trans. on Antennas and Propagation*, vol. 35, pp. 1226 -1234.
- [22] Fallahi, A., Yahaghi, A., Abiri, H., Shahabadi, M., Hafner, C., (2010), Large overlapping sub-domain method- of-moments for the analysis of frequency selective surfaces, *IEEE Trans. on Microwave Theory and Techniques*, vol. 58, no. 8, pp. 2175-2187.
- [23] Taflov, A., Umashankar, K. R., (1989), The finite-difference time-domain (FDTD) method for numerical modeling of electromagnetic scattering, *IEEE Trans. on Magnetics*, vol. 25, no. 4, pp. 3086-3091.
- [24] Kuisheng, F., Na, Li., Jiadong, Xu. (2009), Finite element method analysis for the frequency selective characteristics of dielectric periodic structure with arbitrary profiles, *Proc. of 4th IEEE Conf. on Industrial Electronics and Applications*, Xian, pp. 1957-1960.

- [25] Joozdani, M. Z., Amirhosseini, M. K., (2016), Equivalent circuit model of frequency selective surfaces embedded in non-homogeneous dielectric slab, 2016 24th Iranian Conference on Electrical Engineering (ICEE), pp. 380-383.
- [26] Chen, C. C., (1970), Transmission through a conducting screen perforated periodically with apertures, IEEE Trans. on Microwave Theory and Techniques, vol. 18, no. 9, pp. 627-632.
- [27] Gilles, T., (2011), Advances in the Formulations and Accuracy of the Method-of-Moments Applied to Electromagnetics, 1st Edition, Presses universitaires de Louvain, Belgium.
- [28] Weile, D. S., Michielssen, E., Gallivan, K., (2001), Reduced-order modeling of multiscreen frequency-selective surfaces using Krylov-based rational interpolation, IEEE Trans. on Antennas and Propagation, vol. 49, no. 5, pp. 801-813.
- [29] Prakash, V. V. S., Mittra, Raj, (2003), Characteristic basis function method: a new technique for efficient solution of method of moments matrix equations, Microwave and Optical Technology Letters, vol. 36, no. 2, pp. 95-100.
- [30] Don, N., Bozzi, M., Kirilenko, A., Perregrini, L., (2007), Analysis of inductive frequency selective surfaces by the method of moments with entire-domain basis functions, Microwave and Optical Technology Letters, vol. 49, no. 12, pp. 2929-2932.
- [31] Montagna, M., Bozzi, M., Perregrini, L., (2010), Convergence properties of the method of moments in the modeling of frequency selective surfaces, International Journal of RF and Microwave Computer-Aided Engineering, vol. 20, no. 2, pp. 220-229.
- [32] Davidson, D. B., (2005), Computational electromagnetics for RF and microwave engineering, Cambridge University Press: Cambridge.
- [33] Taflove, A., Hagness, S., (2000), Computational electrodynamics: The Finite-Difference Time-Domain Method, 2nd Edition, Artech House: Boston.
- [34] Yee, K., (1966), Numerical solution of initial boundary value problems involving Maxwell's equations in isotropic media, IEEE Trans. on Antennas and Propagation, vol. 14, no. 3, pp. 302-307.
- [35] Taflove, A., Umashankar, K. R., (1989), Review of FDTD numerical modeling of electromagnetic wave scattering and radar cross section, Proc. of IEEE, vol. 77, no. 5, pp. 682-699.
- [36] Harms, P., Mittra, R., Ko, W., (1994), Implementation of the periodic boundary condition in the finite-difference time-domain algorithm for FSS structures, IEEE Trans. on Antennas and Propagation, vol. 42, no. 9, pp. 1317-1324.
- [37] Yu, W., Yang, X., Liu, Y., Mittra, R., Muto, A., (2011), Advanced FDTD Methods: Parallelization, Acceleration and Engineering Applications, Artech House: Norwood.

- [38] Yu,W., Mittra,R.,Yang, X., Liu, Y., Rao, Q., Muto,A., (2010), High performance conformal FDTD techniques, *IEEE Microwave Magazine*, vol. 11, no. 4, pp. 42-55.
- [39] Bardi,I., Remski, R., Perry, D., Cendes,Z., (2002),Plane wave scattering from frequency selective surfaces by the finite-element method, *IEEE Trans. on Magnetics*, vol. 38, no. 2, pp. 641-644.
- [40] D'Angelo,J., Mayergoyz, I. D., (1991),Three dimensional RF scattering by the finite element method, *IEEE Trans. on Magnetics*, vol. 27, no. 5, pp. 3827-3832.
- [41] Eibert,T. F., Erdemli, Y. E.,Volakis, J. L., (2003), Hybrid finite element-fast spectral domain multilayer boundary integral modeling of doubly periodic structures, *IEEE Trans. on Antennas and Propagation*, vol. 51, no. 9, pp. 2517-2520.
- [42] Archer,M. J.,(1985), Wave reactance of thin planar strip gratings, *Int. Journal of Electronics*, vol. 58, no. 2, pp. 197-230.
- [43] Marcuvitz,N.,(1986), *Waveguide handbook*, Peter Peregrinus Ltd.: New York, vol.21.
- [44] Langley, R. J.,Parker, E. A.,(1982), Equivalent circuit model for arrays of square loops, *Electronics Letters*, vol. 18, no. 7, pp. 294-296.
- [45] Barrera, M. A. R., Carpes,W. P., (2015), Numerical model of the effective permittivity for square-loop frequency selective surfaces, *IEEE Trans. on Magnetics*, vol. 51, no. 3, pp. 1-4.
- [46] Yang,J.,Shen, Z.,(2007), A thin and broadband absorber using double-square loops, *IEEE Antennas and Wireless Propagation Letters*, vol. 6, pp. 388-391.
- [47] Yao, X., Bai, M.,Miao,J., (2011), Equivalent circuit method for analyzing frequency selective surface with ring patch in oblique angles of incidence", *IEEE Antennas and Wireless Propagation Letters*, vol. 10, pp. 820-823.
- [48] Hamdy, S. M. A.,Parker,E. A.,(1982), Influence of lattice geometry on transmission of electromagnetic waves through arrays of crossed dipoles", *IEE Proceedings H Microwaves, Optics and Antennas*, vol. 129, pp. 7-10.
- [49] Parker,E. A., El-Sheikh,A. N. A., (1991), Convolved array elements and reduced size unit cells for frequency selective surfaces, *IEE Proceedings H Microwaves, Antennas and Propagation*, vol. 138, pp. 19-22.
- [50] Shang,Y.,Shen,Z.,Xiao,S., (2014), Frequency-selective rasorber based on square-loop and cross-dipole arrays, *IEEE Trans. on Antennas and Propagation*, vol. 62, no. 11, pp. 5581-5589.
- [51] Anderson,I., (1975), On the theory of self-resonant grids, *The Bell System Technical Journal*, vol. 54, no. 10, pp. 1725-1731.
- [52] Bagby,J. S.,Nyquist, D. P., Drachman, B. C.,(1985), Integral formulation for analysis of integrated dielectric waveguides, *IEEE Trans. MTT-33*, vol. 33, pp. 906-915.

- [53] Koshiba, M., Suzuki, M., (1986), Application of the boundary-element method to waveguide discontinuities (Short Paper)", IEEE Trans. Microw. Theory Tech., vol. 34, pp. 301–307.
- [54] Schimert, T., Koch, M., Chan, C., (1990), Analysis of scattering from frequency-selective surfaces in the infrared, J. Opt. Soc. Am. A, vol. 7, pp. 1545-1553.
- [55] Agahi, S., Mittra, R., (1990), Design of a cascaded frequency selective surface as a dichroic subreflector, International Symposium on Antennas and Propagation Society, Merging Technologies for the 90's, Dallas, TX, USA, vol.1, pp. 88-91.
- [56] Kunz, K. S., Luebbers, R. J., (1993), The finite difference time domain method for electromagnetics, CRC Press: Boca Raton, FL, USA.
- [57] Lambea, M., Gonzalez, M. A., Encinar, J. A., Zapata, J., (1995), Analysis of frequency selective surfaces with arbitrarily shaped apertures by finite element method and generalized scattering matrix, IEEE Antennas and Propagation Society International Symposium. 1995 Digest, Newport Beach, CA, USA, vol.3, pp. 1644-1647.
- [58] Rozanov, K. N., (2000), Ultimate thickness to bandwidth ratio of radar absorbers, IEEE Trans. on Antennas and Propagation, vol. 48, no. 8, pp. 1230-1234.
- [59] Bardi, I., Remski, R., Perry, D., Cendes, Z., (2002), Plane wave scattering from frequency-selective surfaces by the finite-element method, in IEEE Transactions on Magnetics, vol. 38, no. 2, pp. 641-644.
- [60] Farahat, N., Mittra, R., (2002), Analysis of frequency selective surfaces using the finite difference time domain (FDTD) method, IEEE Antennas and Propagation Society International Symposium (IEEE Cat. No.02CH37313), San Antonio, TX, USA, vol.2, pp. 568-571.
- [61] Gianvittorio, J.P., Romeu, J., Blanch, S., Rahmat-Samii, Y., (2003), Self-similar pre fractal frequency selective surfaces for multiband and dual-polarized applications, IEEE Trans. Antennas Propag., vol. 51, pp. 3088–3096.
- [62] Kern, D. J., Werner, D. H., Monorchio, A., Lanuzza, L., Wilhelm, M. J., (2005), The design synthesis of multiband artificial magnetic conductors using high impedance frequency selective surfaces, IEEE Trans. Antennas Propag., vol.53, pp.8–17.
- [63] Blackburn, J., Arnaut, L. R., (2005), Numerical convergence in periodic method of moments analysis of frequency-selective surfaces based on wire elements, in IEEE Transactions on Antennas and Propagation, vol. 53, no. 10, pp. 3308-3315.
- [64] Kiani, G. I., Ford, K. L., Esselle, K. P., Weily, A. R., Panagamuwa, C., Batchelor, J. C., (2008), Single-layer bandpass active frequency selective surface, Microw. Opt. Technol. Lett., vol. 50, pp. 2149–2151.

- [65] Chiu, C. N., Chang, K. P., (2009), A novel miniaturized-element frequency selective surface having a stable resonance, *IEEE Antennas Wirel. Propag. Lett.*, vol. 8, pp. 1175–1177.
- [66] Chen, H., Hou, X., Deng, L., (2009), Design of frequency-selective surfaces radome for a planar slotted waveguide antenna, in *IEEE Antennas and Wireless Propagation Letters*, vol. 8, pp. 1231-1233.
- [67] Yang, F., Samii, Y., (2009), *Electromagnetic band gap structures in antenna engineering*, Cambridge University Press: Cambridge, UK.
- [68] Liu, H. L., Ford, K. L., Langley, R. J., (2009), Design methodology for a miniaturized frequency selective surface using lumped reactive components,” *IEEE Transactions on Antennas and Propagation*, vol. 57, no. 9, pp. 2732–2738.
- [69] Mudar, A., Joumayly, Al, Behdad, N., (2010), A generalized method for synthesizing low-profile, band pass frequency selective surfaces with non-resonant constituting elements, *IEEE Transactions on Antennas and Propagation* , vol. 58, pp. 4033-4041.
- [70] Campos, A. L. P., de Oliveira, E.E.C., da Fonseca Silva, P. H., (2010), Design of miniaturized frequency selective surfaces using Minkowski island fractal, *J. Microw. Optoelectron. Electromagn. Appl. (JMoe)*, vol. 9, pp. 43–49.
- [71] Roig, M., Sazegar, Zheng, M. Y., Jakoby, R., (2012), Tunable frequency selective surface based on ferroelectric ceramics for beam steering antennas, 2012 The 7th German Microwave Conference, Ilmenau, Germany, pp. 1-4.
- [72] Sun, L., Cheng, H., Zhou, Y., Wang, J., (2012), Broadband metamaterial absorber based on coupling resistive frequency selective surface. *Opt. Express*, vol.20, pp. 4675-4680.
- [73] Jang, S., Kim, J., (2012), Wireless structural sensor made with frequency selective surface antenna, *Proc. SPIE 8344, Nanosensors, Biosensors, and Info-Tech Sensors and Systems*.
- [74] Song, K., Mazumder, P., (2013), Design of highly selective metamaterials for sensing platforms, *IEEE Sens. J.* , vol. 13, pp. 3377–3385.
- [75] Lazaro, A., Villarino, R., Ramos, A., Girbau, D., (2013), Active frequency selective surface for time-domain UWB RFID applications, 2013 European Microwave Conference, Nuremberg, Germany, pp. 136-139.
- [76] Li, B., Shen, Z, (2013), Three dimensional band pass frequency-selective structures with multiple transmission zeros, *IEEE Trans. Microw. Theory Tech.*, vol. 61, pp. 3578–3589.
- [77] Cure, D., Weller, T. M., Miranda, F. A., (2013), Study of a low-profile 2.4-GHz planar dipole antenna using a high-impedance surface with 1-D varactor tuning, *IEEE Transactions on Antennas and Propagation*, vol.61, pp. 506-51.

- [78] Zhang, L., Wu, Q., Denidni, T. A., (2013), Electronically radiation pattern steerable antennas using active frequency selective surfaces, *IEEE Antennas and Wireless Propagation Letters*, vol. 12, pp. 6000-6007.
- [79] Pan, W., Huang, C., Chen, P., Pu, M., Ma, X., Luo, X., (2013), A beam steering horn antenna using active frequency selective surface, *IEEE Antennas and Wireless Propagation Letters*, vol. 12, pp.6218-6223, 2013.
- [80] Jazi, M. N., Denidni, T. A., (2013), Electronically sweeping-beam antenna using a new cylindrical frequency-selective surface, *IEEE Antennas and Wireless Propagation Letters*, vol.12, pp. 666-676.
- [81] Agarwal, K., Nasimuddin, Alphones, A., (2013), Unidirectional wideband circularly polarized aperture antennas backed with artificial magnetic conductor reflectors, *IET Microwaves, Antennas & Propagation*, vol. 7, pp. 338-346.
- [82] Moharamzadeh, E., Javan, A. M., (2013), Triple-band frequency-selective surfaces to enhance gain of X-Band triangle slot antenna, *IEEE Antennas and Wireless Propagation Letters*, vol. 12, pp. 1145-1148.
- [83] Seager, R. D., Chauraya, A., Bowman, J., Broughton, M., Philpott, R., Nimkulrat, N.,(2013), Fabric based frequency selective surfaces using weaving and screen printing, *Electronics Letters*, vol. 49, pp.1507- 1509.
- [84] Natarajan, R., Shadrach, S., Kumar, N., (2013), Free space FSS filter for 5GHz WLAN, *International Journal of Engineering Research and Technology (IJERT)*, vol.2 , issue 12, pp. 172-174.
- [85] Genovesi, S., Costa, F., Monorchio, A., (2014), Wideband radar cross section reduction of slot antennas arrays, *IEEE Transactions on Antennas and Propagation*, vol. 62, pp. 163-173.
- [86] Smith, T., Gothelf, U., Kim, O.S., Breinbjerg, O., (2014), An FSS-backed 20/30 GHz circularly polarized reflect array for a shared aperture Land Ka-band satellite communication antenna, *IEEE Transactions on Antennas and Propagation*, vol. 62. pp. 661-668.
- [87] Rashid, A. K., Li, B., Shen, Z., (2014), An overview of three-dimensional frequency-selective structures, *IEEE Antennas Propag. Mag.*, vol.56, pp. 43-67.
- [88] Martinez-Lopez, L., Rodriguez-Cuevas, J., Martinez-Lopez, J. I., Martynyuk, A. E., (2014), A multilayer circular polarizer based on bisected split-ring frequency selective surfaces", *IEEE Antennas Wirel. Propag. Lett.*, vol. 13, pp. 153-156.
- [89] Abdelrahman, A. H., Elsherbeni, A. Z., Yang, F., (2014), Transmission phase limit of multilayer frequency-selective surfaces for transmitarray designs, *IEEE Trans. Antennas Propag.*, vol.62, pp.690-697.
- [90] Abadi, S.M.A.M.H., Li, M., Behdad, N., (2014), Harmonic suppressed miniaturized element frequency selective surfaces with higher order bandpass responses, *IEEE Trans. Antennas Propag.*, vol. 62, pp. 2562-2571.

- [91] Abadi, S.M.A.M.H., Li, M., Behdad, N., (2014), Design of wideband, FSS-based multibeam antennas using the effective medium approach, *IEEE Trans. Antennas Propag.*, vol. 62, pp. 5557-5564.
- [92] Shi, Y., Tang, W., Zhuang, W., Wang, C., (2014), Miniaturized frequency selective surface based on 2.5-dimensional closed loop, *Electron. Lett.*, vol. 50, pp. 1656-1658.
- [93] Yu, Y. M., Chiu, C. N., Chiou, Y. P., Wu, T. L., (2014), A novel 2.5 dimensional ultra miniaturized element frequency selective surface, *IEEE Trans. Antennas Propag.*, vol. 62, pp. 3657-3663.
- [94] Li, B., Shen, Z., (2014), Bandpass frequency selective structure with wideband spurious rejection, *IEEE Antennas Wirel. Propag. Lett.*, vol. 13, pp. 145-148.
- [95] Abdelrahman, A. H., Elsherbeni, A. Z., Yang, F., (2014), Transmit array antenna design using cross-slot elements with no dielectric substrate, *IEEE Antennas and Wireless Propagation Letters*, vol. 13, pp. 177-180.
- [96] Li, L., Li, Y., Wu, Z., Huo, F., Zhang, Y., Zhao, C., (2015), Novel polarization-reconfigurable converter based on multilayer frequency-selective surfaces, *Proc. IEEE*, vol. 103, pp. 1057-1070.
- [97] Xu, N., Gao, J., Zhao, J., Feng, X., (2015), A novel wideband, low profile and second order miniaturized bandpass frequency selective surfaces, *AIP Adv.*, vol. 5, pp. 077157.
- [98] Mahgoub, K., Navigation, T., (2015), Frequency selective surfaces for UHF RFID applications, 2015 IEEE International Symposium on Antennas and Propagation USNC/URSI National Radio Science Meeting, Vancouver, BC, Canada, pp. 987-988.
- [99] Wang, X. C., Zhao, W. S., Hu, J., Yin, W. Y., (2015), Reconfigurable terahertz leaky-wave antenna using graphene-based high-impedance surface, *IEEE Transactions on Nanotechnology* , vol.14, pp. 62-69.
- [100] Jia, Y., Liu, Y., Wang, H., Li, K., Gong, S. (2015), Low RCS, high-gain, and wideband mushroom antenna, *IEEE Antennas and Wireless Propagation Letters*, vol. 14, pp. 277-280.
- [101] Kapoor, A. Jha, K. R., Singh, G., (2016), Design and analysis of frequency selective surface at Ka/K/Ku Band for antenna miniaturization, 2016 International Conference on Computational Techniques in Information and Communication Technologies (ICCTICT), pp. 25-31.
- [102] Hashemi, S., Abdolali, A., (2017), Room shielding with frequency selective surfaces for electromagnetic health application, *International Journal of Microwave and Wireless Technologies*, vol. 9, no. 2, pp. 291-298.
- [103] Yao, X., Liang, B., Bai, M.,(2017), Quasi optical frequency selective surface with phase compensation structure correcting the beam distortion, *Opt. Express*, vol.25, pp. 23014-23023.

- [104] Milici, S., Lazaro, A., Lorenzo, J., Villarino, R., Girbau, D., (2017), Wearable sensors based on modulated frequency selective surfaces, 2017 47th European Microwave Conference (EuMC), pp. 942-945.
- [105] Hussain, T., Cao, Q., Kayani, J. K., Majid, I., (2017), Miniaturization of frequency selective surfaces using 2.5-D knitted structures: Design and Synthesis," IEEE Transactions on Antennas and Propagation, vol. 65, no. 5, pp. 2405-2412.
- [106] Sarika, Tripathy, M., Ronnow, D., (2018), A frequency selective surface reflector for 4G/X-Band/Ku-Band," Progress In Electromagnetics Research C, vol. 81, pp. 151-159.
- [107] Huang, C., Ji, C., Wu, X., Song, J., Luo, X., (2018), Combining FSS and EBG Surfaces for high-efficiency transmission and low-scattering properties, IEEE Trans. Antennas Propag., vol. 66, pp. 1628-1632.
- [108] Hui, X., Sheng, L. J., (2018), Double layer frequency selective surface for terahertz band pass filter, J Infrared Milli Terahz Waves , vol. 39, pp. 1039–1046.
- [109] Anwar, R., Ning, M., Huansheng, L., (2018), Frequency selective surfaces: A Review, Appl. Sci. , vol. 8, no. 9, pp. 1689.
- [110] Elzwawi, G. H., Elzwawi, H. H., Tahseen, M. M., Denidni, T. A., (2018), Frequency selective surface based switched beamforming antenna, IEEE Access, vol. 6, pp. 48042-48050.
- [111] Zhao, P., Zhang, Y., Sun, R., Zhao, W., Hu, Y., Wang, G., (2018), Design of a novel miniaturized frequency selective surface Based on 2.5-Dimensional Jerusalem cross for 5G applications, Wireless Communications and Mobile Computing, vol. 2018, Article 6 pages.
- [112] Anwar, R., Wei, Y., Mao, L., Ning, H., (2019), Miniaturised frequency selective surface based on fractal arrays with square slots for enhanced bandwidth, IET Microwaves, Antennas and Propagation, vol.13, no.11, pp. 1811-1819.
- [113] Kanth, V., Raghavan, S., (2019), EM design and analysis of frequency selective surface based on substrate integrated waveguide technology for airborne radome application, in IEEE Transactions on Microwave Theory and Techniques, vol. 67, no. 5, pp. 1727-1739.
- [114] Vásquez-Peralvo, J. A., Fernández-González, J., Valtr, P., Rigelsford, J. M., (2020), Inductive frequency selective surface: An application for dichroic sub reflectors," in IEEE Access, vol. 8, pp. 22721-22732.
- [115] Sahai, J., Tiwari, G., (2020), A metamaterial based I-shaped frequency selective surface for band pass and band stop applications, 2020 International Conference on Computer Communication and Informatics (ICCCI), Coimbatore, India, pp. 1-3.
- [116] Kapoor, A., Mishra, R., Kumar, P., (2021), Slotted wideband frequency selective reflectors for Sub-6 GHz 5G Devices, 2021 International Conference on Computing, Communication, and Intelligent Systems (ICCCIS), Greater Noida, India, pp. 786-791.

- [117] Li, B., Ne, R., (2021), A novel miniaturized dual-layer frequency selective surface, *AEU - International Journal of Electronics and Communications*, vol. 130, pp. 153580.
- [118] Alvarez, H. F., Cadman, D. A., Goulas, A., et al., (2021), 3-D conformal band-pass millimeter-wave frequency selective surface with improved fields of view, *Sci Rep*, vol. 11, pp. 12846.
- [119] Tang, X., et al., (2019), Ultra wideband patch antenna for sub-6 GHz 5G communications, 2019 International Workshop on Electromagnetics: Applications and Student Innovation Competition (iWEM), pp. 1-3.
- [120] Meneses, G. S. R., Rita, T., Rodríguez, M., (2019), Microstrip antenna design for 3.1 GHz - 4.2 GHz frequency band applied to 5G mobile devices", *EJERS, European Journal of Engineering Research and Science*, vol. 4, no. 10, pp. 111-115.
- [121] Huang, B., Li, M., Lin, W., Zhang, J., Zhang, G., Wu, F., (2020), A compact slotted patch hybrid mode antenna for sub-6GHz communication", *International Journal of Antennas and Propagation*, vol. 2020, Article ID 8262361, 8 pages.
- [122] Huang, B., Li, M., Lin, W., Zhang, J., Zhang, G., Wu, F., (2020), A compact slotted patch hybrid mode antenna for sub-6 GHz communication", *International Journal of Antennas and Propagation*, vol. 2020, Article ID 8262361, 8 pages.
- [123] Gopal, G., Thangakalai, A., (2020), Cross dipole antenna for 4G and sub-6 GHz 5G base station applications, *ACES Journal*, vol. 35, no. 1, pp. 16-22.
- [124] Khalifa, M., Khashan, L., Badawy, H., Ibrahim, F., (2020), Broadband printed-dipole antenna for 4G/5G smartphones, *Journal of Physics: Conference Series*, no. 1447.
- [125] Melchiorre, L., Marasco, I., Niro, G., Basile, V., Marrocco, V., D'Orazio, A., Grande, M., (2020), Bio-inspired dielectric resonator antenna for wideband sub-6 GHz range, *Appl. Sci.*, vol. 10, pp. 8826.
- [126] Saurabh, A. K., Meshram, M. K., (2020), Compact sub-6 GHz 5G-multiple-input-multiple-output antenna system with enhanced isolation, *Int. J. RF Microw Comput Aided Eng.*, vol. 30, no. e22246.
- [127] Zaidi, A., Awan, W. A., Hussain, N., Baghdad, A., (2020), A wide and tri-band flexible antennas with independently controllable notch bands for sub-6 GHz communication system, *Radioengineering*, vol. 29, no. 1, pp. 44-51.
- [128] Jha, P., Singh, S., Yadava, R. L., (2021), Wideband sub-6 GHz microstrip antenna: Design and fabrication, In: Agrawal R., Kishore Singh C., Goyal A. (eds) *Advances in smart communication and imaging systems. Lecture notes in electrical engineering*, vol 721. Springer, Singapore.

- [129] Azim, R., Meaze, A., Affandi, A., Alam, M., Aktar, R., Mia, M., Islam, M., (2021), A multi-slotted antenna for LTE/5G sub 6 GHz wireless communication applications, *International Journal of Microwave and Wireless Technologies*, vol. 13, no. 5, pp. 486-496.
- [130] Mishra, R., Dandotia, R., Mishra, R.G., Kuchhal, P., Pachauri, R. K., (2021), SRR slotted multiband antenna in sub 6 GHz for futuristic communication, *EAI Endorsed Transactions on Energy Web*, vol.8, issue 32, pp. 1-5.
- [131] Aathmanesan, T., (2021), Novel slotted hexagonal patch antenna for sub-6 GHz 5G wireless applications, *ICTACT Journal on Microelectronics*, vol. 06, issue 04, pp. 1010-1013.
- [132] Hakanoglu, B. G., Koc, B., Sen, O., Yalduz, H. Turkmen, M., (2021), Stub loaded patch antenna and a novel method for miniaturization at sub 6 GHz 5G and Wi-Fi frequencies, *Advances in Electrical and Computer Engineering*, vol.21, no.2, pp.23-32.
- [133] Ishteyaq, I., Muzaaffar, K., (2021), Multiple input multiple output (MIMO) and fifth generation (5G): an indispensable technology for sub-6 GHz and millimeter wave future generation mobile terminal applications, *International Journal of Microwave and Wireless Technologies*, pp. 1-17.
- [134] Zada, M., Shah, I. A., Yoo, H., (2021), Integration of sub-6 GHz and mm-Wave bands with a large frequency ratio for future 5G MIMO applications, *IEEE Access*, vol. 9, pp. 11241-11251.
- [135] Chaimool, S., Chung, K. L., Akkaraekthalin, P., (2010), Bandwidth and gain enhancement of microstrip patch antennas using reflective metasurface, *IEICE Transactions on Communications*, vol. E93.B, no. 10, pp. 2496-2503.
- [136] Sharma, A., Gangwar, D., Kanaujia, Dwari, B. K. S., (2013), Gain enhancement and broadband RCS reduction of a circularly polarized aperture-coupled annular-slot antenna using metasurface, *Journal of Computational Electronics*, vol. 17, issue 3, pp. 1037-1046.
- [137] Cure, D., Weller, T. M., Price, T., Miranda, F. A., Van Keuls, F. W., (2014), Low-profile tunable dipole antenna using barium strontium titanate varactors", *IEEE Transactions on Antennas and Propagation*, vol. 62, pp.1185-1193.
- [138] Rana, B., Chatterjee, A., Parui, S. K., (2016), Gain enhancement of a dual polarized dielectric resonator antenna using polarization independent FSS, *Microw. Opt. Technol. Lett.*, vol. 58, pp. 1415-1420.
- [139] Rabbani, M. S., Shiraz, H. G., (2017), Dual frequency selective surface high gain antenna with deep resonant cavity and E-field reflectors, *Microw. Opt. Technol. Lett.*, vol. 59, pp. 2772-2777.
- [140] Imran, A. I., Elwi, T. A., (2017), A cylindrical wideband slotted patch antenna loaded with frequency selective surface for MRI applications", *Engineering Science and Technology, an International Journal*, vol. 20, issue 3, pp. 990-996.

- [141] Gunes, F., Belen, M. A., Mahouti, P., (2018), Performance enhancement of a microstrip patch antenna using substrate integrated waveguide frequency selective surface for ISM band applications, *Microwave and Optical Technology Letters*, vol.60, no.5, pp.1160-1164.
- [142] Singh, D., Thakur, A., Srivastava, V. M., (2018) Miniaturization and gain enhancement of microstrip patch antenna Using defected ground with EBG, *Journal of Communications*, vol. 13, no. 12, pp. 730-736.
- [143] Shukla, H. N., Hasan, Z., (2019), Design of gain enhanced microstrip patch antenna using frequency selective surface, *International Journal of Science & Engineering Development Research*, vol.4, issue 3, pp. 491-495.
- [144] Hussein, E. D., Qasem, N., Jameel, M. S., Ilyas, M., Bayat, O., (2020), Performance optimization of microstrip patch antenna using frequency selective surfaces for 60 GHz, 2020 28th Signal Processing and Communications Applications Conference (SIU), pp. 1-4.
- [145] Nassr, Z. A., Zabri, S. N., Shairi, N. A., Zakaria, Z., Othman, A., Zobilah, A. M., (2020), Performance improvement of a slotted square patch antenna using FSS superstrate for wireless application, *Journal of Physics: Conference Series*, no, 1502, pp. 1-8.
- [146] Raj, A., Gupta, N., (2020), Radiation characteristics of microstrip antenna on frequency selective surface absorbing layer, *International Journal of Microwave and Wireless Technologies*, pp. 1-7.
- [147] Kumar, A., De, A., Jain, R. K., (2021), Gain enhancement using modified circular loop FSS loaded with slot antenna for sub-6 GHz 5G application," *Progress In Electromagnetics Research Letters*, vol. 98, pp. 41-48.
- [148] Anwar, R. S. Mao, L., Ning, H., (2018), Frequency selective surfaces: A review", *Appl. Sci.*, vol. 8, no. 9, pp. 1-46.
- [149] Wang, Z., (2020), Floquet theory, (Accessed 14 September 2020). <https://math.ecnu.edu.cn/zmwang/teaching / Assignments and Some Supplemental Materials /Floquet Theory.pdf>.
- [150] Jha, K. R., Singh, G., Jyoti, R., (2013), A simple synthesis technique of single square loop frequency selective surface, *Progress in Electromagnetic Research B*, vol.45, pp. 165-185.
- [151] Yilmaz, A. E., Kuzuoglu, M.,(2009), Design of the square loop frequency selective surfaces with particle swarm optimization via the equivalent circuit model, *Radioengineering*, vol.18, no. 2, pp.95-102.
- [152] Archer, M. J., (1985), Wave reactance of thin planar strip gratings, *International Journal of Electronics*. vol. 58, pp. 187 – 230.
- [153] Reed, J. A.,(1997), Frequency selective surfaces with multiple periodic elements, Ph.D. Dissertation, University of Texas at Dallas, USA.

- [154] Li, M., Behdad, N.,(2013), Frequency selective surfaces for pulsed high-power microwave applications, *IEEE Transactions on Antennas and Propagation*, vol. 61, no.2, pp.677-687.
- [155] Zhou, X., Luo, K., Chen, B., Wang, Y., (2015), Simulation analysis of frequency selective surface with high power handling capability, 2015 7th Asia-Pacific Conference on Environmental Electromagnetics (CEEM), pp.344-349.
- [156] Farnaz, M., Javad, N., Changiz, G., (2012), A novel dual-wide band monopole like microstrip antenna with controllable frequency response, *IEEE Antenna and Wireless Propagation Letter*, vol. 11, pp. 289-292.
- [157] Alsath, M. G. N., Kanagasabai, M., Balasubramanian, B., (2013), Implementation of slotted meander-line resonators for isolation enhancement in microstrip patch antenna arrays, in *IEEE Antennas and Wireless Propagation Letters*, vol. 12, pp. 15-18.
- [158] Ismail, M., Inam, Y. M., Zain, A. F. M., Mughal, M. A. M., Abdullah, F. L., Ubin, A., (2010), Phase and bandwidth enhancement of reconfigurable reflectarray antennas with slots embedded patch, 2010 *IEEE Antennas and Propagation Society International Symposium*, pp. 1-4.
- [159] Kidre, A., (2014), Wide band dual beam U- slot Microstrip antenna, *IEEE transaction of Antennas and Wireless Propagation Letters*, vol.61, pp. 1415-19.
- [160] Liu, W.C., Wu, C. M., Dai, Y., (2011), Design of triple frequency microstrip fed monopole antenna using defected ground structure , *IEEE Transaction on Antennas and Propagation*, vol.10, pp. 2457-2463.
- [161] Bansal, A., Gupta, R., (2020), A review on microstrip patch antenna and feeding techniques, *Int. j. inf. tecnol.*, vol.12, pp. 149–154.
- [162] Njokweni, S. N., Kumar, P., (2020), Salt and sugar detection system using a compact microstrip patch antenna, *International Journal on Smart Sensing and Intelligent Systems*, vol.13, issue 1, pp.1-9.
- [163] Guo, J. L., Zou, Y. L., Liu, C., (2011), Compact broadband crescent moon-shape patch-pair antenna, *IEEE Antennas Wirel. Propag. Lett*, vol. 10, pp. 435–437.
- [164] Sekeljic, N., Yao, Z., Hsu, H., (2019), 5G broadband antenna for sub-6 GHz wireless applications, 2019 *IEEE International Symposium on Antennas and Propagation and USNC-URSI Radio Science Meeting*, pp. 147-148.
- [165] Tang, X., Jiao, Y., Li, H., Zong, W., (2019), Ultra wideband patch antenna for sub-6 GHz 5G communications, *International Workshop on Electromagnetics: Applications and Student Innovation Competition (iWEM)*, Qingdao, pp. 1-3, China.
- [166] Foroozesh, A., Shafai, L., (2010), Investigation into the effects of the patch type FSS superstrate on the high gain cavity resonance antenna design, *IEEE Transactions on Antennas and Propagation*, vol. 58, no. 2, pp. 258-270.

- [167] Chen, H., Tao, Y., (2011), Bandwidth enhancement of a u-slot patch antenna using dual band frequency-selective surface with double rectangular ring elements, *Microwave Opt Technol Lett.*, vol.53, no. 7, pp.1547–53.
- [168] Rishishwar, D., Shrivastava, L., (2014), Rectangular microstrip patch antenna with FSS and slotted patch to enhance bandwidth at 2.4 GHz for WLAN applications, *Int. J Technol Enhance Emerg Eng Res*, vol. 2, no. 4, pp. 59-62.
- [169] Kakhki, M. B., Mantash, M., Denidni, T. A., (2018), Gain enhancement of col-linear antenna array using a frequency selective surface, 2018 18th International Symposium on Antenna Technology and Applied Electromagnetics (ANTEM), pp. 1-2.
- [170] Filho, A., Valdez A., Campos, A. L. P. S., (2014), Performance optimization of microstrip antenna array using frequency selective surfaces, *J. Microw. Optoelectron. Electromagn. Appl.*, vol.13, no.1, pp. 31-46.
- [171] Sugumaran, B., Balasubramanian, R., (2020), Design and analysis of fractal based monopole antenna backed with modified Jerusalem cross frequency selective surface for wireless personal area communications, *Mobile Netw Appl.*, vol. 25, pp. 2092–2101.

Publications

- [1] A. Kapoor, P. Kumar and R. Mishra, "Analysis and design of a passive spatial filter for sub-6 GHz 5G communication systems," *Journal of Computational Electronics*, vol. 20, pp. 1900-1915, 2021. Status: Published.[IF - 1.9] [SCIE]
- [2] A. Kapoor, R. Mishra, and P. Kumar, "Frequency selective surfaces as spatial filters: Fundamentals, analysis and applications," *Alexandria Engineering Journal*. Status: Published. [IF - 3.7] [SCIE]
- [3] A. Kapoor, R. Mishra, and P. Kumar, "Gain Augmentation of Compact Wideband Printed Patch Radiator Using Frequency Selective Surface for Sub-6 GHz 5G Next Generation Devices," *Alexandria Engineering Journal*. Status: Under Review. [IF - 3.7] [SCIE]
- [4] A. Kapoor, R. Mishra, and P. Kumar, "Wideband miniaturized patch radiator for Sub-6 GHz 5G devices," *Heliyon*, vol. 7, no. 9, pp. 1-10, 2021. Status: Published. [IF - 2.9] [ESCI, SCOPUS]
- [5] A. Kapoor, R. Mishra, and P. Kumar, "Complementary Frequency Selective Surface Pair Based Intelligent Spatial Filters for 5G Wireless Systems," *Journal of Intelligent Systems*. Status: In Press. [ESCI, SCOPUS]
- [6] A. Kapoor, R. Mishra, and P. Kumar, "A Compact High Gain Printed Antenna with Frequency Selective Surface for 5G Wideband Applications," *Advanced Electromagnetics*, vol. 10, no. 2, pp. 27-38., 2021. Status: Published. [ESCI, SCOPUS]

- [7] A. Kapoor, R. Mishra, and P. Kumar, "Compact wideband-printed antenna for Sub-6-GHz fifth-generation applications," *International Journal of Smart Sensing and Intelligent Systems*, vol. 13, no. 1, pp. 1-10, 2020. Status: Published. [ESCI, SCOPUS]
- [8] A. Kapoor, R. Mishra, and P. Kumar, "Slotted Wideband Frequency Selective Reflectors for Sub-6 GHz 5G Devices," *2021 IEEE International Conference on Computing, Communication, and Intelligent Systems (ICCCIS)*, pp. 786-791, 2021. Status: Published. [IEEE, SCOPUS]
- [9] A. Kapoor, R. Mishra, and P. Kumar, "Novel Wideband Frequency Selective Surface Based Space Borne Filters for Sub-6 GHz 5G Devices," *2021 4th Biennial IEEE International Conference on Nascent Technologies in Engineering (ICNTE)*, pp. 1-6, 2021. Status: Published. [IEEE, SCOPUS]

Scholar's Resume

Ankush Kapoor

S/O Prof. Vipin Kapoor H.No-120 Ward No.-2
Haripur, Sundernagar, Mandi, (H.P.), India.
+91-9459679235 ; ankush8818@yahoo.com (mail id)

Career Objective

To make the best use of my technical expertise in logic development and data analysis in a research based career; hence to acquire and apply advanced knowledge in a particular field, "Antenna Design".

Professional Qualification

- M. Tech in ECE (**Gold Medalist**) in 2012 from Jaypee University of Information Technology, Waknaghat (H.P.)
- B. Tech in ECE in 2010 from R.I.E.I.T Ropar, Punjab Technical University.

Skill Set

Computer Proficiency: Working knowledge of HFSS, CST, Labview, VHDL, Verilog, MATLAB, Network Simulator-2 (NS-2) and Communication Simulator (CommSim), OrCAD Software, PSpice, Ansys Designer/ NEXXIM.

Areas of Interest: Frequency Selective Surfaces (FSS), Antenna Design, Satellite Communication, Wireless Communication, Electromagnetic Band Gap Structures (EBG), Spread Spectrum Theory, Software Defined Radio (SDR), Microwave Theory, Computational Electromagnetics, Optical Communication.

Teaching Experience

1. Working as a Assistant Professor in Deptt. Of ECE, Jawaharlal Nehru Government Engineering College Sundernagar Distt. Mandi H.P from 2013 to till date (selection from Himachal Pradesh Public Service Commission).
2. Worked as a Lecturer in Deptt. Of ECE, Jawaharlal Nehru Government Engineering College Sundernagar Distt. Mandi H.P from 2012 to 2013.

Awards and Scholarships

1. Gold Medalist at M.Tech Level in the University.

2. Got Bronze Medal in B.Tech at college level.
3. Brilliance Scholarship from Department of Technical Education and Vocational Training H.P at B.Tech level and M.Tech level.
4. Brilliance Scholarship from Department of Technical Education and Vocational Training H.P at M.Tech level.

Administrative/ Co-Curricular Activities

1. Worked as Officer In charge of ECE Department for one year in Jawaharlal Nehru Government Engineering College Sundernagar.
2. Nodal Officer Procurement (TEQIP-III) for three years in Jawaharlal Nehru Government Engineering College Sundernagar.
3. Coordinator ISTE AND IETE Chapters for one year in Jawaharlal Nehru Government Engineering College Sundernagar.
4. Member of Board of Studies (BOS) of H.P. Technical University Hamirpur to revise and make choice based credit system curriculum and for implementing AICTE modal curriculum in the existing CBCS syllabus of HPTU.
5. Subject Expert in Affiliation Committee visited to Atal Bihari Vajpayee Government Institute of Engineering and Technology, Shimla.
6. Member of Editorial Board of 'International Journal of Electronics and Computer Science Engineering' [IJECS], 'International Association Of Engineers' [IAENG]
7. Member of 'International Association of Computer Science and Information Technology' [ACSIT], 'The Society of Digital Information and Wireless Communications' [SDIWC], and Member of 'Universal Association of Computer and Electronics Engineers' [UACEE]

Journal and Conference

1. Published 8 Journals paper
2. Published 16 Conference paper.

Declaration

I vouch for the accuracy of the above-mentioned data. If given the chance, I pledge to put out my best efforts to meet high standards and contribute to an innovation in the field of Antennas and Spatial filters.

Ankush Kapoor



PLAGIARISM CERTIFICATE

1. We , **Dr. Ranjan Mishra** (Internal Supervisor) and **Dr. Pradeep Kumar** (External Supervisor); certify that the Thesis titled as **“Frequency Selective Surface Based Microstrip Antennas for Wideband Applications”** submitted by the Scholar **Mr. Ankush Kapoor** having SAP ID: 500072301, has been run through a Plagiarism Check Software and the Plagiarism Percentage is reported to be 7 %.
2. Plagiarism Report as generated by the Plagiarism Software is attached herewith.

A handwritten signature in black ink, appearing to read 'Ranjan Mishra', with a horizontal line underneath.

Dr. Ranjan Mishra
Internal Supervisor

A handwritten signature in blue ink, appearing to read 'Pradeep Kumar', with a horizontal line underneath.

Dr. Pradeep Kumar
External Supervisor

A handwritten signature in black ink, appearing to read 'Ankush Kapoor', with a horizontal line underneath.

Ankush Kapoor
(Scholar)

ORIGINALITY REPORT

7%

SIMILARITY INDEX

3%

INTERNET SOURCES

6%

PUBLICATIONS

%

STUDENT PAPERS

PRIMARY SOURCES

- 1** Ankush Kapoor, Pradeep Kumar, Ranjan Mishra. "Analysis and design of a passive spatial filter for sub-6 GHz 5G communication systems", Journal of Computational Electronics, 2021
Publication 2%
 - 2** aemjournal.org
Internet Source 2%
 - 3** "Handbook of Antenna Technologies", Springer Science and Business Media LLC, 2016
Publication 1%
 - 4** www.exeley.com
Internet Source 1%
 - 5** Ankush Kapoor, Ranjan Mishra, Pradeep Kumar. "Frequency selective surfaces as spatial filters: Fundamentals, analysis and applications", Alexandria Engineering Journal, 2021
Publication 1%
-

dyuthi.cusat.ac.in

Ankush Kapoor

Ranjan Mishra

Ankush